Zirconium-89 for Positron Emission Tomography and Hydroxamate Resin Column for Gallium-68 Generator

Azahari Kasbollah

Submitted in total fulfilment of the requirements of the degree of

Doctor of Philosophy

July 2013

School of Medical Sciences

RMIT University

Abstract

Zirconium-89 (^{89}Zr), a radionuclide with a half-life of 78.4 hours, is suitable for imaging tumours using positron emission tomography (PET) when labelled with monoclonal antibodies. ^{89}Zr can be produced from Yttrium-89 (^{89}Y) by a process of cyclotron bombardment with ^{89}Y(p, n)^{89}Zr reaction. Purification and radiolabelling processes must be developed before ^{89}Zr can be used for monoclonal antibody PET imaging.

The main aim of this study was to produce ^{89}Zr using various types of ^{89}Y solid targets through irradiation in a 12 MeV medical cyclotron at low currents using ^{89}Y(p, n)^{89}Zr reaction for PET imaging in a preclinical condition. Five techniques of ^{89}Y solid targets were prepared for the production of ^{89}Zr. Gamma spectrum analyses determined energy peaks of 511 keV and 909 keV indicating that ^{89}Zr radionuclide had been successfully produced. ^{89}Zr was then purified through a hydroxamate resin column and radiolabelled to a monoclonal antibody (trastuzumab). Experiments on biodistribution together with PET imaging of female balb/c nude mice having the HER2 positive LS174T colorectal tumour was undertaken to validate the successful radiolabelling procedure between ^{89}Zr and trastuzumab. PET images at 24 hours showed a selective accumulation of ^{89}Zr-Df-Trastuzumab in tumour-bearing mice with good tumour tracer uptake in the right flank, as well as cardiac uptake, a significant presence of HER2 receptor expression on the heart, demonstrated that the conjugated Df-Trastuzumab was successfully labelled with ^{89}Zr.

In addition, the capability of the hydroxamate resin column as a new potential column was investigated for ^{68}Ga purification and radiolabelling in a ^{68}Ga generator. Hydroxamate resin column was used to trap ^{68}Ga in alkaline solution and the solution was purified and eluted from hydroxamate resin column using citrate buffer at pH 4 as an extraction agent. It was then labelled to a monoclonal antibody to produce ^{68}Ga radiopharmaceutical for PET imaging. The first series of experiments on different quantities of hydroxamate resin column indicated that 50 mg of the resin was suitable for the optimum extraction of ^{68}Ga radionuclide. Series elution tests of ^{68}Ga from the hydroxamate resin column using various buffers including acetate, citrate and citrate in hydrochloric acid (HCl) with different concentrations were performed. The results indicated that 0.1 M citrate buffer was suitable for ^{68}Ga elution and comparable to 0.5 M HCl which is currently being used as ^{68}Ga extraction agent from ^{68}Ge/^{68}Ga generator. Experiments on ^{68}Ga radiopharmaceutical radiolabelling reported that ^{68}Ga-Df-Trastuzumab radiolabelling was successful according to TLC and HPLC analysis results; however, weak radiolabelling efficiency was found for ^{68}Ga-Pentetreotide radiolabelling.

In conclusion, ^{89}Zr was produced through irradiation at 10 µA using ^{89}Y(p, n)^{89}Zr reaction in a 12 MeV medical cyclotron and was successfully radiolabelled to trastuzumab for PET imaging in a preclinical condition. In addition, the potential of hydroxamate resin to be used as a new column in a ^{68}Ga generator was promising, where ^{68}Ga was purified and eluted from a hydroxamate resin column using 0.1 M citrate buffer at pH 4 as an extraction agent. It was successfully labelled to a monoclonal antibody to produce ^{68}Ga radiopharmaceutical for PET imaging.

Declaration

This is to certify that this thesis comprises only my original work towards the PhD, except where indicated. Due acknowledgement has been made in the text to all other material used, and the thesis is less than 100,000 words in length, exclusive of tables, figures, references and appendices.

Azahari Kasbollah

July 2013

Preface

The work presented in this thesis was performed at the School of Medical Sciences at RMIT University, under the supervision of Dr. Pradip Deb and in the Diagnostic Imaging Department at the Peter MacCallum Cancer Center under the supervision of Mr. Peter Eu. Some components of this work were also carried out under the guidance of Jos Campbell in the School of Applied Sciences, RMIT University.

Some components of this work were performed by other researchers and due acknowledgement is given throughout the thesis. Yttrium sputtering production was performed jointly by me and also Jos Campbell from the School of Applied Sciences, in the laboratory of Professor Dr. Kourosh Kalantar-zadeh from the School of Electrical and Computer Engineering, RMIT University.

Most of the work presented in the thesis has been presented at scientific conferences and some parts of the work have been published in peer-reviewed journals.

Acknowledgements

This thesis is exclusively dedicated in loving memory to my parents, Kasbollah bin Jam-jam and Menah binti Seladi. May peace be upon them.

My deepest gratitude for guidance and encouragement throughout this research goes to my supervisors, Dr. Pradip Deb, Mr. Peter Eu and Dr. Simon Cowell. I appreciate their support and patience given to me throughout the entire candidature; particularly Peter, who has given me a great deal of opportunities in training to develop my expertise in cancer research, as well as access to technical equipment that I needed over the four years of my PhD study.

I am grateful to all those who participated in this study and I appreciatively acknowledge the funding sources that made my PhD work possible. My scholarship was sponsored by the Ministry of Science, Technology and Innovation (MOSTI), Malaysia. I also would like to thank the Malaysian Nuclear Agency for giving me the opportunity to pursue my PhD study in Melbourne, Australia. In particular, I wish to thank the staff of RMIT University and the Peter MacCallum Cancer Centre by providing me with all necessary support and advice in making my PhD study possible.

I have been supported by a miraculous group of family and friends. I would like to thank my family, relatives and friends, whose support, inspiration and love have always been the foundation upon which my efforts rely.

Most of all, my thanks go to my loving and encouraging wife, Nurhasliza binti Hashim, with whom I shared my anxiety and joy while conducting this research. Thank you for your patience and faithful support during the four years of my PhD journey. My love is for her. Not forgetting my lovely children who are also my life.

Abbreviations

DOTA	1,4,7,10-tetraazacyclododecane-N,N',N'',N'''-tetraacetic acid
EDAC	1-Ethyl-3-(3-dimethylaminopropyl)carbodiimide
^{18}FDG	18-fluoro-2-deoxy-D-glucose
HEPES	4-(2-hydroxyethyl)-1-piperazineethanesulfonic acid
MeCN	acetonitrile
^{76}Br	bromine-76
^{11}C	carbon-11
CLI	Cerenkov luminescence imaging
^{64}Cu	copper-64
Df	desferrioxamine
DMSO	dimethyl sulfoxide
DOTATOC	DOTA-d-Phe(1)-Tyr(3)-octreotide
EGFR	epidermal growth factor receptor
EDTA	ethylenediaminetetraacetic acid
FISH	fluorescence *in situ* hybridization
^{18}F	fluorine-18
FDA	Food and Drug Administration
^{68}Ga	gallium-68
^{68}Ge	germanium-68
LS174T	human caucasian colon adenocarcinoma
HER2	human epidermal growth factor receptor 2
IGF1R	insulin-like growth factor 1 receptor

LOR	line of response
MRI	magnetic resonance imaging
MBq	megabequerel
MeOH	methanol
mAbs	monoclonal antibodies
Df-Bz-NCS	*p*-isothiocyanatobenzyl-desferrioxamine
PET	positron emission tomography
PET-CT	positron emission tomography-computed tomography
PSMA	prostate-specific membrane antigen
SPECT	single photon computed emission tomography
$NaHCO_3$	sodium bicarbonate
Na_2CO_3	sodium carbonate
NaCl	sodium chloride
NaOH	sodium hydroxide
SSTR	somatostatin receptor
TFP	tetrafluorophenol
UV	ultraviolet
VEGF	vascular endothelial growth factor
WFI	water for injection
^{86}Y	yttrium-86
^{89}Y	yttrium-89
^{89}Zr	zirconium-89

Table of Contents

List of Tables

List of Figures

Chapter 1: Introduction

1.1 Radioactivity

Radioactivity refers to a spontaneous emission of radiation from atomic nuclei, either from the unstable atom or as a consequence of a nuclear reaction. Radioactivity is a decomposition process where unstable atomic nuclei spontaneously release energetic subatomic particles to form nuclei with a higher stability. The energy and particles which are released during the decomposition process are called radiation. There are three major types of radioactivity emitted by a radioactive substance, namely:

- Alpha Radiation - Alpha radiation has an atomic mass of 4 and a charge of +2 (a helium nucleus). It contains a stream of positively charged particles which are also called alpha particles. When an alpha particle is ejected from a nucleus, the mass number of the nucleus decreases by four units and the atomic number decreases by two units. For example:

  $$^{238}_{92}U \rightarrow ^{4}_{2}He + ^{234}_{90}Th$$

  The helium nucleus is the alpha particle. Although alpha particles are normally highly energetic, they travel only a few centimetres in the air and are then stopped by a sheet of paper or the outer layer of dead skin.

- Beta Radiation - Beta radiation is a stream of electrons, called beta particles. When a beta particle is ejected, a neutron in the nucleus is converted to a

proton, so the mass number of the nucleus is unchanged, but the atomic number increases by one unit. For example:

$$^{234}_{90}Th \rightarrow ^{0}_{-1}e + ^{234}_{91}Pa$$

The electron is the beta particle. Beta particles may travel metres in air and several millimetres into the human body. Most beta particles may be stopped by a small thickness of a light material such as aluminium or plastic.

- Gamma rays are high-energy photons with a very short wavelength (0.0005 to 0.1 nm). The emission of gamma radiation results from an energy change within the atomic nucleus. Gamma emission does not change either the atomic number or the atomic mass. Alpha and beta emissions are often accompanied by gamma emission, as an excited nucleus drops to a lower and more stable energy state. Gamma particles travel in a wave-like pattern at the speed of light. They can only be stopped by a dense material such as lead, steel, concrete or several metres of water.

Apart from the natural process of unstable nuclei decomposition in nature (which is also known as natural radioactivity), there is another process of unstable nuclei decomposition that is prepared in the laboratory, known as induced radioactivity. In this process, positron (a particle with the same mass as an electron, but a charge of +1 instead of -1) emission is a common mode of decay in induced radioactivity but not observed in natural radioactivity. Basically, positron emission is used in preparing radioactive isotopes in the lab by using bombardment reactions in order to

convert a stable nucleus into a radioactive one. Bombardment reactions can be used to produce very heavy elements which do not occur in nature.

Radiation can also be artificially produced in conventional X-ray machines and CT scanners, while radioisotopes can be produced in nuclear reactors or particle accelerators such as medical cyclotrons. Radioactivity has many applications in medicine, both in therapy and imaging. Medical imaging uses either structural or functional imaging. Structural imaging includes x-rays, computed tomography (CT) and magnetic resonance imaging (MRI); whereas functional imaging typically involves the Nuclear Medicine modalities of single photon emission computed tomography (SPECT) and positron emission tomography (PET). Nuclear medicine makes use of the tracer technique whereby targeted radioisotopes emit radiation with sufficient energy to enable them to be detected outside of the body. When these radioisotopes are attached to biologically active molecules, the resulting compounds are known as radiopharmaceuticals. They can either localize in certain body tissues or follow a particular biochemical pathway [1].

Radiopharmacology is the study and preparation of radiopharmaceuticals (radioactive pharmaceuticals) used in the field of nuclear medicine as tracers in the diagnosis and therapeutic treatment of many diseases. It consists of two parts, specifically; a radionuclide (which is a radioactive isotope that can be injected safely into the body) and a pharmaceutical which acts as a carrier molecule delivering the isotope to the area to be treated or examined within the body. Currently, about 95% of radiopharmaceuticals are used for diagnostic purposes and around 5% are used for radionuclide therapy [2-4]. In order for a radiotracer to be used safely in humans, for

imaging or therapy, it must meet high quality standards that include chemical and radiochemical purity, sterility and freedom from pyrogenic material. For functional nuclear medicine imaging there are few ideal radiopharmaceuticals [5]. Table 1.1 outlines the ideal diagnostic radiopharmaceutical for imaging. The ability to measure regional biochemical functions requires a careful design process with these principles in mind. However, in reality, it is not possible to meet all of these criteria. For example, all decay processes involve the emission of particles, as in the case of the pure γ-emitters which emit Auger electrons during some segment of the decaying process. Thus, in addition to the quest of designing an ideal radiopharmaceutical in the development of a biochemical probe area, the following three factors must be considered [6], specifically: (i) the radiotracer must be able to bind preferentially to a specific site; (ii) the radiotracer must be sensitive to minor changes in biochemistry and (iii) if possible, the specific biochemical change should be a function of a specific disease that matches that sensitivity.

Table 1.1

Properties of Ideal Diagnostic Radiopharmaceutical for Imaging [6]

Properties	Expectations
1) Easy availability	Be readily available at a low cost.
2) Particle Emission	(a) Diagnostic purpose - Be a pure gamma emitter, i.e. no particle emission such as α and β, as these particles contribute a radiation dose to the patient while not providing any diagnostic information. (b) Therapeutic purpose – Particles such as α and β are very useful for treating radiation damage of abnormal cells.
3) High Target-to-Nontarget Activity Ratio	To provide maximum efficacy in the diagnosis (therapy) and minimum radiation dose to the patient.
4) Possess proper metabolic activity	Ideal radiopharmaceutical should possess the proper metabolic activity, in that it follows or is trapped in the metabolic process of interest.

Many radiotracers have been synthesised to probe metabolic turnover such as oxygen consumption, glucose utilisation and amino acid synthesis. Enzymatic activity, neurotransmission, receptor density and occupancy have all been measured through appropriately designed radiotracers. It should be emphasised that the development of radiotracers for PET fundamentally violates rule No. 2 (a) in Table 1.1 for the ideal diagnostic radiopharmaceutical for imaging, since PET radionuclides emit β^+ particles by nature. However, the resulting coincident γ rays from the β^+ annihilation form the basis for the technique.

Additionally, in consideration of the above principles, a plan must be considered as to how to insert the radionuclide into the molecule at a point in the synthetic process

with minimal handling, yet still be late enough in the synthesis to minimise loss due to chemical yield and radioactive decay. For these reasons, the preparation of radiopharmaceuticals requires good planning and techniques which are not encountered in traditional synthetic chemistry.

In diagnosis, radioactive substances are administered to patients and the radiation emitted is detected. The diagnostic tests involve the formation of an image using a gamma camera or PET.

1.2 Positron Emission Tomography (PET)

1.2.1 Introduction

Positron emission tomography (PET) is a type of diagnostic medical imaging technology that uses a nuclear medicine imaging modality to produce a three-dimensional image of functional processes in the body. It detects gamma rays emitted by a positron-emitting radioisotope or radionuclide, which is introduced into the body on a metabolically active molecule. The functional images produced of metabolic activity in space are then reconstructed by computer analysis. PET is commonly used for diagnostic purposes to determine the level of cancer inside the body. PET scanners nowadays are mainly aided by results from a CT X-ray scan performed on the patient at the same time using the same machine. Usually, in order to conduct a scanning procedure, a short-lived positron emitting radioisotope tracer is used and injected into the body of a living subject (usually into blood circulation).

However, the radioisotope tracer has to be chemically incorporated into a metabolically active molecule before it can be injected into the blood circulation. Before the patient or research subject is placed in the imaging scanner, there is a waiting period so that the metabolically active molecule accumulates and becomes concentrated in tissues of interest. The most commonly used molecule for this scanning procedure is fluorodeoxyglucose (FDG), a sugar, for which the waiting period is typically an hour.

At the beginning of the 1950s, Wren et al. proposed the idea of using coincidence technique to image positron emitting radionuclides [7]. With this technology, they wanted to study ^{64}Cu in brain tumours using opposing sodium iodine detectors. The Anger camera was launched in the market in 1954 and was quickly applied for positron emitters [8]. Na(I) detectors with coincidence measurements were used in clinical investigations during the 1960s [9]. In 1970, a very important progression in this field was accomplished through the introduction of the tomography principle [10]. The PET technique is thus the outcome of two Nobel Prize awards, specifically: the tracer principle (de Hevesy in 1943) and the tomographic principle (Houndsfield and Cormack in 1979) [11].

Since PET images generate physiological and functional information to the observer and the anatomic structures are sometimes hardly distinguished, PET is nowadays often combined with CT in order to yield the anatomical information [3]. An example of PET facilities at one of the cancer centres in Victoria, Australia is shown in Figure 1.1.

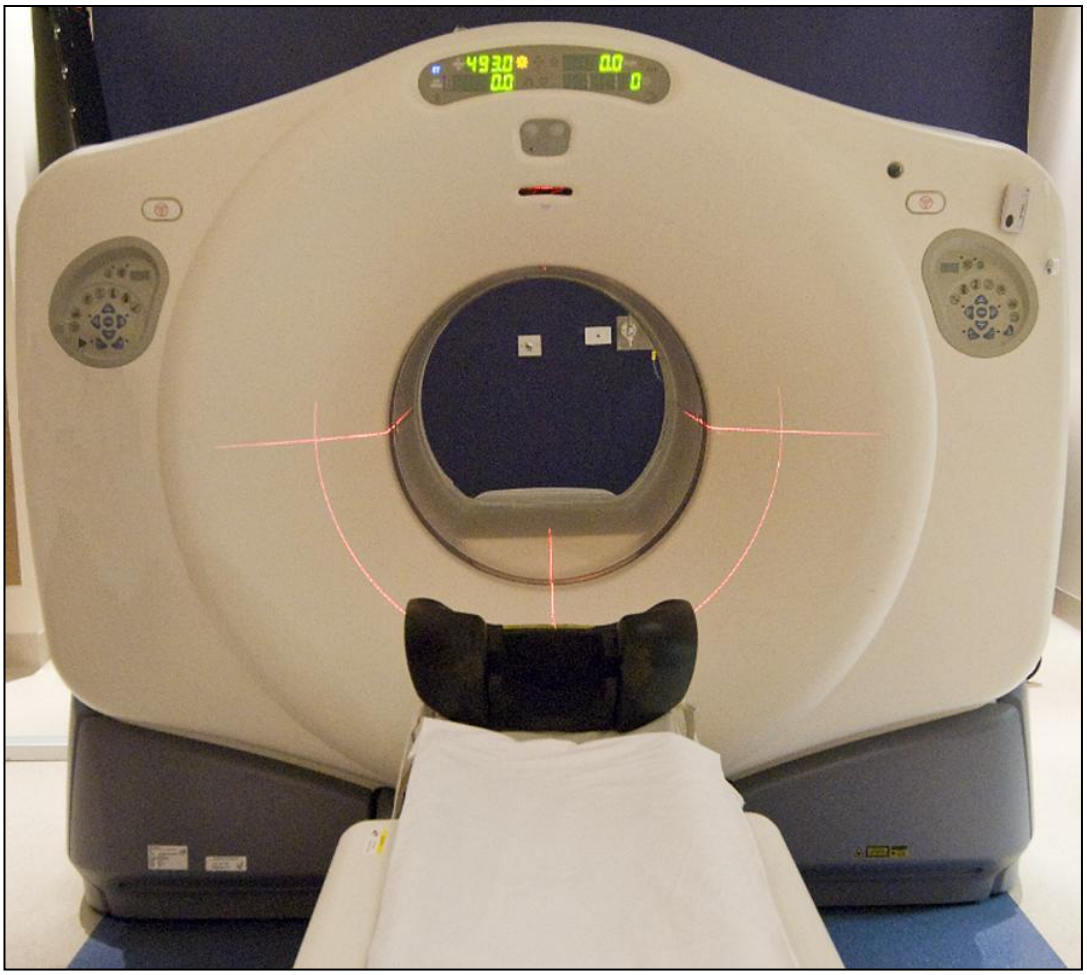

Figure 1.1 PET facilities at Peter MacCallum Cancer Centre, Victoria, Australia

1.2.2 Basic Principle

PET uses gamma rays produced by positrons annihilating with electrons emitted from positron-emitting radionuclides or radiopharmaceuticals, which are then introduced into the body on a metabolically active molecule [12]. Images of metabolic activity in space are then reconstructed by computer analysis, aided by results from a CT X-ray scan performed on the patient at the same time, in the same scanner machine. PET is based on the coincidence detection principle of the two annihilation photons emitted after positron decay [13]. A radioactive isotope,

together with an excess of protons, may disintegrate through positron decay. A proton in the nucleus is converted into a neutron and at the very same moment a positron (β+) and a neutrino (ν) is emitted. The positron has the same mass as an electron but the opposite electric charge, i.e. it is the antiparticle of an electron. In the case of ^{89}Zr, positron decay would look like the following:

$$^{89}\mathrm{Zr} = \mathrm{Y} + \beta^{+} + \nu$$

The energy released in the decay is divided between the positron and neutrino (and the residual energy of the daughter), which means that the positron energy is not monoenergetic but emits in a range of energies. The neutrino is always ejected simultaneously with the positron but is not detected. For radionuclides used in PET, the range of the positron in tissue is in the order of 1-10 mm [14]. Finally, when the positron reaches thermal energy, it interacts with an electron to form an unstable formation - positronium. Positronium eventually decays by emitting two anti-parallel annihilation photons corresponding to the rest masses of the electron and positron respectively, i.e. 511 keV each [15]. Due to inelastic collisions between the positron and atomic electrons, the positron can change its direction substantially from one collision to another.

The PET camera consists of a ring of detectors placed around the object to examine. If these two annihilation photons are registered in a very short period of time (~5-15 ns) the algorithms assume that anywhere along this line an event has happened, which refers to line of response (LOR). By calculating all LORs, the place where the annihilation occurred can be reconstructed. This is basically the principle of coincidence systems. Notice that this location does not refer to the location where the

positron decay took place, but rather to the line along which the decay occurred [16]. The spontaneous decay of a positron emitter produces a positron, which travels a certain distance (depending on its energy) to finally react with one electron of a surrounding atom which is called annihilation. Consequently, two gamma photons are emitted (511 keV each, emitted at 180^{o} to each other). Figure 1.2 shows the basic principles of positron decay and its following annihilation. The generation of these gamma rays forms the basis of PET.

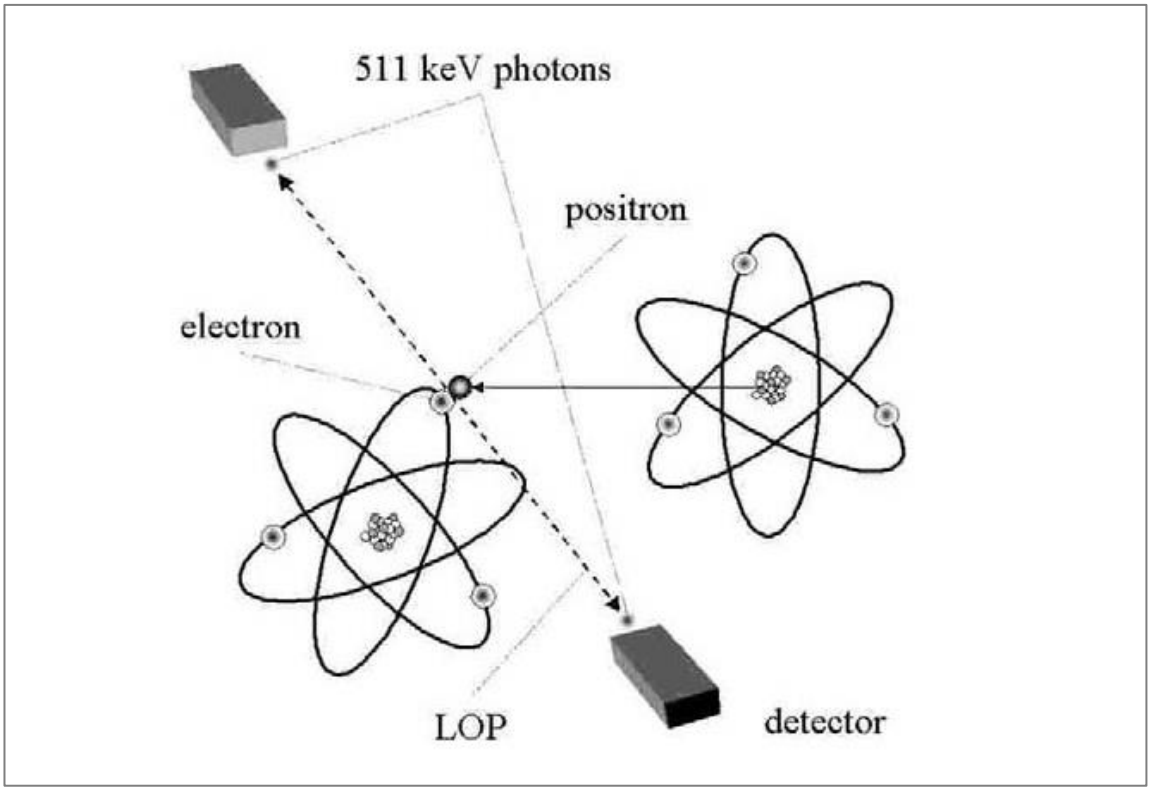

Figure 1.2 Basic principle of positron decay and the following annihilation [17]

1.2.3 Immuno-PET

Immuno-PET, a combination of monoclonal antibodies (mAbs) and PET, associates the high resolution and sensitivity of PET imaging with the specificity of a mAb. This occurs in order to improve diagnostic tumour characterisation that enables the confirmation of tumour targeting and the quantification of mAb accumulation by radioactivity uptake in a modified therapeutic approach [16, 18]. Furthermore, immuno-PET might also have an important role in the characterisation and optimisation of new potential mAbs for diagnosis and therapy [19]. Each mAb can target to an extracellular matrix component or specific tumour cell surface marker for use in immuno-PET. This then permits the development of new potential imaging probes based on mAb. Apart from that, PET also has the potential of molecular interactions quantification, in instances where immuno-PET is used as an introduction to the therapy with the approved mAbs.

In a modified therapeutic method, immuno-PET enables the confirmation of tumour targeting and the quantification of mAb accumulation. Therefore, patients who have the best chance to benefit from the therapy based on mAb could be selected, whereas treatment schedules can be adjusted to improve treatment efficiency and reduce harmfulness.

Currently, intact mAbs are the format of choice for therapeutic procedure because of their long residing time in humans, ranging from a few days to weeks, compared to mAb fragments that have a much faster blood clearance. However, the optimal format for diagnostic purpose is still under review. Innovative approaches for optimal diagnostic procedure include the pretargeting techniques that involve

separating the targeting antibody from the consequent delivery of an imaging or therapeutic agent that binds to the tumour-localised antibody [20].

1.2.4 Positron Emitters for Immuno-PET

A positron emitter which is suitable to be used for immuno-PET has to fulfil several requirements. First and foremost, the positron emitter should have suitable decay characteristics for optimum resolution and quantitative accuracy. Secondly, the production ought to be easy and cheap so as to allow efficient and stable coupling to mAbs. Finally, maintenance of the antibody's in vivo binding and biodistribution characteristics is important, while the half-life ($t_{1/2}$) of the positron emitter should be well-suited with the time needed for a mAb to achieve optimal tumour-to-nontumour ratios. Table 1.2 shows the positron emitters which are suitable for immuno-PET, to be precise: gallium-68 (^{68}Ga; $t_{1/2}$ = 1.13 hours), fluorine-18 (^{18}F; $t_{1/2}$ = 1.83 hours), copper-64 (^{64}Cu; $t_{1/2}$ = 12.7 hours), yttrium-86 (^{86}Y; $t_{1/2}$ = 14.7 hours), bromine-76 (^{76}Br; $t_{1/2}$ = 16.2 hours), zirconium-89 (^{89}Zr; $t_{1/2}$ = 78.4 hours), and iodine-124 (^{124}I; $t_{1/2}$ = 100.3 hours) [21]. ^{68}Ga and ^{18}F are short-lived positron emitters, so they can only be used in combination with mAb fragments or in pretargeting methods. ^{89}Zr and ^{124}I, on the other hand, are predominantly suitable in combination with conjugated mAbs because of their long half-lives which allow imaging at later time points for gaining optimum information. The long half-life of a positron emitter is also an added advantage in terms of logistics related to transportation. However, a possible disadvantage of the use of a long-lived positron emitter is a higher radiation burden to patients. However, as scanners are becoming more sensitive nowadays, this aspect will become less critical. ^{76}Br and ^{124}I can be coupled directly with mAbs,

while the others require indirect labelling methods, using bifunctional chelates or other prosthetic groups.

Table 1.2

Characteristics of positron emitters used in preclinical and clinical radioimmunoscintigraphy studies [21]

Positron emitter	Production	Half-life (hours)	Main β^+ energies (keV)	(%)	Intrinsic spatial resolution loss (mm)
^{68}Ga	^{68}Ge/^{68}Ga generator	1.13	1,899	87.9	2.4
^{18}F	^{18}O(p,n)	1.83	634	100	0.7
^{64}Cu	^{20}Ne(d, ^{64}Ni(d,2n) ^{64}Ni(p,n)	12.7	653	17.4	0.7
^{86}Y	^{86}Sr(p,n)	14.7	1,221	11.9	1.8
			1,545	5.6	
^{76}Br	^{75}As(3He,2n)	16.2	871	6.3	5.3
	^{76}Se(p,n)		990	5.2	
			3,382	25.8	
			3,941	6	
^{89}Zr	^{89}Y(p.n)	78.4	897	22.7	1
^{124}I	^{124}Te(p,n)	100.3	1,535	11.8	2.3
	^{124}Te(d,2n)		2,138	10.9	
	^{125}Te(p,2n)				

Another important consideration in the choice of positron emitter is whether the mAb becomes internalized after binding to the target antigen. Degradation of ^{76}Br- and ^{124}I-labelled mAbs upon internalization results in rapid clearance of these radionuclides from the target cells, and therefore the PET image shows less tumour contrast and does not reflect the actual mAb distribution. In contrast, the positron emitters are trapped intracellularly in lysosomes when ^{68}Ga, ^{64}Cu, ^{86}Y, and ^{89}Zr labelled mAbs are being processed. Thus, when selecting a positron emitter for immuno-PET applications, the occurrence of these residualisations should be taken into account. For example, imaging of trastuzumab, bevacizumab and cetuximab can best be performed using a residualizing positron emitter.

Four important PET radionuclides (^{11}C, ^{13}N, ^{15}O and ^{18}F) were known to all of medical society and this trend is still ongoing. However, apart from these radioisotopes, many other PET radionuclides were prepared and some of them entered the human application phase due to the need for tracing the related elements in human diseases and conditions. Some others were used in radiolabelled form and demonstrated interesting diagnostic tools in various biological phenomena.

Usually, radionuclides which are suitable for labelling to monoclonal antibodies to be used in immuno-PET imaging studies are produced in a cyclotron.

1.3 Cyclotron

1.3.1 Introduction

A cyclotron is a particle accelerator that makes use of electric and magnetic fields to accelerate ions in a small space. Cyclotrons accelerate charged particles using a high-frequency with alternating voltage. A vertical magnetic field causes the particles to spiral almost in a circle so that they re-encounter the accelerating voltage many times. A cyclotron consists of two D-shaped regions known as dees; where in each dee there is a magnetic field perpendicular to the plane of the page. There is a uniform electric field pointing from one dee to the other in the gap separating the dees. A charge is accelerated by the electric field when it is released from the rest in the gap and carried into one of the dees. The charge which is caused by magnetic field in the dee follows a half-circle that carries it back to the gap [22]. When the electric field in the gap is reversed, the charge is once again accelerated across the gap while the charge is in the dee. The cycle continues with the magnetic field in the dees continually bringing the charge back to the gap and every time the charge crosses the gap it picks up speed. This phenomenon causes the half-circles in the dees to increase in radius and, finally, the charge emerges from the cyclotron at high speed.

The electric field is generated by the application of an electric potential difference to two electrodes (called dees and counter-dees) which are connected to the alternating current source. A high voltage is applied to hydrogen or deuterium gas to generate negative ions in the ion source which is placed in the centre of the cyclotron. By

applying an electrical field, negative ions are extracted from the centre of the cyclotron. The counter dee is negatively charged when the dee is positively charged. As a result, the ion is accelerated towards the dee by the electric field [23].

Cyclotrons are one of the earliest types of particle accelerators to be developed and currently used for the preparation of a wide variety of radionuclides that find application in SPECT as well as in PET. Consequently, the cyclotron-produced radioisotopes are in high demand within a worldwide market.

The first cyclotron dedicated to medical applications was installed at Washington University in St. Louis, in 1941 and produced radioactive isotopes of phosphorus, iron, arsenic and sulphur. A cyclotron in Boston also provided a steady supply of radionuclides for medical purposes during World War II. In the middle of the 1950s, a group at Hammersmith Hospital in London put into operation a cyclotron wholly dedicated to radionuclide production [24].

Cyclotrons come in many sizes depending on the function and the scope of the work to be performed in each facility. For example, the widely used PET radionuclides can be prepared in large quantities in a cyclotron with energy ranging from 9 to 19 MeV, whereas higher energy machines (~30 MeV) are needed for preparation of the commonly used SPECT radionuclides. The basic characteristics of all cyclotrons are the same, having an ion source, an acceleration chamber and a magnetic field to produce ions and accelerate them along a circular trajectory. Figure 1.3 shows a deuteron machine designed to produce only ^{15}O for PET. The machine shown in Figure 1.4 is a 500 MeV cyclotron which is located at TRIUMF in Vancouver,

Canada. This 500 MeV cyclotron is a huge facility and a place where a wide variety of radionuclides are produced and other experiments are carried out [24].

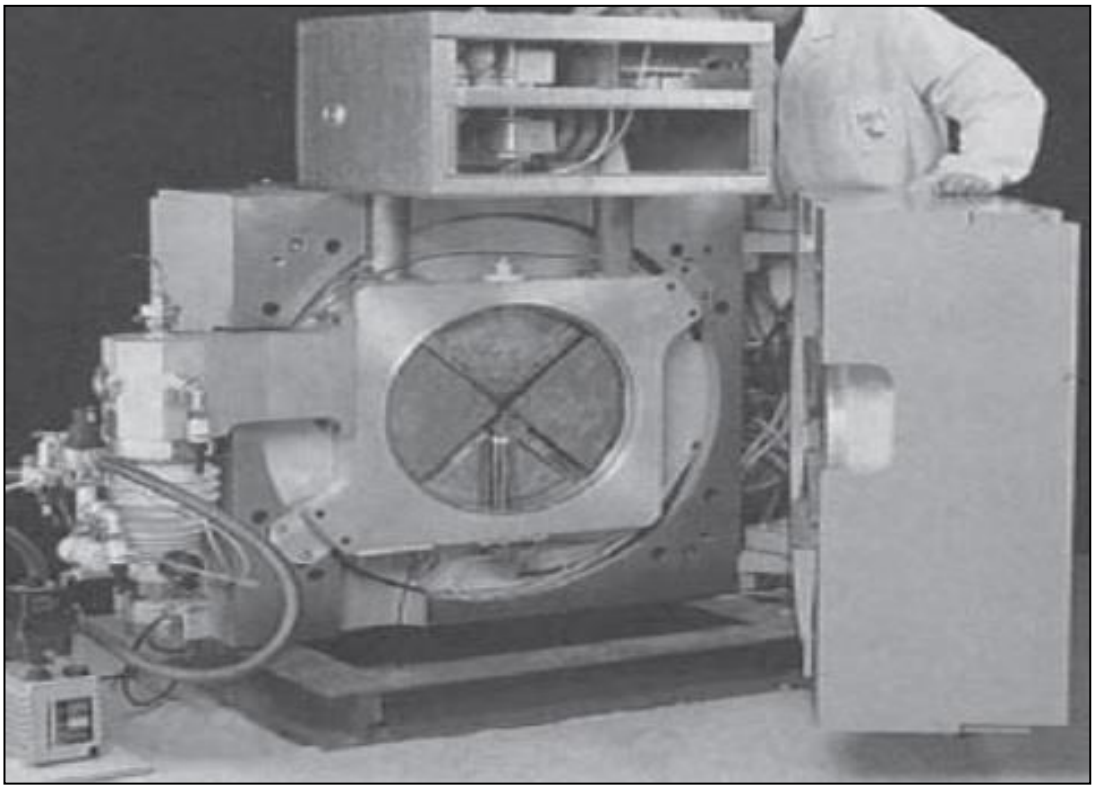

Figure 1.3 A small single isotope cyclotron machine [24]

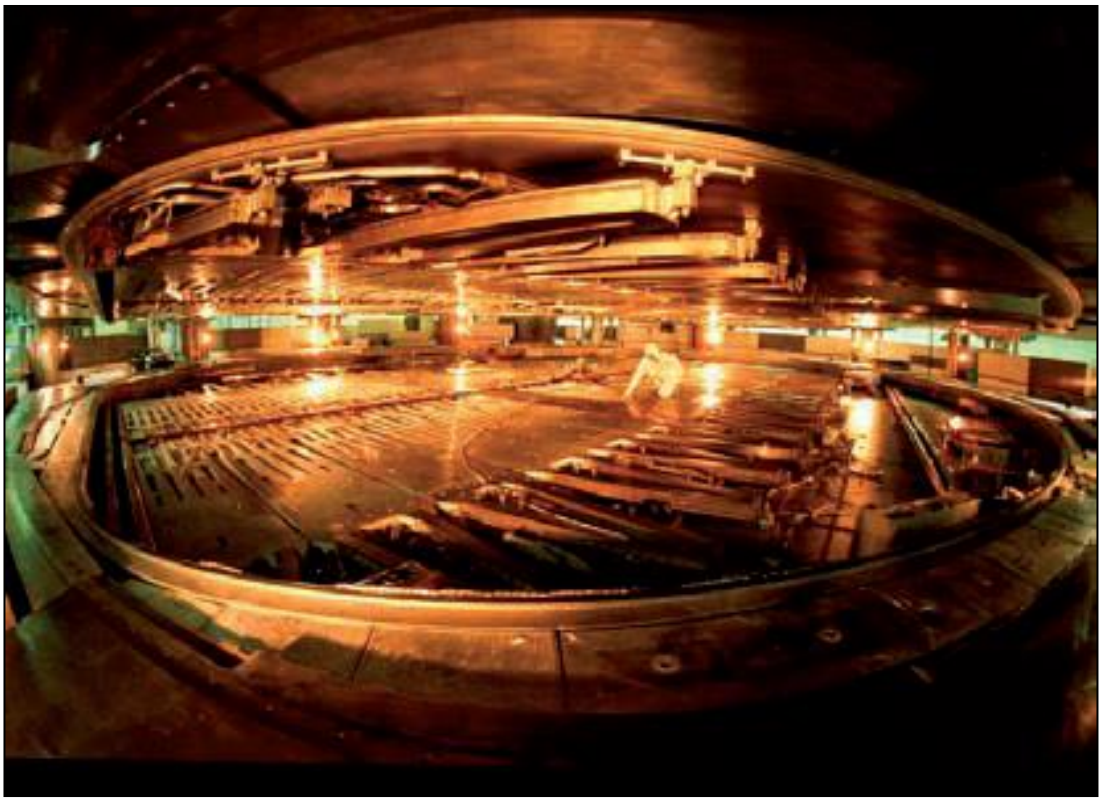

Figure 1.4 A large multipurpose research cyclotron machine [24]

Based on the scope of the work to be performed, five categories of cyclotrons were formally defined by a task group on the PET site and facility planning set up by the American Association of Physicists in Medicine (AAPM). It is obvious that there is really a continuum of facilities and the lines of definition are purely arbitrary [25]. Categories have been defined based on the assumption that a cyclotron will be in place in the facility and the differences will be in the mission and scope of the facility. Table 1.3 outlines the categories of the cyclotron facility [24].

Table 1.3

Types of Cyclotron Facility [24]

Type II	Cyclotron facility with radionuclide production for PET Similar to Type I, this type of facility also has a cyclotron in the proton energy range of 9–19 MeV, with the production of FDG as the principal objective. However, this facility is designed to produce other short-lived positron emitters, e.g. ^{11}C, ^{13}N and ^{15}O, convert them into radiopharmaceuticals and distribute them locally. The facility may also distribute FDG to nearby hospitals with little involvement in basic radiotracer development research and nearly complete dependence on the vendor for maintenance, equipment upgrades, and the development of new radiotracers.
Type III	Cyclotron facility with a research support staff Along with a cyclotron in the 13–19 MeV range and automated synthesis modules, this facility has a scientific support staff of chemist(s), physicist(s), or other scientists capable of developing procedures and radiopharmaceuticals that have been described in the literature. The major emphasis is to provide radiopharmaceuticals for routine patient studies, but some independent research can be carried out, including biodistribution and biokinetic animal studies with micro-PET. In addition to the production of the four traditional PET radionuclides,

	mentioned earlier, this type of facility may also produce other radionuclides such as ^{123}I, ^{124}I, ^{64}Cu and ^{86}Y.
Type IV	Radionuclide production and distribution facility This type of facility is devoted to the large scale production of radionuclides and radiopharmaceuticals for distribution to users. If FDG is the major product, then the cyclotron is probably a small one. If other radioisotopes such as ^{201}Tl, ^{123}I, ^{124}I, ^{67}Ga, ^{64}Cu, ^{86}Y and others are being produced, the cyclotron should be larger(~30 MeV) than those used only for PET. Separate laboratory areas may be required for target preparation, recovery and processing. Separate laboratories or similar places should also be required for sterile setup, quality control (QC) and shipping. There are also possibilities of setting up cyclotron centres dedicated to the production of a single radionuclide such as ^{103}Pd for therapy.
Type V	Cyclotron facility with an extensive research program The facility will have a team of research scientists performing basic research on developing new radiotracers and procedures, along with a larger (30 MeV) cyclotron used for the production of PET and SPECT radionuclides and radiopharmaceuticals. Considerable space is allocated for laboratories and animal facilities. There is little or no pure clinical work done, but there may be an extensive clinical research program. This program may involve production of non-traditional PET radioisotopes such as ^{64}Cu, ^{86}Y, ^{123}I, and ^{124}I as well as many other radionuclides that can be produced by proton (p, xn), deuteron (d, xn) or alpha (α, xn) reactions.

In summary, if the cyclotron is used for radionuclide production and scientific or industrial applications, a multi particle, variable energy and variable beam current (a few nA up to a few hundred μA) accelerator with several beam lines is the preferred cyclotron to be installed. In a word, a cyclotron can be divided into two classes; one with low energy (which is also known as medical cyclotron and produces short lived

PET isotopes such as ^{18}F, ^{15}O and ^{11}C), while the other with higher energy produces SPECT isotopes such as ^{67}Ga, ^{111}In and ^{201}Tl.

In 2006, the International Atomic Energy Agency (IAEA) reported that there are 262 entries for cyclotrons operating in 39 member states of the IAEA. This is an increase of 7% over the 246 reported in the 2002 cyclotron directory. This can be compared to the 350 or more cyclotrons believed to be presently operating in the world, which are involved in some aspects of radionuclide production. The number of cyclotrons have increased recently, not only in developed countries, but also even more in the developing countries [26].

1.3.2 Targets

A cyclotron target is a container where the target material (gas, liquid or solid materials) is introduced in order to be irradiated in a cyclotron. There are some key parameters which have to be considered for target body design, specifically:

- The minimal energy needed to generate the radioactive atom that is the threshold energy for the reaction.
- The energy where the maximum cross-section (probability for the nuclear reaction to occur) is obtained.
- The physical form of the target material: gas, liquid or solid. Heat transfer properties and potential effects due to heating while irradiation takes place should be carefully considered for each particular case.

- The chemical which is formed from the target material.
- The physical form of the product.
- The chemical form of the product.
- The ease of separation of the product from the target.

Target material can be gas, liquid or solid depending on the radioisotope of interest. Targets specially designed for the production of the most common positron emitters (^{18}F, ^{11}C, ^{13}N and ^{15}O) are implemented in commercially available cyclotrons and the design to improve its performance has been optimized for many years. ^{89}Zr is an example of a non-conventional positron emitter which is produced from a solid target of ^{89}Y).

1.4 Zirconium-89

In recent years, there has been increased interest in such non-conventional positron emitters [27-31] and one of them is ^{89}Zr [31-34]. Large-scale production procedure of ^{89}Zr and its stable coupling to mAbs have been developed since the introduction of the long-lived positron emitter ^{89}Zr as a residualizing radionuclide for immuno-PET [18, 35-37]. In order to have a successful diagnostic in PET imaging for solid tumours, a radionuclide's half-life must be suitable for target accumulation and nonspecific clearance. ^{89}Zr has a half-life of 78.4 h (3.3 d) with a positron emission β^+ (897 keV, 23%) decay and electron capture (77%). ^{89}Zr is produced by cyclotrons from the nuclear reaction $^{89}Y(p, n)^{89}Zr$, but the separation of ^{89}Zr requires both solvent extraction and ion-exchange chromatography [38-40]. A simplified

production method using the $^{89}Y(d, 2n)^{89}Zr$ reaction requires only a one-step ion-exchange separation. Theoretically, all the bifunctional chelating agents, such as DTPA and DOTA derivatives, for ^{111}In and ^{90}Y-labeling can be used for ^{89}Zr-labeling of biomolecules [41]. Due to ^{89}Zr's long half-life, it is an attractive isotope for ^{89}Zr-labeling of biomolecules.

Zirconium is a metallic element which has a positive ionic charge and 4+ oxidation state [36]. The isotope ^{89}Zr was first found to be well suited to the field of immuno-PET by O'Brien and Link [42]. It has been known for many years that Desferrioxamine binds well to Zirconium and that the terminal amino group can be used as a linker without affecting Zirconium binding [36]. However, the ability for ^{89}Zr to chelate with any given chelating agent is based on the ability to have a high specificity, highly pure radioisotope [35].

Shure and Deutsch were the first to produce ^{89}Zr at M.I.T. via (d, 2n) reaction on Y_2O_3 in 1951 [43]. At that time, production via a (p,n) reaction on a foil of ^{89}Y as target material took place as a preferable production as the natural abundance of 100% ^{89}Y makes it ideal [44].

1.5 PET in Cancer Diagnosis

Cancer is a class of disease in which abnormal cells in the body display uncontrolled growth (division beyond the normal limits), invasion (intrusion on and destruction of adjacent tissues), and sometimes metastasis (spreading to other locations in the body via lymph or blood). There are differences between cancers and benign tumours where benign tumours are self-limited, and do not invade or metastasize [45].

In many cases, a PET scan produces digital images that can identify many of the most common forms of cancers including lymphoma, melanoma, breast, lung and colorectal. In principle, PET is a medical imaging technology that images the biology of disorders at the molecular level before anatomical changes are visible. A PET scan is very different from an X-ray, MRI, CT or ultrasound. A PET scan can distinguish between benign and malignant disorders in contrast to other imaging technologies which merely confirm the presence of a mass. A PET scan can also detect abnormalities in cellular activity before there is any anatomical change. Once cancer is diagnosed, the PET scan is an essential "next step" by which to adequately stage the cancer, thereby identifying the primary tumour and the extent, if any, of the metastases. Furthermore, PET can help physicians monitor the treatment of disease. For instance, chemotherapy leads to changes in cellular activity and is observable by PET before structural changes can be measured by X-ray, MRI, CT or ultrasound. As a consequence, before an evaluation can be made using other imaging technologies, a PET scan might help to provide physicians with another tool to evaluate treatments, leading to a modification in treatment. PET also plays a role in identifying the recurrence of cancer. Malignant processes can be separated from scarring, edema and necrosis since PET is dependent on metabolic and not structural changes.

Breast cancer is a disease in which abnormal cells in the breast tissues multiply and form an invasive or malignant tumour which can attack and damage the tissue around them and spread to other parts of the body through the lymphatic or vascular systems. Breast cancer is known to be related to human epidermal growth factor receptor-2 (HER2) [46]. HER2 is a transmembrane tyrosine kinase receptor

belonging to the family of epidermal growth factor receptors. It is encoded by the HER2/neu proto-oncogene located on chromosome 17q21 [47]. HER2 is overexpressed in approximately 25–30% of all breast cancer cases [48, 49]. HER2 overexpression stimulates cancer cell growth and correlates with a shorter relapse-free interval and overall survival time [50]. The unfavourable prognosis associated with HER2 overexpression has been confirmed by numerous studies [46]. HER2 overexpression is determined immunehistochemically. Some cancers express high levels of growth factors as well as their receptors. The growth of cells of breast cancer is regulated by the autocrine or paracrine stimulation of HER2.

Breast cancer is also a disease prevalent throughout the world and studies on imaging and therapy in variety preclinical and clinical models are being undertaken. One of the latest drugs to become available is a monoclonal antibody called Herceptin® (Trastuzumab) [51, 52].

1.6 Monoclonal Antibodies

Monoclonal antibodies (mAbs) are monospecific antibodies for the reason that they are made by one type of immune cell which is cloned from a unique parent cell. The applications of monoclonal antibodies are limited by the number of different receptors found on any given cell. Radiolabelled mAbs have shown considerable potential for diagnosis and treatment of cancers; in particular, solid tumour cancers [37, 53, 54]. Nowadays, hundreds of monoclonal antibodies (mAbs) and mAb fragments are under clinical development because of their excellent potential for the systemic treatment of cancer and other pathological conditions [55-57].

Monoclonal antibodies (mAbs) have been approved for therapeutic use in a broad range of medical indications and form the most rapidly expanding category of pharmaceuticals, especially in oncology [58]. Intact mAbs typically achieve optimal tumour-to-non-tumour ratios at 2-4 days after injection, but mostly 1-6 hours after injection for the smaller fragments. Presently, nine mAbs have been approved by the FDA for cancer therapy, all being intact mAbs which are listed in Table 1.4. Five of the mAbs have been approved for treatment of haematological malignancies, specifically: rituximab, gemtuzumab ozogamicin, alemtuzumab, ibritumomab tiuxetan, and tositumomab. Another four mAbs have been approved for therapy of solid tumours. These are: trastuzumab, cetuximab, bevacizumab, and panitumumab respectively. Trastuzumab is used for treatment of metastatic breast cancer, while cetuximab, bevacizumab, and panitumumab have been approved for treatment of metastatic colorectal cancer. Cetuximab and bevacizumab have also been approved for the treatment of head and neck cancer and non-small cell lung cancer, respectively. These ‘‘solid tumour mAbs’’ are most effective when combined with chemotherapy or radiotherapy which interfere with signal transduction pathways by targeting growth factors or their receptors. Furthermore, most of the free therapeutic mAbs can also act via other effector mechanisms such as induction of apoptosis, complement-depending cytotoxicity or antibody-dependent cellular cytotoxicity. Gemtuzumab has been armed with the supertoxic drug ozogamicin to increase its therapeutic potency, whereas ibritumomab tiuxetan (Zevalin^{TM}) and tositumomab (Bexxar^{TM}) are radiolabelled mAbs containing the β-emitters ^{90}Y and ^{131}I, respectively. Apart from the aforementioned mAbs, one naked mAb and one radioimmunoconjugate have been approved in China [59]. The therapeutic value of

the mAbs has been outlined in several excellent reviews [55, 60, 61]. Clinical successes with the aforementioned therapeutic mAbs have boosted research and development on new mAbs directed against validated and novel targets [62]. In 2007, Reichert and Valge-Archer reported on 206 unique therapeutic mAbs in clinical trials during the time period 1980-2005 by commercial companies worldwide for a variety of cancer [56].

Table 1.4

Monoclonal Antibodies Approved for Cancer Treatment [58]

FDA Approved	Generic name (trade name)	Target	Type	Indication
1997	Rituximab (Rituxan)	CD20	Chimeric IgG1	Lymphoma
1998	Trastuzumab (Herceptin)	HER2/neu	Humanized IgG1	Breast cancer
2000	Gemtuzumab ozogamicin (Myelotarg)[a]	CD33	Humanized IgG4 conjugated to calicheamicin	Acute myeloid leukemia
2001	Alemtuzumab (Campath-1H)	CD52	Humanized IgG1	Chronic lymphatic leukemia
2002	^{90}Y-Ibritumomab tiuxetan (Zevalin^{TM})[a]	CD20	^{90}Y-radiolabelled murine IgG1	Non-Hodgkin's lymphoma
2003	^{131}I-Tositumomab (Bexxar^{TM})[a]	CD20	^{131}I-radiolabelled murine IgG2a	Non-Hodgkin's lymphoma
2004	Bevacizumab (Avastin)	VEGF	Humanized IgG1	Colorectal cancer
2006				Non-small cell lung cancer
2004	Cetuximab (Erbitux)	EGFR	Chimeric IgG1	Colorectal cancer
2006				Head and neck cancer
2006	Panitumomab (Vectibix)	EGFR	Human IgG1	Colorectal cancer

Trastuzumab (Herceptin®) is a humanised monoclonal antibody that is specific to human epidermal growth factor receptor 2 (HER2) breast cancer cells [51, 52]. Trastuzumab consists of two antigen-specific sites that bind to the juxtamembrane portion of the extracellular domain of the HER2 receptor and that prevent the activation of its intracellular tyrosine kinase [63]. The remainder of the antibody is human IgG with a conserved Fc portion. A number of promising mechanisms by which trastuzumab might decrease signalling include: prevention of HER2-receptor dimerisation, inhibition of shedding of the extracellular domain, immune activation and increased endocytosis of the receptor [64]. Pertuzumab, which is a newer antibody that binds farther from the cell membrane, appears to be more efficient because of increased inhibition of heterodimerisation; however this is not the only mechanism of the action of trastuzumab [65, 66]. Preclinical models suggested that trastuzumab recruits immune effector cells that are responsible for antibody-dependent cytotoxicity [67]. The finding that animals deficient in immune-cell–activating Fc receptors (on effector cells) do not have a response to trastuzumab provides support for this hypothesis [68]. Preoperative administration of trastuzumab has been reported to increase tumour infiltration by lymphoid cells and modulation of in vitro antibody-dependent cytotoxicity [69]. Ongoing studies are examining the effect of combining trastuzumab with HER2-targeted vaccines and activated CD8+ lymphocytes to make use of the immunomodulatory facets of trastuzumab [70]. Antibodies to the HER2 receptor might serve as targeted delivery mechanisms for conjugated toxins or radioisotopes [71].

Studies in an animal model of breast cancer in which HER2 is overexpressed indicate that angiogenesis may be inhibited by modulating proangiogenic and antiangiogenic factors from trastuzumab which induces normalisation and regression of the vasculature [72, 73]. Heregulin (a ligand of HER3 and HER4) regulates the production of vascular endothelial growth factor (VEGF), and a HER-family receptor blockade leads to reductions in VEGF [74]. A preliminary clinical trial designed to increase this effect by combining trastuzumab with bevacizumab, which simultaneously reduces VEGF, displayed promising activity against HER2-positive breast cancer [75, 76]. Clinical trials found patients with HER2 receptor over-expression benefited most by trastuzumab therapies; thus, these patients would benefit most by ^{89}Zr labelled trastuzumab studies [33, 51, 77]. The pharmacology of trastuzumab works on both the extracellular and intracellular functions of the cancer cell [51, 78]. With regard to the extracellular surface, the antibody will bind the HER2 receptor thus prohibiting the growth factor signal to connect to the cell. The lack of a growth factor specific to HER2 receptors binding to the receptor has a cascading effect within the cell, as it will not be instructed to switch on the genes that will result in proliferation [51]. Therefore, the binding of trastuzumab will cause stasis of the cancer cells preventing tumour growth. There are ongoing studies being conducted to further investigate the role trastuzumab plays in breast carcinoma, in particular, metabolism in vivo [79, 80].

1.7 Bifunctional Chelates for Metal Nuclides

Radiolabeling of metal nuclides to small molecules, proteins, monoclonal antibodies, peptides and nanoparticles are compulsory for active investigation on both diagnostic and therapeutic applications. Consequently, they require a common variable that is needed for appropriate chelation chemistry for adequate sequestration of the metallic radionuclide that is equal to the intended application. Metallic radioisotopes will not bind directly to an antibody nor maintain stability in vivo. Therefore, a chelating agent is necessary to ensure ligation between the biological tracer and the radioactive marker [41, 54]. This form of chemical is known as a bifunctional chelating agent and acts as a linker for immuno-PET binding between antibodies and radioisotopes [41, 54]. The chelating agents have been termed “bifunctional chelating agents” since they have a metal binding moiety function and also possess a chemically reactive functional group. The utility of metallic radionuclides is crucial for the development of metal chelating agents in order to effectively provide a handle on their behaviour. The chelating agent formed then provides for the sequestration of the metallic radionuclide while the latter aspect provides the requisite chemistry for covalent attachment to a targeting vector of interest, such as small molecules peptides (octreotide) [81], proteins (monoclonal antibody, Zevalin) [82], or nanoparticles [83].

There are numbers of fundamental criteria that must be met in the design of bifunctional chelating agents. The main criterion is based on the stability of the metal complex. Obviously, the consequences of loss or dissociation of the radionuclide are associated with toxicity in the case of therapeutics and poor image qualities for

diagnostics. Other fundamental coordination chemistry criteria such as: (1) charge; (2) matching cavity size of the chelating agent with the ionic radius of the radionuclide; (3) providing the appropriate chelate denticity or number of donor binding groups and (4) providing donor binding groups of appropriate chemical character are also important elements. It is also critical to consider two additional properties, specifically: the rate at which the metal complex forms and the rate of dissociation. All of these criteria are correlated. Cavity size must accommodate the ionic radius of the radionuclide, which requires donor groups to align with optimal binding to the metal ion in such a way as to adequately encapsulate the ion thereby providing high stability and limiting dissociation. The suitable radiometals are varied in properties and coordination chemistry, unfortunately there is no bifunctional chelating agent suitable for all radionuclides [84].

After a bifunctional chelating agent (BFCA) has been prepared, validation of its suitability for biological applications still remains to be executed. There are a number of properties that can be used to certify a novel BFCA, such as: (1) thermodynamic stability constants; (2) transchelation studies; (3) acid catalyzed dissociation constants; and (4) serum stability studies. These properties provide some information that can be used to suggest potential *in vivo* suitability. Serum stability can be a helpful tool as is model use to predict and eliminate from contention those BFCAs that are unsuitable for *in vivo* applications. However, none of these properties is predictive of actual *in vivo* stability of the radiolabelled compound. To measure real *in vivo* stability of the radiolabelled compound, validation and evaluation in an appropriate animal model is crucial. The meaning of appropriate animal model is

variable, however it clearly should reflect closely to the ultimate intended biological application. Nevertheless, no *in vitro* model system replicates all of the ongoing processes and components of a living organism, just as the therapeutic efficacy of a macromolecule cannot be predicted from *in vitro* results [85].

Despite all considerations, the development of bifunctional chelating agents has been rooted in making derivations from well-established and defined inorganic chemistry chelating agents such as diethylenetriamine pentaacetic acid (DTPA) and ethylenediamine tetraacetic acid (EDTA). Fundamental thermodynamic stability constants are known for these ligands with a variety of metal ions that have provided a starting point for their derivation into an array of bifunctional chelating agents [86].

One of the earliest reports of a BFCA conjugated to an antibody made use of a natural product, desferrioxamine, for radiolabeling with ^{111}In [87]. Desferrioxamine and related compounds are well-known chelators of Fe(III), and thus, their derivation for use with In(III) and Ga(III) has precedence. Desferrioxamine has been investigated for conjugating ^{89}Zr through an elegant protocol that exploits that same Fe(III)/(II) chemistry for antibody labeling in support of immunoPET applications [36, 54]. The Fe(III) complex was formed at first with the desferrioxamine, then activated for conjugation through extension of the terminal amine with succinic anhydride followed by conversion of the formed carboxylate into an active ester [36]. After conjugation, the Fe(III) was displaced with ^{89}Zr by a reduction process.

Desferrioxamine (also known as desferrioxamine B, desferoxamine B, desferal or Df) is a bacterial siderophore produced by the actinobacter Streptomyces pilosus. It has medical applications as a bifunctional chelating agent used to remove excess iron

from the body [39]. As suggested by previous research, desferrioxamine is the bifunctional chelating agent of choice as a linker for binding radionuclide with mAb [54]. The utility of this approach has been demonstrated through high-quality ^{89}Zr–mAb–PET images and quantification results reported in preclinical [37, 44, 88-90] and clinical studies [91-95]. In these studies, typically 370 kBq and 37–74 MBq ^{89}Zr–mAb was used for immuno PET in mice and humans, respectively. In both preclinical and clinical studies neither pharmacokinetic changes nor a specific accumulation in non-target organs were observed, except for an uptake in catabolic organs such as the liver and kidneys. The incidence of a high radiation dose to the patient is the only concern which is inherent to the use of long-lived positron emitters like ^{89}Zr and ^{124}I, as these might limit repeated applications of ^{89}Zr–immuno-PET [91]. Desferrioxamine is an attractive chelate because it has been used clinically in a safe way for many years [91, 92, 94].

1.8 Radiolabeling of ^{89}Zr

^{89}Zr labelling of antibodies can be achieved through various types of chelators, primarily desferrioxamine B (Df) which can form a stable chelate with ^{89}Zr through the 3 hydroxamate groups [54]. Generally, mAbs are conjugated with a bifunctional derivative of Df via an amide linkage for subsequent labeling with ^{89}Zr [96]. The hydroxamate groups within Df need to be temporarily blocked with Fe(III) before mAb conjugation. Consequently, Fe(III) is removed by transchelation to EDTA before the conjugate is exposed to ^{89}Zr. The choice of Df as the chelator for ^{89}Zr is attractive because it has been safely used in the clinic for many years. Neither

adverse reactions nor significant changes in blood and urine values were observed after injection of Df-containing conjugates from either past or ongoing clinical studies. Moreover, no antibody responses directed against the Df chelate were observed, demonstrating that its immunogenicity is quite low [92].

Despite the success of this approach, the multi-step technique procedure is quite complicated and time-consuming which makes it challenging to produce ^{89}Zr-labelled mAbs in compliance with the current Good Manufacturing Practice (cGMP) for clinical investigations. A novel bifunctional chelate was reported for ^{89}Zr labeling: *ρ*-isothiocyanatobenzyl-desferrioxamine B (Df-Bz-NCS) [97] with labeling of ^{89}Zr has been significantly simplified into a 2-step procedure (the initial strategy has 6 steps) [36]. Coupling of Df-Bz-NCS to mAbs was very efficient and it has been reported that a reproducible chelate:mAb with a ratio of 1.5:1 could be obtained using only a three-fold molar excess of Df-Bz-NCS [97]. Such a low chelate:mAb ratio can avoid alteration of the pharmacokinetics or immunoreactivity of the mAb. By comparing the 2 techniques of preparation, the rate of ^{89}Zr complexation was comparable, indicating that different chemical linkages (e.g. S instead of O in the side chain which might be involved in $^{89}Zr^{4+}$ coordination) have little influence on the radiochemistry. Almost quantitative complexation was achieved after a 30 minute incubation period at room temperature at the optimal pH (7.0), with no resulting impairment of the immunoreactivity of the mAbs.

The need for protection of radioimmunoconjugates against radiation damage during storage has been demonstrated in various studies [36, 98]. The presence of the antioxidant ascorbic acid during storage of high-dose ^{90}Y/^{131}I-labelled mAbs has

been proven to be advantageous. Nevertheless, ascorbic acid cannot be used for ^{89}Zr-labelled mAbs storage since it can cause detachment of ^{89}Zr from Df by reducing Zr^{4+} to Zr^{2+} [36]. It was suggested that ^{89}Zr-Df-mAb can best be stored at 4°C in sodium acetate buffer in the presence of the antioxidant gentisic acid. It is worth noticing that under certain storage conditions, the ^{89}Zr-Df-mAb conjugate is slightly less stable than the conjugate obtained from the 6-step strategy. Particularly, the integrity of the radioimmunoconjugates can be impaired by the presence of Cl^- in the storage buffer. This is probably due to radiation-induced formation of OCl^- which can react with the thiol group of the enolised thiourea unit that can lead to a series of events such as coupling reactions and cleavage of methionyl peptide bonds.

Apart from the two abovementioned methods, an investigation on the reaction between N-(S-acetyl)thioacetyl-Df (SATA-Df) and maleimide-conjugated mAb was also carried out [99, 100]. However, the resulting conjugates were found to be unstable in human serum at 37°C [36]. Several thiol-reactive Df ligands were tested recently for labeling mAbs in a site-specific manner [101]. In this study, engineered mAbs containing selectively-positioned cysteine residues were used where the amino group of Df was acylated by various chemicals in order to obtain thiol-reactive reagents maleimidocyclohexyl-desferrioxamine (Df-Chx-Mal), iodoacetyl-desferrioxamine (Df-Iac) and bromoacetyl-desferrioxamine (Df-Bac), respectively. Df-Chx-Mal led to the conjugate Df-Chx-Mal-thio-trastuzumab, while Df-Bac and Df-Iac alkylated the thiol groups of thio-trastuzumab by nucleophilic substitution. Each Df-modified thio-trastuzumab conjugate was labelled with ^{89}Zr in high yield

and the resulting tracers exhibited good tumour-to-blood ratio in a breast cancer model [102].

1.9 PET imaging with ^{89}Zr

In PET imaging, the need for stable chelation chemistry remains an important consideration with this element since uncomplexed and unlabelled radioisotopes localise in the bone and will consequently deliver a high radiation dose to the bone marrow [103]. Considering the success of ^{90}Y-labelled mAbs in clinical radioimmunotherapy [104, 105], ^{86}Y-labelled mAbs are currently being developed in preclinical models for clinical dosimetry purposes [106, 107]. The half-life of ^{90}Y is nearly 4 times greater than that of ^{86}Y, and therefore, predicting ^{90}Y dosimetry of slowly clearing antibody may not be feasible or even appropriate. For these reasons, ^{89}Zr was explored as being one of the possible radionuclides that could be used for dosimetry analysis of ^{90}Y-labelled mAbs [16]. Clinically used antibodies such as: HER1-targeted cetuximab [108], VEGF-targeted bevacizumab [90], and CD-20-targeted ibritumomab tiuxetan have been labelled with the ^{89}Zr-Df conjugate [94]. All the above studies demonstrated the use of ^{89}Zr-labelled antibodies in quantitative PET imaging. In addition, the tumour localization of the ^{89}Zr-mAb was similar to that of the ^{111}In/^{90}Y-mAb. Due to the feasibility in production and purification of ^{89}Zr labelled mAb, clinical studies were performed with CD44V6-specific chimeric mAb, U36 labelled with ^{89}Zr [92]. In this study, ^{89}Zr-U36 was evaluated in patients having squamous cell carcinoma of the head and neck (HNSCC), who were at high risk of developing neck lymph node metastases. All primary tumours (n =17), as well as

lymph node metastases in 18 of 25 positive levels (sensitivity 72%) and in 11 of 15 positive sides (sensitivity 73%), were detected using PET radioimmunoimaging. Interpretation of PET was correct in 112 of 121 operated levels (accuracy 93%) and in 19 of 25 operated sides (accuracy 76%). For CT/MRI, sensitivities of 60% and 73% and accuracies of 90% and 80% were found per level and side, respectively. ^{89}Zr-immunoPET demonstrated a sensitivity of 85% and accuracy of 95% as compared to sensitivity of 62% and accuracy of 88% for ^{18}F-FDG-PET. Thus, this study demonstrated the utility and advantages of ^{89}Zr PET radioimmunoimaging in a clinical setting in comparison with CT/MRI and ^{18}F-FDG [92]. Similarly, all known tumour lesions previously identified by ^{18}F-FDG were successfully imaged by ^{89}Zr-Df-Zevalin in a pilot PET imaging study in a patient having Non-Hodgkin's lymphoma [94].

1.9.1 ^{89}Zr imaging with Epidermal Growth Factor Receptor (EGFR)

The epidermal growth factor receptor (EGFR) is a 170 kDa protein which plays a critical role in tumour cell proliferation, differentiation and survival [109, 110]. EGFR is a member of the ErbB family with its overexpression being associated with a number of cancers such as lung cancer, breast carcinoma, colon carcinoma and bladder cancer [111, 112]. Furthermore, EGFR expression is often associated with more aggressive tumours, poor prognosis, and resistance to treatment with cytotoxic agents. For this reason, EGFR is one of the most extensively-studied targets in oncology and many mAbs have been developed against EGFR for cancer therapy [113].

Cetuximab (Erbitux) is a chimeric IgG1 mAb that can block EGFR activation by binding to the ligand-binding domain. Cetuximab induces internalization of EGFR, thus preventing downstream signalling [114]. ^{89}Zr-labelled cetuximab has been investigated in several preclinical studies [37, 108]. In the early report, ^{89}Zr-cetuximab PET was used as a scouting procedure before radioimmunotherapy (RIT) to confirm tumour targeting and allow estimation of radiation dose delivery to tumours and normal tissues [108]. It was concluded that ^{89}Zr-cetuximab could serve as a surrogate for scouting the biodistribution of ^{90}Y-cetuximab and ^{177}Lu-cetuximab in tumour-bearing mice.

In another study, a difference between ^{89}Zr-cetuximab uptake in the tumours and in vivo EGFR expression level in mouse models was observed. This suggested that additional pharmacokinetic or pharmacodynamic mechanisms may influence the tumour uptake of cetuximab, as well as the therapeutic efficacy of this agent [37]. It was recommended that these additional mechanisms may explain why receptor expression levels alone are insufficient to predict patient response to anti-EGFR therapies. Numerous studies have discovered that a majority of tumours responding to EGFR kinase inhibitors harbor activating mutations in the EGFR kinase domain [115]. Therefore, imaging of EGFR mutant expression might be more useful in selecting the right patient population for modified treatment, as well as accurately predicting the therapeutic response [116].

1.9.2 ^{89}Zr imaging with Vascular Endothelial Growth Factor (VEGF)

Vascular endothelial growth factor (VEGF) is a potent mitogen in embryonic and somatic angiogenesis. VEGF plays an important role in both normal vascular tissue development and many disease processes such as tumour development and metastasis [117]. Overexpression of VEGF and/or VEGF receptors (VEGFRs) has been implicated as being a marker of poor prognosis in various clinical studies [118]. The humanized anti-VEGF mAb, bevacizumab (i.e. Avastin), can block VEGF-induced tumour angiogenesis and has been approved by the FDA to treat multiple metastatic cancers [119].

In 2007, ^{89}Zr-labelled bevacizumab was investigated in nude mice bearing human ovary cancer SKOV-3 xenograft tumours [90]. Comparing ^{89}Zr-bevacizumab and ^{89}Zr-IgG, which served as a control, PET showed an uptake of ^{89}Zr-bevacizumab in well-perfused organs at 24 h post-injection and clear tumour localization after 72 h. The uptake of ^{89}Zr-bevacizumab was significantly higher than that of ^{89}Zr-IgG, suggesting target specificity of the tracer. Recently, ^{89}Zr-bevacizumab was also successfully used to detect the early anti-angiogenic tumour response to treatment with a Hsp90 inhibitor, indicating that ^{89}Zr-bevacizumab PET can be a sensitive and non-invasive technique for monitoring the antitumour effect [120].

1.9.3 ^{89}Zr imaging with CD44v6

CD44 is a cell-surface glycoprotein involved in a wide variety of biological processes such as: adhesion of cells to extracellular matrix proteins, homotypic

adhesion, lymphocyte-endothelial cell interactions, lymphohematopoiesis, T cell activation/adherence, metastasis formation, cytokine release and lateral movement of cells [121, 122]. The CD44 protein family is composed of several isoforms which are encoded by standard exons and many alternatively spliced variant exons that are expressed in a tissue-specific manner. The splice variant v6 of CD44 (denoted as "CD44v6") has been implicated in tumourigenesis, tumour cell invasion, and metastasis [123, 124]. Although CD44v6 is expressed only in a subset of normal epithelial tissues, such as prostate glands and thyroid, homogeneous expression of CD44v6 has been found in various solid tumour types such as squamous cell carcinoma of the head and neck (HNSCC), esophageal, skin, cervical, and lung cancer respectively [125]. Additionally, heterogeneous expression of CD44v6 has been found in adenocarcinomas of the stomach, breast, colon, lung and pancreas.

In order to avoid human anti-mouse immune responses, the chimeric IgG1 derivative of a murine mAb (U36 which binds to CD44v6) was constructed. ^{186}Re-labelled chimeric mAb (cmAb), termed as "cU36", was then tested in phase I trials which showed promising anti-tumour effects in patients with HNSCC [126, 127]. Subsequently, ^{89}Zr-labelled cU36 was investigated in xenograft-bearing mice [36]. Further, ^{89}Zr-cU36 was also tested for the first time in HNSCC patients who were at high risk of having neck lymph node metastases [92]. Serial PET scans after injection of 2.0 mCi of ^{89}Zr-cU36 successfully detected the primary head and neck tumours, as well as metastases in the neck, which is as good as CT or MRI in terms of sensitivity. Conversely, a few patients developed an antibody response directed against cU36, even though no evidence was found for antibody reactions against the

chelate. Moreover, ^{89}Zr-cU36 was not able to detect micrometastases in patients which were comparable to the findings of a previous biodistribution study with the mAb U36 [128]. In another study of cU36, it was reported that ^{89}Zr-labelled mAbs are more suitable for scouting of therapeutic doses of ^{90}Y-labelled mAbs, while ^{124}I-labelled mAbs are better for scouting of ^{131}I- and ^{186}Re-labelled mAbs [88].

Radiation dosimetry estimation in patients injected with ^{89}Zr-cU36 revealed that ^{89}Zr-cU36 was safe and well-tolerated in all patients [91]. The continuous improvement of new clinical PET/CT scanners may allow the acquisition of better-quality PET images with a lower injected radioactivity dose, even though the malicious radiation dose was estimated to be around 40 mSv for patients in this study. This would consequently limit repeated applications of ^{89}Zr immuno-PET. In a recent study, different ^{89}Zr-labeling chemistry was compared between the 2-step and 6-step methods, for PET imaging of cU36 in a mouse model [97]. This indicated that, for both tracers, a high level accumulation of ^{89}Zr-labelled cU36 in the tumours and a low level of tracer uptake in normal tissues were observed.

1.9.4 ^{89}Zr imaging with HER2

HER2 overexpression is determined using immunohistochemistry and fluorescence *in situ* hybridization (FISH) at the time of diagnosis of the primary tumour. Non-invasive imaging of HER2 expression and localisation of HER2-overexpressing tumour lesions using immuno-PET could be a practical method in the clinic to guide HER2-targeted therapy.

Trastuzumab (i.e. Herceptin®), an anti-HER2 mAb, has been extensively investigated for imaging applications over the last decade [109, 129]. Trastuzumab was approved by the FDA to treat HER2-positive breast cancer. In one study, clinical grade ^{89}Zr-trastuzumab was developed for potential clinical immunoPET imaging applications [93]. In nude mice bearing HER2-positive tumours, ^{89}Zr-trastuzumab exhibited excellent tumour uptake (~30%ID/g) with high tumour-to-nontumour ratios. The biodistribution pattern of ^{89}Zr-trastuzumab was similar to that of ^{111}In-trastuzumab, which was reported in a previous clinical study [130]. In addition, ^{89}Zr-trastuzumab was very stable in both buffer solutions and human serum.

The first-in-human study of ^{89}Zr-labelled trastuzumab for PET imaging of HER2-positive lesions has been reported [131]. The tracer showed excellent tumour uptake which allowed detection of most of the known lesions and some lesions that had not been detected earlier. This occurred where the dose of trastuzumab for optimal PET imaging performance was chosen to be 37 MBq of ^{89}Zr-trastuzumab in a total of 50 mg protein for trastuzumab-naive patients or 10 mg protein for patients that are already on trastuzumab treatment.

Another study indicated that trastuzumab pharmacokinetics and organ distribution can also be heavily affected by an extensive tumour load [132]. Consequently, a study concentrating on a more patient-tailored trastuzumab dosing schedule on the basis of tumour volume in addition to bodyweight should be considered in the future. It could be deliberated that such dose-dependent pharmacokinetics may not be appropriate to ^{89}Zr-labelled antibodies which bind to other cancer-related targets.

1.9.5 ^{89}Zr imaging with PSMA

Prostate-specific membrane antigen (PSMA) is a 100 kDa type II transmembrane glycoprotein and PSMA is one of the best characterised targets in oncology [133]. PSMA expression levels have been shown to exhibit a positive correlation with development of castration resistance, resistance to hormone-based therapies and increased tumour progression. Even though PSMA expression has also been detected in a selectively limited range of normal tissues, including: renal proximal tubule, benign prostatic epithelium, the brain and small bowel, these normal tissue sites only express PSMA at levels 2-3 orders of magnitude, which is lower than that observed in more than 95% of clinical prostate cancer specimens [134]. Additionally, expression of PSMA in normal tissues is highly polarized to the apical or luminal sides of various tissues which are not readily accessible to circulating mAbs, therefore making anti- PSMA mAbs functionally tumour-specific.

Recently, a study on quantification of PSMA expression *in vivo* of ^{89}Zr-labelled anti-PSMA mAb, J591, was reported for immuno-PET [135]. PET imaging of male athymic nude mice bearing subcutaneous LNCaP (PSMA-positive) or PC-3 (PSMA-negative) tumours was conducted and ^{89}Zr-J591 provided an excellent image contrast for delineating the LNCaP xenografts a few days after tracer administration. Interestingly, a "multimodality" approach to image PSMA expression has also been carried out using ^{89}Zr-J591, which may potentially be used in the clinic to non-invasively identify and quantify PSMA-positive prostate tumours in patients [136]. Cerenkov luminescence imaging (CLI) of tumours *in vivo*, using a small animal optical scanner, was carried out. This procedure took advantage of the phenomenon

known as the Cerenkov Effect, where the emission of light from a transparent substance travels through the material with a speed faster than the speed of light in that material. The results obtained from immuno-PET studies correlated well with those obtained from optical scans in a quantitative manner. CLI can be used to image radionuclides that do not emit either positrons or γ-rays and are thereby unsuitable for use with current nuclear imaging modalities. Therefore, it may serve as a potential new imaging modality for rapid and high-throughput screening of radiopharmaceuticals.

1.9.6 ^{89}Zr imaging with other targets

A number of other proteins have also been investigated using ^{89}Zr-based PET. Hypoxic tumour cells are resistant to radiotherapy and various chemotherapeutic agents. Carbonic anhydrase IX (CAIX), an endogenous hypoxia-related protein, is upregulated in many tumour types [137]. Therefore, pre-therapeutic assessment of intratumoural hypoxia may allow for selection of patients having intensified treatment regimens. Recently, ^{89}Zr radiolabelled with an anti-CAIX antibody fragment (cG250-F(ab')$_2$), was reported to allow visualization of tumour hypoxia with PET in a xenograft tumour model, which correlated spatially to the microscopic distribution of CAIX-expressing cells [138]. This study suggested a potential role of ^{89}Zr-cG250-F(ab')$_2$ for non-invasive imaging of hypoxia in head and neck carcinomas, upon which subject further investigation in the future can be deliberated.

In one report, expression of the insulin-like growth factor 1 receptor (IGF1R) was measured by PET with ^{89}Zr-labelled R1507, a mAb against IGF1R [139]. Excellent

contrast and prominent tracer uptake in the tumour was observed in a mouse bearing triple-negative breast cancer tumours. This may enable future patient selection for IGF1R-targeted therapy in the clinic since currently there is no effective therapeutic regime for this sub-population of breast cancer patients.

Single-walled carbon nanotubes (SWCNTs) have unique properties which make them suitable for applications in a wide variety of imaging modalities such as: radionuclide-based imaging, Raman spectroscopy, photoacoustic tomography, MRI and near-infrared fluorescence [140, 141]. Recently, SWCNTs were conjugated to an antibody, E_4G_{10}, which specifically binds to the monomeric vascular endothelial cadherin (VE-cad) epitope expressed in angiogenic tumour vessels, and labelled with ^{89}Zr [142]. Dynamic and longitudinal PET imaging of this agent in LS174T human colorectal tumour-bearing mice demonstrated rapid blood clearance and target-specific tumour accumulation. A single construct could be designed to incorporate both imaging and therapeutic agents onto the same platform due to the large surface areas of SWCNTs. Moreover, it was suggested that a single agent may potentially be employed to image or treat a variety of different tumour types since VE-cad is expressed by the tumour vasculature.

To date, a wide variety of mAbs have been labelled with ^{89}Zr and several of these ^{89}Zr labelled mAbs have entered clinical investigation with promising results. It is expected that, in the future, many new PET tracers based on ^{89}Zr will be developed with the comprehensive availability of ^{89}Zr and simpler chemistry for radiolabeling.

1.10 Hydroxamate Resin Column

In a growth development of a sustainable ^{89}Zr labelled monoclonal antibody, a construction of hydroxamate resin column will enable the ^{89}Zr to be purified from its impurities. This will accordingly result in extraction of the radioisotope into elution to be labelled to a monoclonal antibody conjugated with a bifunctional chelating agent. The first synthesis of a hydroxamate resin was reported by Herscheid *et al.* in 1983 for use in a ^{52}Fe/^{52m}Mn generator [143]. Subsequently, in 1994, Meijs *et al.* studied the separation of ^{89}Zr from ^{89}Y starting material through a hydroxamate resin column using oxalic acid as an extraction agent [35].

Nevertheless, the availability of ^{89}Zr for column testing is limited in Australia due to its cost and no cyclotron producing is available at this time. As a result, ^{68}Ga is the isotope of choice following the design of the column.

1.11 Gallium-68

With a half-life of 1.13 hr, ^{68}Ga decays from ^{68}Ge via electron capture. ^{68}Ga electrochemistry consists of 3 available valence electrons. ^{89}Zr, the final isotope to be tested in a future study, has a half-life of 78 h and a valency of 4+. The ^{68}Ge/^{68}Ga generator is easily accessible within a PET centre and makes an easy alternative as ^{89}Zr is not currently available. The ultimate aim is to develop a novel procedure for production of ^{89}Zr labelled monoclonal antibodies and to improve the specificity of detecting cancer cells via PET imaging. However, in order for this to be achieved, a

viable hydroxamate exchange column that will bind ^{68}Ga was constructed to prove it can bind ^{89}Zr.

The ^{68}Ge/^{68}Ga generator is a closed system and due to the nature of decay of the parent and daughter isotope, purification is inherent within the system [144]. The column bound with ^{68}Ge is constructed from Tin-Dioxide polyethylene and uses non-metallic parts such as polyethylene tubing to ensure no carriers are added. The column simply has 0.6M hydrochloric acid passed through it and 80% ^{68}Ga abundant elution is produced. The breakthrough of ^{68}Ge, which is considered a radiochemical impurity, has been referenced as 0.002% by the manufacturer [144]. Thus, straight after the elution of ^{68}Ga it is possible to bind it to the monoclonal antibody deferoxamine complex. In conclusion, the purification of ^{68}Ga before chelation with an antibody is negligible when compared to the purification processes of ^{89}Zr.

1.12 Statement of research

The first activity in this research was the preparation of Yttrium-89 (^{89}Y) solid targets followed by production of Zirconium-89 (^{89}Zr) in a medical cyclotron using ^{89}Y as a starting material. The ^{89}Zr was then dissolved in hydrochloric acid (HCl) and loaded to a hydroxamate resin column in order to purify the ^{89}Zr from its impurities and then labelled to a monoclonal antibody in clinical condition to be used for small animal PET imaging study.

Table 1.5

Decay Characteristics of ^{89}Zr [53]

Isotope	Half Life	Energy	Abundance
Zirconium-89	78.4hr	0.909 MeV	99.9%
	(3.27 day)	1.202 MeV	0.014%
		1.622 MeV	0.070%

Decay characteristics of ^{89}Zr, including half-life, percentage abundance and energies of the decay types are shown in Table 1.5 [53]. ^{89}Zr has good gamma energies allowing imaging using PET scanners. Without this property, visualisation of the antibodies would not be possible. Another factor to consider is the daughter nuclides formed by the positron decay of ^{89}Zr; ^{89}Y. This isotope is stable and will not cause any damage in vivo [34]. The ^{89}Zr has been chosen in this study because of its ideal physical characteristics and suitable properties for immuno-PET, such as its long half-life of 3.27 day. This is well-matched with the time needed for conjugated mAbs to reach the tumour site, as intact antibodies need around 2 to 4 days to penetrate a solid tumour [36, 53, 145]. In contrast, to achieve good visualisation, a large dose would need to be administered. This is costly and, more importantly, dangerous to the patient with regard to radiation exposure [88]. The most commonly used PET radionuclides are ^{18}F and ^{11}C which have short half-lives of 110 min and 20 min respectively. These radionuclides are not suitable to be used to detect solid tumours as they would undergo appreciable radioactive decay before reaching the centre of the tumour [14]. Although ^{18}F-FDG is used to find tumours since the FDG molecule

targets quickly, the clearance time of radioimmunoconjugates is relatively long. Thus, good target-to-blood ratios are not achieved within 24 h after administration given the relatively short half-life of ^{18}F [53, 54, 146]. ^{124}I, on the other hand, has a half-life of 4.2 days, but there are considerable isotopic enrichment costs involved. In addition, there is the added danger of exposure of thyroid tissue (in particular) to free radioactive iodine. ^{89}Zr fits perfectly within the range of antibody localisation with its 78.4 h half-life [36]. Thus far, one of the greatest challenges preventing ^{89}Zr from becoming a widely used radioisotope for Immuno-PET is its purification from other impurities. Firstly, the bombardment of the yttrium metal target results in a large number of radiochemical impurities, along with the radionuclide impurity of trace ^{88}Zr around 0.01% [36]. The target itself contains a copper metal backbone as well as trace amounts of titanium, iron and gadolinium [36]. After bombardment, trace products of Zinc-65, Vanadium-48, Cobalt-56 and Terbium-156 are formed respectively to the trace metals located on the target [36]. These unwanted impurities must be separated from ^{89}Zr as they might compete in the labelling step with the antibodies [35]. The latest method of removing these impurities uses a hydroxamate column [36]. In 1990, O. T. Dejesus concluded that the hydroxamate column can produce 99.9% carrier free ^{89}Zr. However, the extraction technique was found to be quite difficult for purification process as the Zirconium was ionically bonded to the column, which a stronger anion exchanger is needed to remove it [53]. In 2003, Verel *et al.* successfully transchelated 97% of the total activity from the hydroxamate column using 1 mol/L oxalic acid over 5 separate elutions with an initial 40% yield in the first two elutions and a purity of > 99.9% [36]. However, two main issues arise from the use of oxalic acid as an extraction chemical for purifying ^{89}Zr. Firstly;

oxalic acid is highly toxic to the human body, causing decalcification of blood which is crucial to neural and muscle function, as well as renal tubule obstruction via calcium oxalate precipitation [34]. Hence, the *in vivo* use of ^{89}Zr bound oxalic acid cannot be considered. It was demonstrated that removing the oxalic acid required the use of another strong anion exchange column and flushing a large volume of water through the column, followed by chloride exchange using HCl [36]. The resultant acid solution can now be boiled off at 110°C under a continuous stream of argon and then reconstituted in 0.9% NaCl solution [36]. Following this purification process, a carrier-free, purified ^{89}Zr was then able to be bound to a monoclonal antibody desferrioxamine (Df) complex [54].

In this research, production of ^{89}Zr in a medical cyclotron was undertaken using ^{89}Y as a starting material and purified using a hydroxamate resin column to be labelled to a monoclonal antibody in a preclinical condition, which finally can be used for small animal PET imaging study.

1.13 Aims of the research

The specific aims of all studies in this research are:

- To develop an efficient method for making a solid target of ^{89}Y to produce ^{89}Zr more effectively.
- To study a production of ^{89}Zr in a medical cyclotron using ^{89}Y as a starting material.
- To develop a separation column for the purification of ^{89}Zr.

- To develop a method of ^{89}Zr isolation and purification.

- Quality control and validation using PET imaging of the labelled compound.

- To examine the potential of hydroxamate resin to be used as a column in a ^{68}Ga generator for purification and radiolabelling of ^{68}Ga.

The ultimate goal of this research was to create a shortcut in the long and complex steps of the purifying and labelling procedures by avoiding the use of oxalic acid as an extraction chemical for purifying ^{89}Zr. This would achieve a result near the Good Manufacturing Practice (GMP) standard.

The development in separation and purification of longer-lived ^{89}Zr PET radioisotopes and its labelling to a monoclonal antibody can be adapted to many other applications within the disciplines of nuclear medicine. This refers particularly to heavy PET radioisotopes that have previously been avoided due to inherent impurities upon cyclotron production. There are some research questions which need to be answered in this research such as:-

- Can ^{89}Y prepared in-house be used as a solid target in production of ^{89}Zr?
- How good is hydroxamate resin column to isolate and purify ^{89}Zr?
- Can oxalic acid be replaced by other chemicals to elute ^{89}Zr from a hydroxamate resin column?
- How effective is Trastuzumab-Df-^{89}Zr labelling compound to be used in vivo?

PET is a dedicated imaging modality which produces a three-dimensional image of functional processes in the body. Currently, PET is widely being used in nuclear

medicine area. Radioisotopes used in PET send out a positron that eventually finds an electron, forming a complex atom called positronium that rapidly decays and emits two annihilation photons. A PET camera detects the 511 keV photons that are emitted at 180° from each other and enable the production of a three–dimensional image [11]. Immuno-PET, a combination of monoclonal antibodies (mAbs) and PET, is an attractive tumour imaging option as it has the potential to improve diagnostic tumour characterisation by combining the high sensitivity and resolution of PET/CT imaging with the specificity of a mAb localisation [147]. In fact, each of the mAbs that targets a specific tumour cell is a candidate for use in immuno-PET, allowing for the development of a new generation of mAb-based imaging probes.

Zirconium is a transition metal in Group IVB of the periodic table. ^{89}Zr is a radioisotope of zirconium which decays through electron capture (77%) and positron emission (23%). For that reason, ^{89}Zr is suitable for PET imaging with the important 511 keV gamma radiations from positron annihilation and 909 keV gamma from the ^{89m}Y de-excitation [148] respectively. Currently, ^{89}Zr is widely used for radiolabelling studies for immuno-PET. Basically, the production of ^{89}Zr is through cyclotron irradiation, which uses ^{89}Y solid target as a starting material where the proton bombardment procedure to the ^{89}Y solid target (which occurs in the cyclotron) creates ^{89}Zr radionuclide. The ^{89}Zr radionuclide is then purified and labelled with monoclonal antibody (mAb) through chelation and conjugation, thus enabling the radionuclide to target and bind with the mAb and finally be ready to be used for PET imaging study. At the moment, the purification of ^{89}Zr from its impurities is one of the greatest challenges for the ^{89}Zr from becoming a widely used

radioisotope for immuno-PET. Unwanted impurities must be separated from ^{89}Zr as they might compete in the labelling step with the mAbs [35].

1.14 Thesis outline

The remaining chapters of this thesis are structured as below;

- Chapter 2 reports the production of ^{89}Zr via cyclotron bombardment using five different types of ^{89}Y solid target preparation. This chapter describes types of yttrium solid targets and methods that have been performed during the preparation of the solid targets. These include: the utilisation of yttrium foil, compacted yttrium nitrate, electrodeposited yttrium nitrate using two different methods of preparation and yttrium sputtering technique. A few technical recommendations that can improve the yield of the targets are also highlighted in the last section of this chapter. Quality control (QC) analysis of the radioisotope produced is also reported in this chapter.

- Chapter 3 describes the ^{89}Zr purification from the starting materials and other impurities. Purification of ^{89}Zr involves the separation and elution of ^{89}Zr radioisotopes from the soluble ^{89}Y ions starting materials and other impurities using a hydroxamate resin column. In addition, this chapter demonstrates the experiments on the potential of phosphoric acid to be used as ^{89}Zr extraction agent from hydroxamate resin column, thus labelling it with Df-Bz-NCS-Trastuzumab. The preparation and construction of the hydroxamate resin column for the separation and elution process is also reported in this chapter.

- Chapter 4 details the experiments on radiolabelling of monoclonal antibodies and ^{89}Zr using the novel *p*-isothiocyanatobenzyl-desferrioxamine B (Df-Bz-NCS) as a bifunctional chelating agent. Firstly, the chapter describes the conjugation of a monoclonal antibody with the Df-Bz-NCS according to a slightly modified procedure from the previous work. Herceptin (Trastuzumab) was the monoclonal antibody of interest for this series of experiments as it showed a stable conjugation with the chelating agent. Secondly, the chapter discusses the radiolabelling of the conjugated Df-Bz-NCS-Trastuzumab, together with ^{89}Zr and QC analysis of the radiolabelled product.

- Chapter 5 explains the PET imaging studies of ^{89}Zr-labelled with a monoclonal antibody.

- Chapter 6 examines the potential of hydroxamate resin to be used in a ^{68}Ga generator. It demonstrates a series of experiments on the elution of ^{68}Ga from hydroxamate resin column continued with experiments on ^{68}Ga-labelled with Trastuzumab and Pentetreotide using hydroxamate resin column as an ion exchanger.

- Chapter 7 summarises the findings of this research work, and, based on this, the conclusions that have been drawn. Future studies that can be developed from this research are also suggested.

- Appendix A shows the amount of ^{89}Zr in MBq extracted from hydroxamate resin column using 1.0 M oxalic acid and 1.0 M phosphoric acid as extraction agents.

- Appendix B indicates the amount of ^{68}Ga in MBq from 50, 100 and 200 mg hydroxamate resin column using 0.01, 0.05 and 0.1 M Citrate Buffer at pH 4.

- Appendix C demonstrates the amount of ^{68}Ga in MBq eluted from 50 mg hydroxamate resin column using 0.01, 0.05 and 0.1 M HCl.

- Appendix D exhibits the amount of ^{68}Ga in MBq eluted from hydroxamate resin column using various solutions.

- Appendix E shows PET images using ^{89}Zr-Df with phosphoric acid as an extraction agent, applied to a female Balb/c nude mouse model with subcutaneous LS174T tumour (HER2-expressing colorectal model) on the right flank.

- Appendix F indicates PET images using free ^{89}Zr, applied to a female Balb/c nude mouse model with subcutaneous LS174T tumour (HER2-expressing colorectal model) on the right flank.

- Appendix G demonstrates PET images using ^{89}Zr tracer bound to mAb as ^{89}Zr-Df-Trastuzumab, applied to a female Balb/c nude mouse model with subcutaneous LS174T tumour (HER2-expressing colorectal model) on the right flank.

- Appendix H details the publications and conference presentations from this research work.

- Appendix I shows my publication paper entitled “Review on Production of ^{89}Zr in a Medical Cyclotron for PET Radiopharmaceuticals.”

- Appendix J shows my publication paper entitled “Establishing Reliable Production of the PET Isotope ^{89}Zr for Research Use: From Target Fabrication to Preclinical Imaging.”

Chapter 2: Production of Zirconium-89

2.1 Preparation of Yttrium Target

Yttrium is introduced in a cyclotron for irradiation in order to produce ^{89}Zr radioisotope. Yttrium targets can be prepared by various methods [149];

- Electron Beam Physical Vapour Deposition (EBPVD) is a form of physical vapour deposition in which a target anode is bombarded with an electron beam given off by a charged tungsten filament under high vacuum. In this process, atoms from the target are transformed into the gaseous phase caused by the electron beam. The atoms are then precipitated into solid form and coat everything in the vacuum chamber with a thin layer of the anode material (within the line of sight).

- Sputtering technique is a process whereby atoms are ejected from a solid target material due to bombardment of the target by energetic particles.

- Chemical vapour deposition (CVD) is a generic name for a group of processes that involve depositing a solid material from a gaseous phase.

- Physical vapour deposition (PVD) is similar in some respects to CVD but differs in that the precursors are solid, with the material to be deposited being vaporised from a solid target and deposited onto the substrate.

- Pulsed laser deposition (PLD) is a thin film deposition technique where a high power pulsed laser beam is focused inside a vacuum chamber to strike a

target of the material that is to be deposited. The material is then vaporised from the target, in a plasma plume, which deposits it as a thin film on a substrate.

Dejesus and Nickles used water cooled yttrium foils to produce ^{89}Zr via the (p, n) reaction on ^{89}Y using 11 MeV protons [53]. The target was bombarded with protons (1 cm diameter beam) typically for 2 h with a beam current of 10 µA. The target was then dissolved in concentrated HCl (5 mL), as reported by Link *et al*., since they found this acid to produce less insoluble material [150]. In 1991, Zweit and collegues reported the production of ^{89}Zr for PET from deuteron irradiation of natural yttrium targets. The target material, natural yttrium powder (100% ^{89}Y), was pressed into 10 mm diameter pellets ranging in thickness from 240 to 340 mg/cm^2 which were placed in the target holders. The pellets were then covered with high purity aluminium foil of 0.005-0.36 mm thickness depending on the incident deuteron energy required. The beam currents used were 3 and 5 µA with irradiation times of 12 and 20 min respectively. The energy window used for the ^{89}Y (d, 2n) ^{89}Zn reaction was from 16 to 7 MeV. This was considered to be optimum in order to minimize the production of the long-lived ^{88}Zr produced by the ^{89}Y (d, 3n) reaction with a threshold energy of 15.5 MeV. After bombardment, the irradiated target pellet was dissolved and heated in 3 mL 12 M HCl. When the target was completely dissolved, 1 mL of 20 % H_2O_2 was added to ensure the oxidation of Zr to Zr (IV). The heating was continued until the solution was completely dry, after which it was redissolved in 12 M HCl and left to cool [151]. Another ^{89}Y target can be prepared using the sputtering technique. Meijs *et al.* (1994) reported that the target can be

prepared by sputtering a Y-layer (25 µm) on a Cu support. In this process, the Y-atoms are ejected as a result of momentum transfer between accelerated Ar-ions and the Y-source. The Y-atoms cross a vacuum chamber and finally deposit on the Cu support. After irradiation, the Y on the Cu support is dissolved in four successive portions of 0.5 mL of 1 M HCl. At this HCl concentration the Cu is insoluble. To ensure the oxidation of Zr to the IV-oxidation state, 1 mL of H_2O_2 was added. Hereafter, concentrated HCl was added to obtain a final 3 M HCl solution, in order to prevent hydrolysis of the Zr-chlorocomplex [35]. Films of yttrium are usually produced by vapour deposition, dry processes and sputtering, but electroplating would be very advantageous in view of the cost and productivity. Matsuda *et al.* (1993) studied the formation of yttrium oxide by electrodeposition in organic electrolyte using dimethylformamide (DMF) containing YCl_3 and a small amount of water. Firstly, yttrium metal was deposited on the substrate after which it would react with water to form yttrium oxide [152]. Reischl *et al.* (2002) on the other hand, performed the electrolytic deposition in 60 min with a constant current of 450 mA at 50^oC. The irradiated ^{86}Y target material was dissolved in 3 mL of 4 % HNO3 (0.6 N) in a cylindrical beaker and then diluted with 47 ml of water with the pH of the solution being between 2.5 and 3.0. During electrolysis, a strong gas was observed when electrolysing an acidic aqueous solution, where hydrogen and oxygen are formed and the yttrium-86 was electrodeposited on the cathode [153]. In 1995, Kumbhar and Lokhande reported the electrodeposition of yttrium from a non-aqueous bath. In this investigation, the electrodeposition of yttrium from nonaqueous (ethanol) baths was reported. The distance between anode and cathode was 0.2 cm. Deposition was carried out under unstirred conditions and in the potentiostatic mode.

The study indicated that, at room temperature, the thickness of the deposit increases linearly with times of up to 1 hour. The effect of temperature showed that good quality, uniform, white-gray deposits could be obtained up to 45^{o}C [154]. In 2010, Sadeghi *et al.* reported two special sedimentation methods to deposit a thick layer of yttrium oxide on copper substrate for the production of ^{89}Zr. A thick layer of Y_2O_3 was deposited on the copper substrate (11.69 cm^2 surface areas) by ethyl cellulose (EC) and methyl cellulose (MC) methods. The target was irradiated up to 20 μA current with 13 MeV protons and no degradation was observed. Improvement of the cooling system that contains a circulating flow of chilled helium in front of the target, in addition to the water cooling used in this work, would improve thermal conductivity. Hence, it is expected to allow the usage of higher beam currents up to 30 μA [155].

2.1.1 Methodology

Most experimental components of the methods were conducted at Peter MacCallum Cancer Centre, East Melbourne, Victoria, Australia and the School of Electrical and Computer Engineering, RMIT University. Five different targets were prepared, namely: yttrium nitrate direct application (99.9 %; Sigma, St. Louis, MO USA), aqueous and non-aqueous electrodeposited yttrium nitrate, yttrium foil application (99.9 %, Thickness: 0.25 mm, American elements, Los Angeles, CA USA) and yttrium sputtering on a copper target plate using a sputtering machine (SPI-Module Sputter Coater, Imbros Pty. Ltd.).

Yttrium nitrate direct application - A gold target plate was cleansed with absolute ethanol before applying 0.4-0.5 g of yttrium nitrate covering the beaming area of the target plate. Aluminium foil was used to cover the target plate so as to avoid the yttrium nitrate which would be melted from leaking out of the target plate during bombardment.

Yttrium electrodeposition in aqueous bath - Two copper plates (which served as anode and cathode and were able to fit the target slot in the cyclotron) were put together with a 0.2 cm distance to each other (Figure 2.1). For the acidic aqueous bath, 4.7 % HNO_3 (Merck, Whitehouse Station, NJ USA) was used to dissolve the yttrium nitrate. The electrodes were then put inside the bath to begin electrolysis and the power supply (Lab Power Supply 0-30 V 2.5 Amp Digital Display; Dick Smith Electronics, Melbourne, VIC Australia) is set on 0.2-0.5 A, creating a current for 60 minutes (Figure 2.2). Further, to prepare a 10.4 mmol $Y(NO_3)_3$, distilled water was added. Electrolysis was started with a 0.20 Amp current for 60 minutes and then the electrodes were removed. The cathode plate that would have yttrium deposited on it was then cleansed in acetone for a minute and left to dry [153].

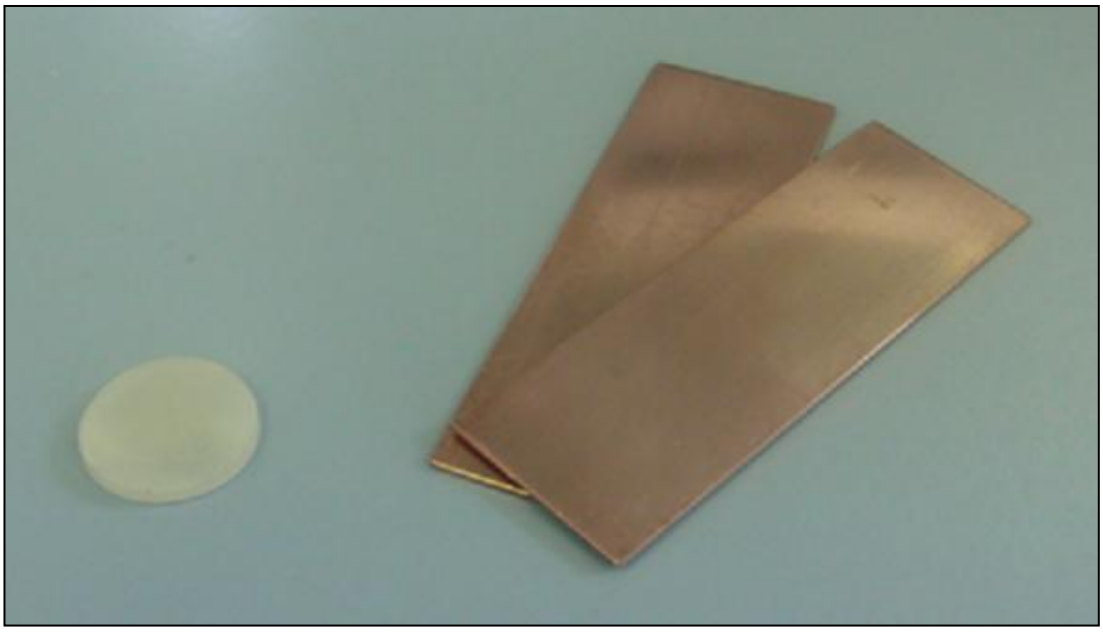

Figure 2.1 Copper plates served as anode and cathode for yttrium-89 electrodeposition.

Figure 2.2 Experiment set up for ^{89}Y aqueous and non-aqueous electrodeposition.

Yttrium electrodeposition in non-aqueous bath - Using basically the same techniques as the electrodeposition with aqueous bath, two copper plates (which served as anode and cathode and were able to fit the target slot in the cyclotron) were put together with a 0.2 cm distance to each other. For the non-aqueous bath, a 10.4 mM $Y(NO_3)_3$ (yttrium nitrate) diluted in absolute ethanol was used. After 60 minutes electrodes were removed and the cathode plate that would have yttrium deposited on it was cleansed in acetone for a minute and left to dry [154].

Yttrium foil - Firstly, an aluminium target plate was cleansed with absolute ethanol and then 0.15 – 0.20 g of yttrium foil was cut and placed on the beaming area of the aluminium plate. The copper plate was then covered by a piece of aluminium foil to make sure the yttrium foil would not be lost during bombardment.

Yttrium sputtering technique - A copper plate was cleansed with absolute ethanol and then loaded onto a target mount in a sputtering machine (Figure 2.3). A circle diameter of 57 mm x 57 mm yttrium metal foil and 0.25 mm thickness was then placed into the sputtering machine, with the distance between the top of the yttrium metal foil and the copper target being about 2.5 cm. Next, the black top cover assembly was replaced and the air admit valve on it was closed. After that, the valve of the argon gas line next to the pressure regulator was opened and the argon pressure was set to 100 kPa at the regulator. Following that, both the power on the sputter coater unit and on the control module were switched on which immediately started the rotary pump. The indication of vacuum was shown on the meter. Next, the yttrium was sputtered onto the copper target plate. The sputtering process took about 10 minutes to complete (Figure 2.4).

Figure 2.3 Yttrium Sputtering Machine

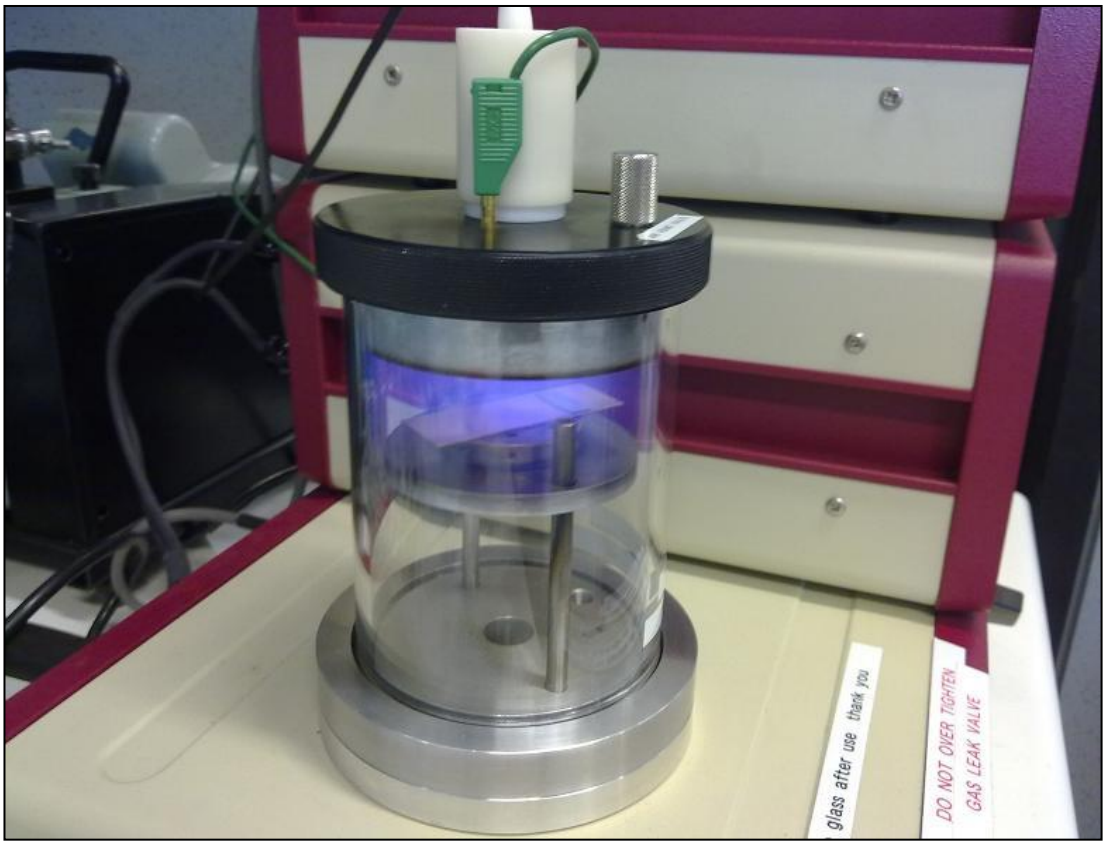

Figure 2.4 Sputtering process in progress

2.1.2 Result

All yttrium solid targets were successfully prepared (Figure 2.5) using various techniques of ^{89}Y targets preparation. The preparation time and amount of ^{89}Y produced is shown in Table 2.1. For yttrium nitrate compacting (Figure 2.5 (a)), the amount of yttrium nitrate used was 0.45g and around 10 minutes was spent on the preparation.

Preparation time on both aqueous and non-aqueous electrodeposition took around 60 minutes. After electrodeposition in the non-aqueous bath, the deposited yttrium appeared to be adhesive, thin, non-homogenous and light blue-white in colour (Figure 2.5 (b)); whilst after electrodeposition in the aqueous bath, the deposited yttrium appeared to be non-adhesive, thick and bluish in colour (Figure 2.5 (c)).

For the preparation of yttrium foil target plate, the preparation time took around 10 minutes and used 0.16 g of yttrium foil which was placed directly on the aluminium target plate (Figure 2.5 (d)).

For the yttrium sputtering preparation technique, the final amount of yttrium produced was around 0.01 g after 10 minutes of the sputtering process (Figure 2.5 (e)).

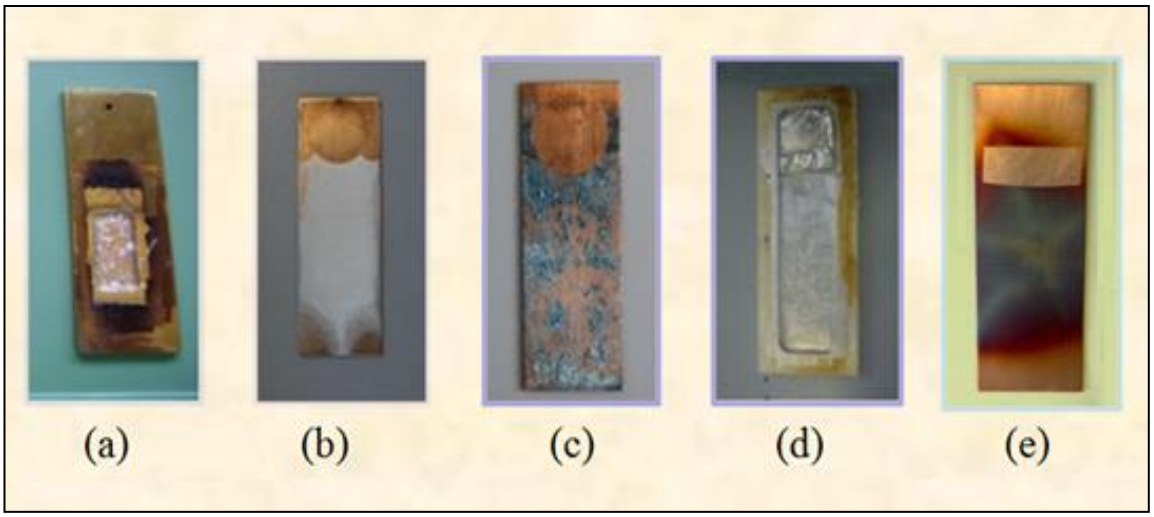

Figure 2.5 Yttrium-89 Solid Targets; (a) Direct Application; (b) Non Aqueous Electrodeposition; (c) Aqueous Electrodeposition; (d) Yttrium Foil; (e) Yttrium Sputtering

Table 2.1

Various techniques of ^{89}Y targets and preparation time and amount of ^{89}Y produced

Yttrium preparation technique	Amount of yttrium (g) used	Preparation time (min)	Amount of yttrium (g) produced
Direct Application	0.45	10	0.45
Aqueous Electrodeposition	0.20	60	0.05
Non Aqueous Electrodeposition	0.20	60	0.05
Foil	0.16	10	0.16
Sputtering	0.01	10	0.01

For a direct application of yttrium nitrate, the amount of yttrium nitrate used was 0.45 g and around 10 minutes was taken for the preparation. To avoid having the yttrium nitrate leak out of the target plate during bombardment, the target plate can be covered with aluminium foil.

Preparation time on both aqueous and non-aqueous electrodeposition took around 60 minutes because the thickness of the deposit increases linearly with time up to 1 hour at room temperature. It has been demonstrated from literature reviews that the effect of temperature could be obtained in an amount of up to 45^{o}C for good quality, uniform, white-gray deposits [154]. The electrodeposition technique carried out in our lab was possible, although the yield is low in both the aqueous and non-aqueous baths. Collecting the deposited yttrium and packing it in a gold or aluminium target plate to gain a higher yttrium yield could be considered, since the initial deposition method produced approximately 0.05 g to be bombarded in the cyclotron.

For the preparation of the yttrium foil target plate, yttrium foil was cut to size and placed directly on the targeted area of the aluminium plate using a cello tape as a sticker. It was covered with a piece of aluminium foil to ensure the yttrium foil would not fall and become lost during bombardment. Usually for a layer of placement, around 0.15 to 0.20 g can be placed directly on the target area of the aluminium plate. From our experience, up to 3 layers of yttrium foil can be placed on the aluminium plate to obtain a higher yield of the ^{89}Zr radioisotope produced after bombardment in the cyclotron.

For the yttrium sputtering preparation technique, the process requires an optimum diameter of 57 mm disk of the metal foil to be used as a target; this can coat a sample

up to about 4 cm in diameter. The final amount of yttrium produced was very low, around 0.01 g after 10 minutes of sputtering process. The suggested maximum processing time was limited to 10 minutes only because the typical time limit for the sputtering technique usually took not more than 5 minutes to complete.

2.2 Production of ^{89}Zr in a Cyclotron

There are some valuable properties required in order for the radioisotope to work efficiently. It needs to have a long-lasting half-life in order to prevent the isotope from decaying before reaching the target; in addition, the isotope needs to emit enough energy for the gamma camera to acquire an image. As an alternative to the approach of modifying the antibody to match the physical characteristics of ^{18}F, the use of longer-lived positron emitters has been explored for radioimmunoimaging with intact antibodies [156-158]. Table 2.2 shows the properties of selected PET radionuclides for radioimmunoimaging [28]. The table indicated that the half-lives of longer-lived positron emitters such as ^{124}I and ^{89}Zr have a much closer match with the biological half-life of most intact antibodies. Antibodies labelled with longer-lived positron emitters can be imaged for 2-5 days after injection, when the radioactivity in the blood pool has been cleared and target to background ratio is higher.

^{89}Zr is an ideal physical characteristic for immuno-PET and has been suggested for use in quantifying slow processes as well as deposition of monoclonal antibodies in tissue and tumour. The relatively low translational energy of the emitted positron for ^{89}Zr results in high resolution of the image quality, which is comparable to those

observed with the ^{18}F and ^{64}Cu radionuclides, respectively [28, 30, 159]. Currently, ^{89}Zr radioisotope is not widely used for immuno-PET, due to its limited availability, but with the use of medical cyclotron, which is commonly available in major hospitals and cancer centres. Hence, production of ^{89}Zr can be carried out through cyclotron bombardment using ^{89}Y as a starting material.

Table 2.2

Properties of Selected PET Radionuclides for Radioimmunoimaging [28]

Radionuclide	Half Life	Production	β^+_{max} in MeV (β^+ yields)	γ-energies in MeV (yields)	Intrinsic spatial resolution loss (mm)
^{89}Zr	78.4 h	$^{89}Y(p, n)^{89}Zr$ $^{89}Y(d, 2n)^{89}Zr$	0.909 (23%)	-	1.0
^{124}I	100.2 h	$^{124}Te(p, n)^{124}I$ $^{124}Te(d, 2n)^{124}I$ $^{125}Te(p, 2n)^{124}I$	2.14 (24%)	0.60 (61%)	2.3
^{18}F	1.83 h	$^{20}Ne(d, \alpha)^{18}F$ $^{18}O(p, n)^{18}F$	0.63 (97%)	0.14 (41%)	0.7

There are two nuclear reactions that have been explored for the production of ^{89}Zr and typically by cyclotron bombardment of ^{89}Y. The first, and most commonly used, is the $^{89}Y(p, n)^{89}Zr$ reaction [53, 160]. This has gained in popularity because a higher yield of ^{89}Zr can be produced from ^{89}Y, which is 100% naturally abundant in the earth's crust. Typically in this reaction, a proton beam with 14-14.5 MeV energy is used to bombard an yttrium foil solid target for 2-3 hours with 65-80 μA beam

current. Since yttrium has only one stable isotope and the product can be made relatively pure at low energy, this is an ideal reaction for production of ^{89}Zr. The other reaction that has been used for the production of ^{89}Zr in the cyclotron is the ^{89}Y(d, 2n)^{89}Zr reaction [151]. Usually in this reaction, an yttrium pellet is used and irradiated with a 16 MeV deuteron beam and ^{89}Zr can be purified and separated from the target by ion exchange chromatography.

The dominant oxidation number of zirconium is +4 which, when combined with a relatively small size, leads to an extensive hydrolysed aqueous chemistry with a largely covalent nature. Donor ligands (ions or molecules attached to a metal atom by coordinate bonding) containing oxygen, nitrogen and chloride are especially stable, commonly creating complexes having coordination numbers of seven, eight and higher. High coordination numbers (seven and eight) are characteristic of zirconium complexes and the ligands are normally labile, which results in the great variety of stereochemistries. Different radiometals have significant differences in their coordination chemistry. While biological properties can be influenced by the radiometal chelate, the biodistribution of a target-specific radiopharmaceutical can be scientifically changed. This can be achieved by either modifying the coordination environment around the radiometal with a variety of chelators, or by the use of various coligands if the radiometal chelate contains two or more ligands.

Table 2.3 shows the list of metallic radionuclides useful for PET imaging. Generally for PET imaging, it is highly desirable that the radionuclide has no radiation decays other than 511-keV gamma photons from positron annihilation. This will minimize impairment of spatial resolution due to high β+ energy and reduce the radiation

burden to the patient. The half-life of desired radionuclide for PET imaging should be long in the parent isotope, but short in the daughter isotope. Radiolabeling should be completed and preferably ready after around 10–30 minutes of preparation. A generator-based isotope would be ideal to achieve high specific activity for target-specific radiopharmaceuticals so that their target uptake can be maximized. Using a generator-produced isotope is also much easier for transportation and delivery. In addition, the cost for parent isotope production and availability of the enriched source should also be considered.

Table 2.3

A selection of metallic radionuclides useful for PET imaging

Isotope	Half-life (h)	Decay mode	$E\beta^+$ (keV)	Production method
^{61}Cu	3.3	β^+ (62%)	1220, 1150	cyclotron, ^{61}Ni(p,
^{62}Cu	0.16	EC (38%)	940, 560	n)^{61}Cu
^{64}Cu	12.7	β^+ (98%)	2910	
		EC (2%)		^{62}Zn/^{62}Cu generator
^{68}Ga	1.1	β^+ (19%)	656	
^{89}Zr	78.5	EC (41%)		cyclotron, ^{64}Ni(p,
^{94m}Tc	0.9	β (40%)		n)/^{64}Cu
		β^+ (90%)		
		EC (10%)	1880, 770	
		β^+ (23%)	897	^{68}Ge/^{68}Ga generator
		EC (77%)	2.47	
		β^+ (72%)		cyclotron, ^{89}Y(p, n)/^{89}Zr
				cyclotron, ^{94}Mo(p,n)^{94m}Tc

Recently, a study on establishing reliable production of the PET isotope ^{89}Zr for research use was undertaken from target fabrication to preclinical imaging. In this study, an in-house semi-automated external beamline with <40 µA at 11.7 MeV for 120 min (degraded from 18 MeV to suppress ^{88}Y & ^{88}Zr co-production) produced ^{89}Zr from ^{89}Y(p,n)^{89}Zr. End of bombardment activity (by HPGe γ-spectr.) of ^{89}Zr in target discs, derived from multiple runs, was 1.36 GBq (±0.53 GBq [SD], n=3) which was 64% (±25%, n=3) of the theoretical activity, with a maximum of 1.84 GBq (87% of theory) achieved. Recovery was 93 % (±17%, n=3), radionuclidic purity >99 % (n=3) and chemical purity 0.2 ppm Zr (±0.3 ppm, n=3, ICP-MS) [161].

Another study was carried out where ^{89}Zr radionuclide was produced by irradiation of Y_2O_3, as a thick target, which was prepared by means of the sedimentation method and separated in 95 ± 5% radiochemical yield using anion exchange chromatography [162]. The target was irradiated up to 20 µA current with 15 MeV. Development of a cooling system that contains a circulating flow of chilled helium in front of the target, besides the water cooling used in this study, would improve thermal conductivity. Hence, it would be expected to allow the use of higher beam current up to 30 µA.

The possible production routes of ^{89}Zr isotope have been discussed and the development of the production procedure for the most suitable route using a low energy cyclotron has been described. For the cyclotron production of no-carrier-added ^{89}Zr, sedimented $^{89}Y_2O_3$ target was irradiated by 15 MeV protons. End of bombardment yielded about 60.77 MBq and ^{89}Zr per µA h was experimentally obtained in 20 min irradiation at 20 µA. ^{89}Zr integral thick target yield and nuclear

model calculations of the $^{89}Y(p,n)^{89}Zr$, $^{89}Y(d,2n)^{89}Zr$, and $^{nat}Sr(a,xn)^{89}Zr$ nuclear processes up to 50 MeV have also been calculated [163].

Degrading the proton beam to 10 MeV produces radionuclidically pure ^{89}Zr with yields from 8 to 9 MBq/μAh [164]. This is enough for preclinical use, but the yield is not sufficient for either clinical use or commercial supply. The use of thinner beam degraders to increase the proton beam energy increases the radionuclidic yield but it is not yet possible to exclude the presence of radionuclidic impurities.

2.2.1 Methodology

All experimental components of the methods were conducted at Peter MacCallum Cancer Centre, East Melbourne, Victoria, Australia. Radiation protection for radiation safety was in accordance with the guidelines issued by the Australian Radiation Protection and Nuclear Safety Agency (ARPANSA). This guidance seeks to promote practices which protect human health and the environment from the possible harmful effects of radiation and to address safety concerns.

Each of the ^{89}Y solid targets which were prepared earlier in Section 2.1.1, were bombarded separately in a 12 MeV medical cyclotron (Oxford) for 30 minutes at 10 μA currents using the (p, n) reaction. During irradiation, the target holder was cooled with water at the back side of the target. Radioactivity measurements were made by using a dose calibrator (Capintec CRC-15R) with a calibration factor of 465 for ^{89}Zr. The presence of ^{89}Zr was determined through gamma spectroscopy that involves the use of a multi-channel analyser (MCA) gamma counter to detect which gamma energies are present. For quantification of radioactivities, samples were counted on a

calibrated Atomlab 950-MCA Operation (BIODEX-Medical System Inc. Version 3.42) Gamma Counter by using a dynamic energy window of 0–1500 keV for ^{89}Zr. The energies of interest are those that originate from the photons with 511 keV and 909 keV energy peaks, respectively.

Before the bombardment procedure was carried out, a target plate covered with a paper was placed in a target boat of the cyclotron in order to determine the specific target location for bombardment (Figure 2.6).

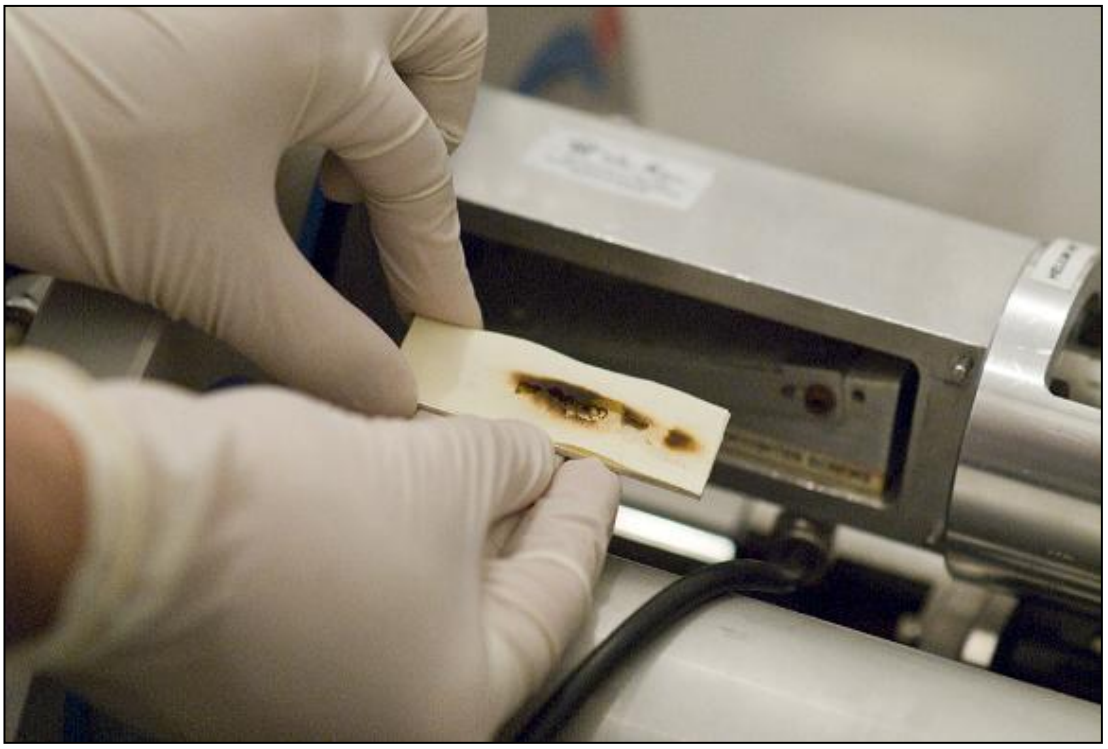

Figure 2.6 Determining target location before bombardment

Figure 2.7 shows the determination of optimum irradiation angle with 10^{o} of irradiation angle showing the optimum surface area for the bombardment procedure. This enables a greater area to be targeted for bombardment.

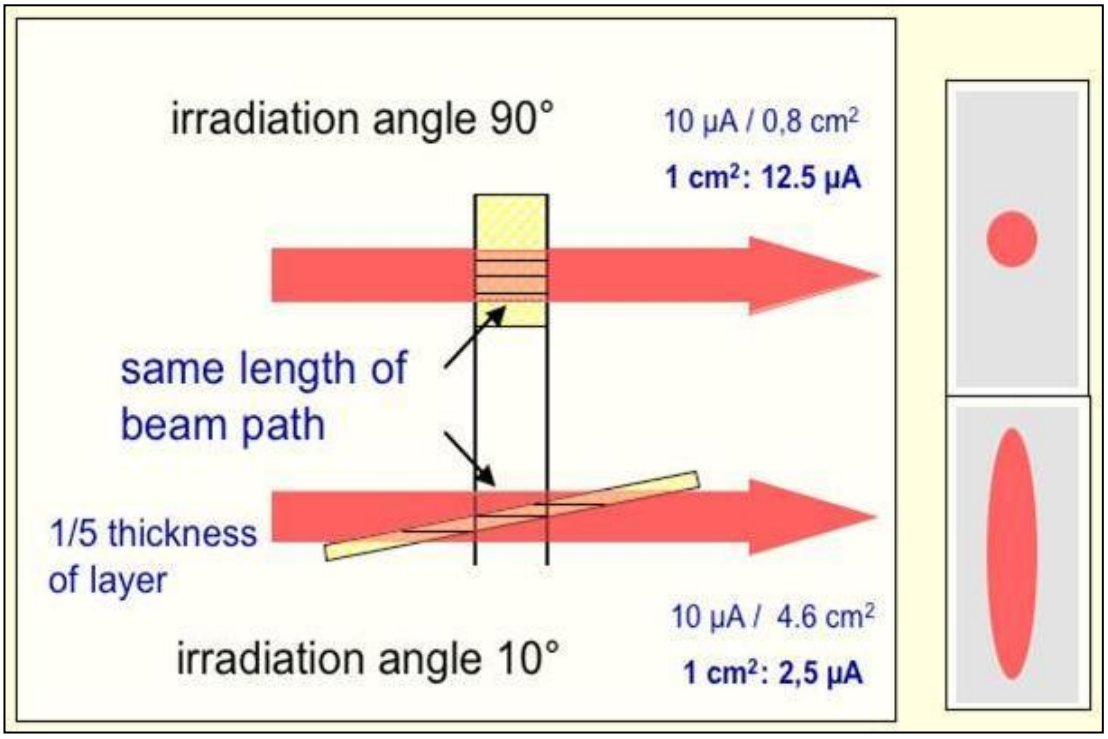

Figure 2.7 Determination of optimum irradiation angle

Figure 2.8 shows the drawing of irradiation technique for the production of ^{89}Zr radioisotope in the cyclotron.

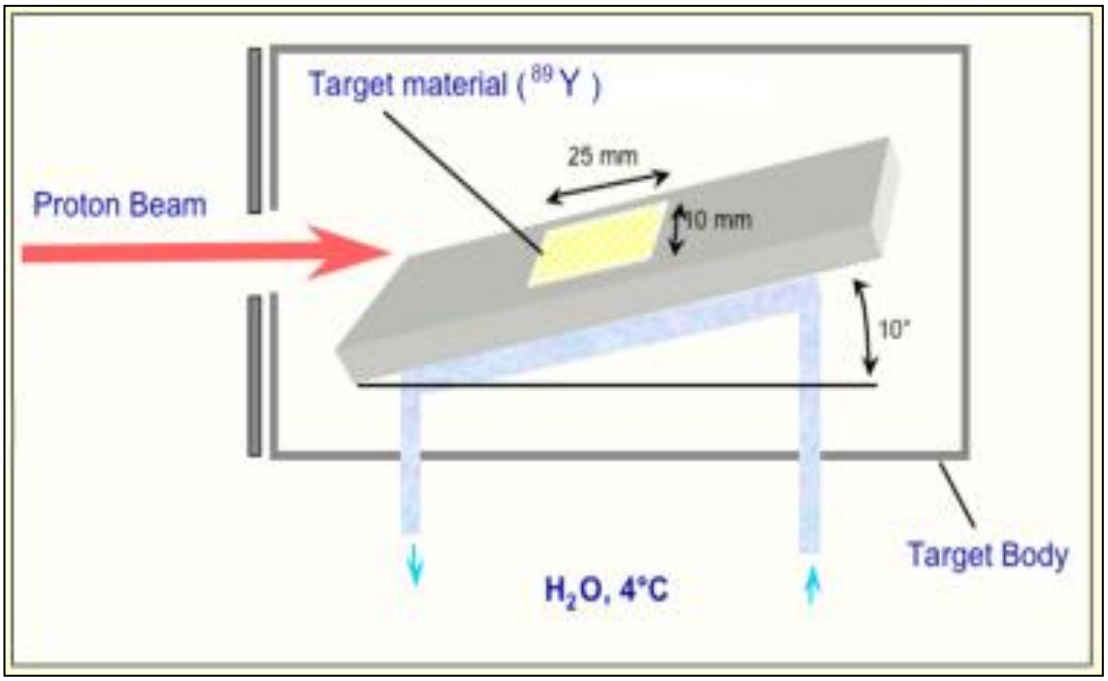

Figure 2.8 Irradiation techniques for the production of ^{89}Zr radioisotope

Each of the ^{89}Y solid targets which were prepared as described in Chapter 3 were then bombarded separately in a 12 MeV medical cyclotron (Figure 2.9) for 30 minutes at 10 μA currents using the (p, n) reaction. During irradiation, the target holder was cooled with water at the back side of the target. Finally, ^{89}Zr radioisotope produced after bombardment was then left overnight for cooling to allow decay of the short-lived isomeric product, $^{89m}Zr[t_{1/2}=4.161(17)$ min].

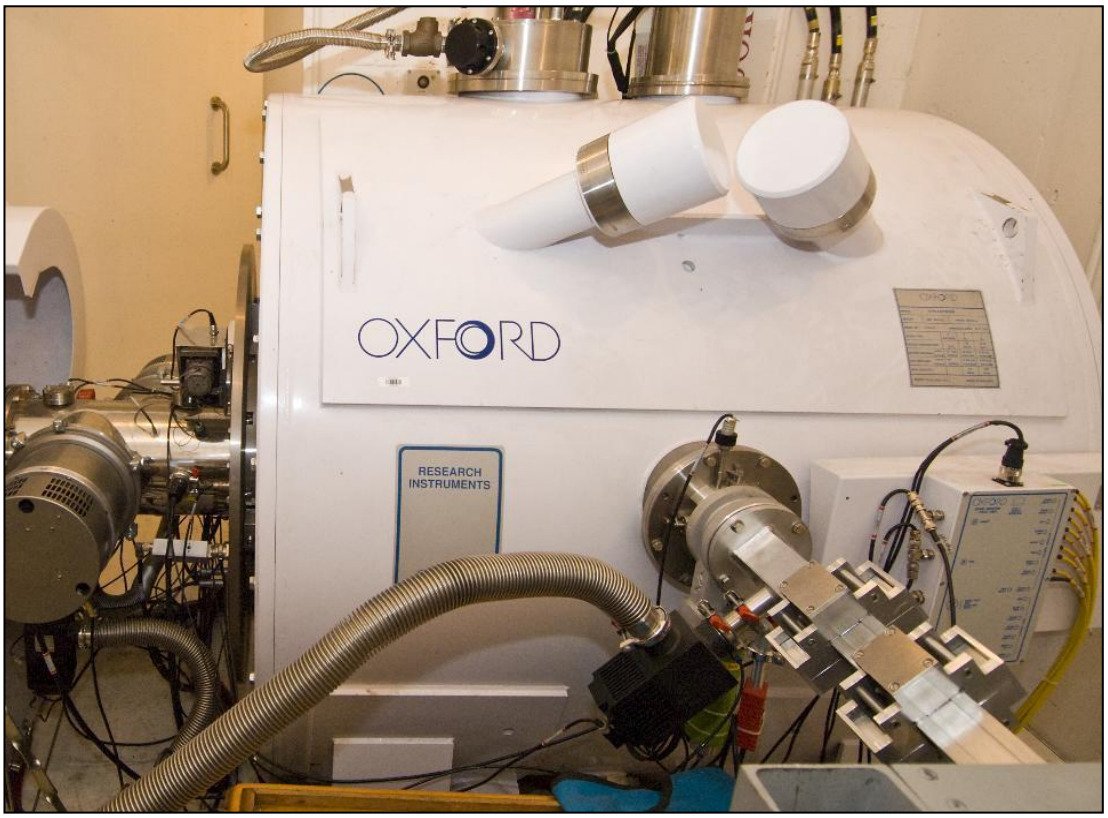

Figure 2.9 Cyclotron Facilities at Peter MacCallum Cancer Centre, Victoria, Australia

After cooling, the target was dissolved in 2.5 ml of 6 M HCl. Dissolution was complete within 30 min. Small traces of a black insoluble material were observed in the remaining suspension. These were likely to be an insoluble form of yttrium chloride and were found not to contain any ^{89}Zr activity. The ^{89}Zr solution in HCl was then oxidised to the IV-oxidation state with 0.1 ml H_2O_2 (hydrogen peroxide) and diluted with distilled water to set the final concentration at 2 mol/L HCl.

2.2.2 Gamma spectroscopy of ^{89}Zr

The production of ^{89}Zr must be verified. This radionuclide can be identified through its decay mode, emission energies and half-life. After bombardment, the samples were measured for their respective levels of radioactivity and then purified using a hydroxamate resin column. Radionuclidic purity was determined by measuring the energy peaks using a multi-channel analyser (MCA). The presence of gamma energies in the sample can be analysed by gamma spectroscopy, showing the presence of radioactive isotopes. To verify that ^{89}Zr is actually produced, a gamma spectroscopy test with an MCA gamma counter is done. By measuring the peak at 511 keV in ^{89}Zr and comparing it to a known amount of ^{18}F in the same experimental set-up and in the same region of interest (ROI) as ^{89}Zr, quantification is possible. The ROI consisted of 21 channels (495-526 keV) around the peak of 511 keV. In this relative quantification, the contribution from background activity is (within a very good approximation) assumed to be equal. However, the contribution from the 909 keV photons in ^{89}Zr is corrected by defining a check-ROI of 21 channels located 10 channels to the right at the ending of 511 keV ROI (542-573 keV). Within the check-ROI, the background is subtracted to quantify only the photons originating from 909

keV. The counts from the check-ROI are then subtracted from the gross counts in the 511 keV peak of ^{89}Zr. The ion chamber is used to ensure that the irradiation has successfully produced a radioisotope.

2.2.3 Result

All Yttrium solid targets were successfully prepared and bombarded in a 12 MeV medical cyclotron (Oxford) at 10 μA beam current. The bombarded yttrium targets (Figure 2.10) underwent gamma spectrum analysis that determined 511 keV and 909 keV energy peaks (Figure 2.11) indicating that ^{89}Zr radionuclide had been successfully produced. During the bombarding process of the different targets, a standard setting was applied. The settings, beaming with 10 μA current for 30 minutes, were chosen so that it would be an equal comparison for all the bombarded targets.

To measure the amount of ^{89}Zr radioactivity produced, a dose calibrator (Capintec), which was described in Section 2.2.1, was used after a cooling time period of 1 day. This step was undertaken to ensure that all the short half-life impurities which were also produced during the production of ^{89}Zr had fully decayed.

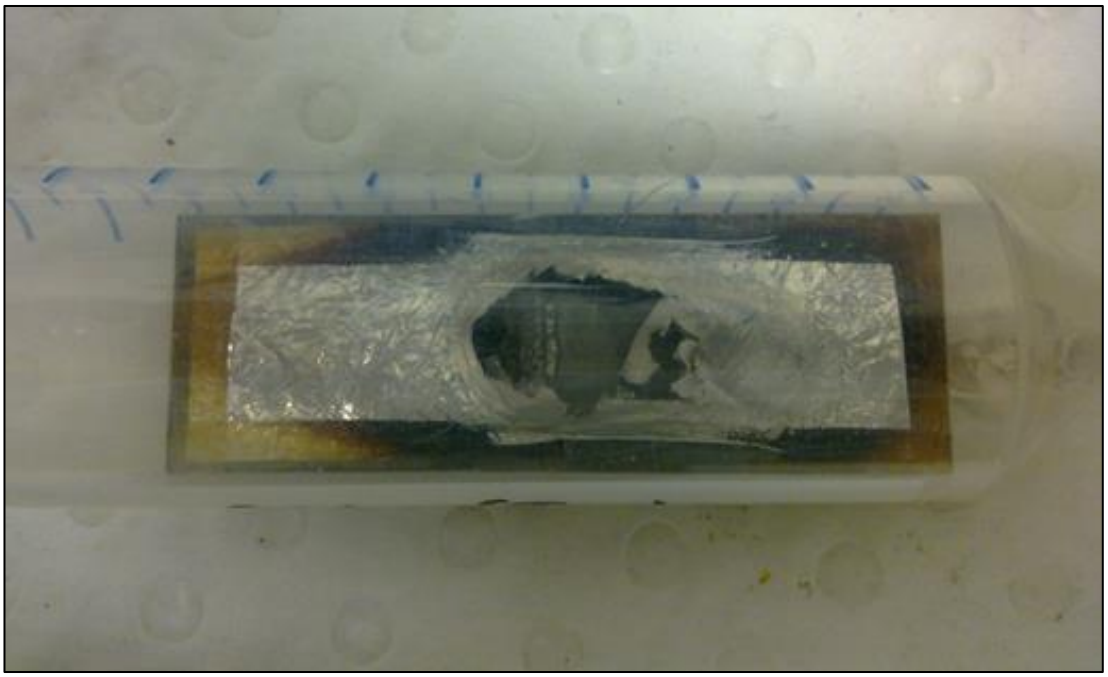

Figure 2.10 Bombarded ^{89}Y producing ^{89}Zr

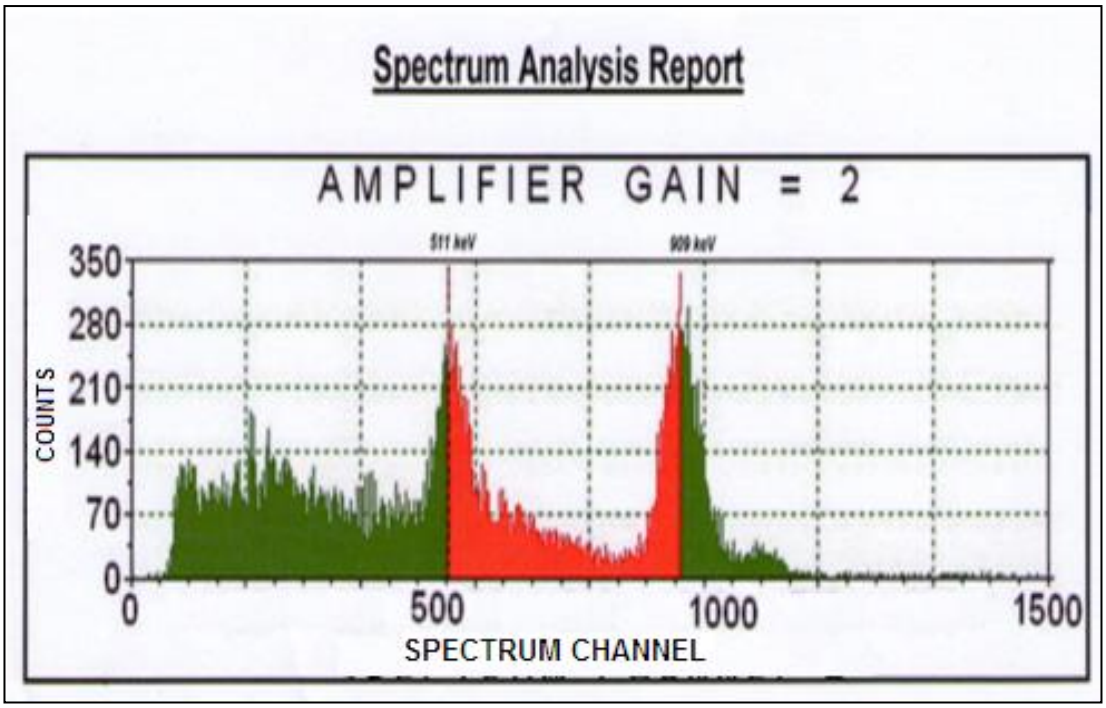

Figure 2.11 Gamma spectrum analysis of ^{89}Zr radioisotope

Table 2.4 shows a series of experiments conducted on the ^{89}Zr production from cyclotron bombardment using 5 different techniques of yttrium target preparation. The data from the table indicated that using yttrium foil as a target produced the highest yield of ^{89}Zr activity; with approximately 77 MBq after bombardment with 1 day cooling time compared to the other methods. Production of ^{89}Zr using compacting yttrium nitrate target produced approximately 9 MBq whilst yttrium sputtering bombardment produced approximately 1 MBq of ^{89}Zr radioactivity. Both electroplating aqueous and non-aqueous targets produced approximately 0.6 MBq of ^{89}Zr radioactivity each.

Table 2.4

^{89}Y targets and ^{89}Zr produced from cyclotron bombardment

Yttrium preparation technique	Yield of yttrium (g)	Preparation time (min)	Irradiation time (min)	Activity after bombardment (1 day cooling time)
Compact	0.45	10	30	9 MBq
Aqueous Electroplating	0.05	60	30	0.6 MBq
Non Aqueous Electroplating	0.05	60	30	0.6 MBq
Foil	0.16	10	30	77 MBq
Sputtering	0.01	10	30	1 MBq

Table 2.5 shows the no-carrier-added (NCA) specific activity of ^{89}Zr from our experiment [161] compared to the other related publications from scientific literature [34, 165]. The table indicated that NCA specific activity of ^{89}Zr from our experiment was 408 MBq/ µg (±26 MBq/µg) which comparable to published data of Holland *et al.*, 2009 [34] of 196-496 MBq/µg and Hong *et al.*, 2011 [165] of 225 (±24 MBq, n=6).

Table 2.5

NCA Specific Activity of ^{89}Zr

Publications from Scientific Literature	**Specific Activity of NCA ^{89}Zr**
Scharli *et al.*, 2012 [161]	408 MBq/µg (±26 MBq/µg)
Holland *et al.*, 2009 [34]	196-496 MBq/µg
Hong *et al.*, 2011 [165]	225 MBq/ µg (±24 MBq)

Chapter 3: Purification of Zirconium-89

Purification of ^{89}Zr usually involved the separation process of ^{89}Zr radionuclide from its impurities and starting materials followed by elution of the radionuclide from the retention column. The development in separation and purification of longer-lived ^{89}Zr PET radioisotope and its chelation with a monoclonal antibody hopefully can be adapted to many other applications within the disciplines of nuclear medicine. Details of radiopharmacy applications of purifying other radioisotopes for use in medical research can also be examined.

The ^{89}Zr can be dissolved in hydrochloric acid and separated from other radioisotopes and the target material on an ion exchange column [35, 53, 151]. In some cases, a wet chemical extraction preceded the ion exchange separation [150]. It was found that the hydroxamic function had a high specific affinity for Zr, even at high acid concentrations (> 1 M HCl), meaning that, at concentrations higher than 1 M HCl, Zr is able to form complexes with hydroxamates, whereas its impurities are not [151]. As ^{89}Zr was ionically bonded to the column, a stronger anion exchanger is needed to remove it. It was found that the most convenient solution for transchelating ^{89}Zr from the column was ≥ 0.5 M oxalic acid [35]. According to Dejesus (1990), the hydroxamate column can produce 99.9% carrier free ^{89}Zr, but the extraction technique proved to be counterintuitive to the purpose of purification [53]. In 2003, the oxalic acid was proven to be able to successfully remove 97% of the total activity from the column over 5 separate elutions with an initial 40% yield in the first two elutions [36].

3.1 Preparation of Hydroxamate Resin Column

^{89}Zr is purified from its radionuclidic impurities using a hydroxamate resin column. The column is based on a modified cation exchange where hydroxamate groups are introduced [143]. To receive a high proportion of these added hydroxamate groups, the carboxylic acid groups of the cation exchange mass are esterfied in two steps using 2,3,5,6-tetrafluorophenol (TFP, Acros Organics) solution (200 mg/mL in MeCN). Firstly, 1 g of cation exchange mass (Accell Plus CM, Waters) is suspended in 8 mL water for injection (WFI) and mixed well. 75 µL 3M Hydrochloric Acid (HCl), 1 mL TFP-solution and 384 mg of 1-(3-Dimethylaminopropyl)-3-ethylcarbodiimide hydrochloride (EDAC, Acros Organics) are then added. The pH measured is to be within the acceptance level of 5.7-6.0. Following that, the solution is mixed end over end in 1 h.

Secondly, in the esterfication step, 105 µL 3 M HCl, 1 mL TFP-solution and 384 mg EDAC are added, after which the pH is again measured to be within 5.7-6.0. To remove EDAC and unreacted TFP, the solution is poured into a funnel having a suitable filter and washed with 30 mL acetonitrile (MeCN). In the meantime, the hydroxlaminehydrochloride solution, i.e. the solution containing the hydroxamate groups, is prepared. To a solution of 1 mL 1 M sodium hydroxide (NaOH) and 2 mL methanol (MeOH), 690 mg of hydroxylamine hydrochloride (Sigma-Aldrich) is added. After 5 minutes, another portion of 1 mL 1 M NaOH is added and pH was expected to be within the range of 5.3-5.4. The washed esterfied cation exchange mass is then introduced to the hydroxylamine hydrochloride solution. The acceptance interval of pH is now 5.1-5.2. This solution is then mixed end over end over the night

before being washed in a funnel with filter as above. This time, the column mass is washed with 140 mL sterile WFI and 70 mL MeCN. The mass is then dried for 3 h in a vacuum chamber at room temperature. In the final batch, after the column mass has dried in room temperature during low pressure, the vacuum chamber is filled with argon to prevent entry of humid air. After this step, the column mass could be stored at room temperature for up to 4 months without decreasing the labelling capacity of ^{89}Zr [36].

For the preparation of a hydroxamate column experimental setup, an Extract-Clean tube (1.5 mL; Alltech) with a frit placed at the bottom (pore size, 20 µm) was packed with a suspension of 100 mg of hydroxamate resin column material in 0.9% NaCl (Sigma-Aldrich).

3.2 Isolation and Purification of ^{89}Zr

Once the irradiation procedure in the cyclotron has been completed, the irradiated targets then need to be purified. Purification of ^{89}Zr involves the isolation of ^{89}Zr radioisotope from the soluble Y(III) ions starting material and other impurities and then eluting the ^{89}Zr from the hydroxamate resin column. Before purification, each of the irradiated targets was dissolved in hydrochloric acid (HCl) in different concentrations, respectively. ^{89}Zr produced from yttrium foil is dissolved in 12 M HCl [53, 150] and ^{89}Zr prepared from yttrium nitrate and electrodeposited yttrium is dissolved in 3 M hydrochloric acid [35]. For ^{89}Zr produced from the yttrium sputtering bombardment, 1 M of HCl is sufficient for washing out the ^{89}Zr from the copper plate. Hydrogen peroxide (H_2O_2) can be added to ensure complete oxidation,

however it was found not to affect the separation or subsequent chelation chemistry [34]. The solution was then diluted with distilled water or more concentrated HCl was added to ensure that the final concentration of ^{89}Zr was 2 M HCl.

Before starting the purification process, the hydroxamate column is rinsed with 4 M HCl and distilled water, which was initiated by connecting vacuum tubes (Becton Dickinson) to the column with a 10 mL syringe pump (Figure 3.1). Then, 100 mg of the hydroxamate column mass is suspended in 0.9% NaCl (Sodium Chloride) before being packed into the column. Thereafter, the column is rinsed with 5 mL MeCN, 10 mL 0.9% NaCl and 2 mL 2 M HCl.

The ^{89}Zr solution was then transferred to the pre-washed hydroxamate resin column. To ensure that as many impurities as possible are absent from the resin, the column is washed with 6 mL 2 M HCl and 6 mL of distilled water. This separation protocol will cause the ^{89}Zr to bind to the column and the remaining impurities will then be eluted and discarded. The zirconium isotopes were subsequently slowly eluted with 2.5 mL of 1 mol/L oxalic acid. The activity of the elution was then measured in the dose calibrator and sent for spectrum analysis using MCA gamma counter.

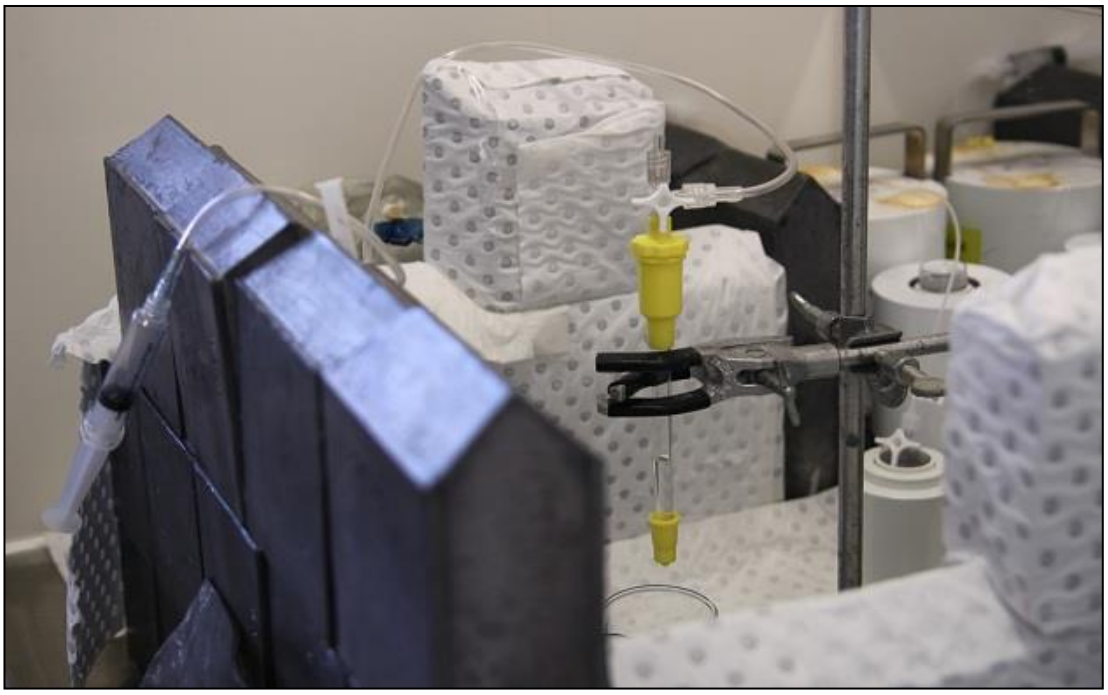

Figure 3.1 Experiment setup for purification of ^{89}Zr

3.3 Result

Table 3.1 shows the ^{89}Zr production from cyclotron bombardment using 5 different techniques of yttrium target preparation and its extraction from hydroxamate resin column using 1 M oxalic acid. The table indicated that oxalic acid extracted more than 80% of ^{89}Zr radioactivity from the column for all types of yttrium targets. For compact yttrium nitrate, which was producing 9 MBq amount of ^{89}Zr radioactivity, the amount of ^{89}Zr trapped in the hydroxamate resin column was 1 MBq and the activity extracted was 8 MBq. The percentage of ^{89}Zr extracted from hydroxamate resin column calculated when using compact yttrium nitrate as a starting target material was approximately 88.9%. Both aqueous and non-aqueous targets, which produced radioactivity approximately 0.6 MBq ^{89}Zr each, showed the lowest

percentage of ^{89}Zr radioactivity, with 83.3% (0.5 MBq) extracted from the column. For yttrium foil which was producing approximately 77 MBq amount of ^{89}Zr radioactivity, the amount of ^{89}Zr trapped in the hydroxamate resin column was 6 MBq and the activity extracted was 71 MBq, which was the highest elution percentage of 92.3%. For yttrium sputtering bombardment which produced approximately 1 MBq of ^{89}Zr radioactivity, the activity trapped in the hydroxamate resin column measured in the dose calibrator was 0.1 MBq and the activity extracted using 1 M oxalic acid was 0.9 MBq (90.0%).

Table 3.1

^{89}Zr produced and purified using 1 M oxalic acid

Yttrium preparation technique	Activity after bombardment (1 day cooling time)	Activity extracted using 1 M oxalic acid	Activity trapped in the column	% Extracted
Compact	9 MBq	8 MBq	1 MBq	88.9
Aqueous Electroplating	0.6 MBq	0.5 MBq	0.1 MBq	83.3
Non Aqueous Electroplating	0.6 MBq	0.5 MBq	0.1 MBq	83.3
Foil	77 MBq	71 MBq	6 MBq	92.3
Sputtering	1 MBq	0.9 MBq	0.1 MBq	90.0

When ^{89}Zr acquired from bombarding ^{89}Y is being eluted after loading it to a hydroxamate resin column, the ^{89}Zr is bound to the resin if 2 M HCl or less is added. This technique could be used to get rid of its impurities. This occurs when loading the ^{89}Zr, lower concentrations of hydrochloric acid should be used for higher yield

(using <2 M solution 99.5% ^{89}Zr will bind). If a higher concentration of hydrochloric acid is used when loading, the affinity with the resin will decrease [34]. The ^{89}Zr is dissolved in HCl and, according to a previous study, hydrogen peroxide is added to keep it in an oxidised state before loading it to the column [35, 36]. Nevertheless, it was not found to affect the separation or subsequent chelation [34] because in an aqueous solution, Zr(IV) ions dominant and the $Zr(IV)+4e^{-}\rightarrow Zr(0)$ reaction has a reduction potential of $E^{o}=-1.51$ V versus the standard hydrogen electrode [166]. Experiments in which H_2O_2 was omitted showed no difference in the observed separation and chelation chemistry of the isolated ^{89}Zr samples.

Hydroxamate resin column was chosen in this experiment because of the relative ease of preparation and simplicity. It resulted in a higher Zr-recovery (> 95% in 2 mL of 1 M oxalic acid) and a better radionuclidic purity [35].

3.4 Alternative ^{89}Zr Extraction Agent

In this research, a few protocols relating to the isolation and purification of ^{89}Zr from its impurities were studied without the use of oxalic acid as an extraction agent. The methodology for this part of the whole research project predominantly followed the work published by Holland *et al.* (2009) and Vosjan *et al.* (2010), in which a step-by-step revised method to conjugate and radiolabel monoclonal antibodies with ^{89}Zr is outlined [32, 34].

For production of ^{89}Zr, ^{89}Y foil target which was described in Chapter 2 was irradiated for two and a half hours in a medical cyclotron (Oxford, 12 MeV) using 10 μA beam current. Post-irradiation, the target was dissolved in 4 mL of concentrated

hydrochloric acid (HCl) whilst heat was applied to instigate the dissolution process. The presence of ^{89}Zr was determined via gamma spectroscopy, which involves the use of a MCA gamma counter as described in Chapter 2 (Section 2.2.2) in order to detect which gamma energies are present.

Once the presence of ^{89}Zr had been verified, it was purified by chemically separating it from the ^{89}Y target material. A hydroxamate resin column was prepared by activating the carboxylate groups of the silica-based weak cation exchange resin (Waters Accell Plus CM) as described in Section 3.1.

A Sep-Pak Accell Plus QMA Plus Light cartridge contains a silica-based, hydrophilic, strong anion-exchanger with large pore size (300 Å), 37–55 μm particle size, 0.22 mmol/g ligand density with surface functionality of –$C(O)NH(CH_2)_3N(CH_3)_3^+Cl^-$ was used to trap and convert [^{89}Zr]Zr-oxalate to [^{89}Zr]Zr-chloride. The anion exchange cartridge was pre-washed with 6 mL MeCN, 10 mL 0.9% saline and 10 mL H_2O before use.

3.4.1 ^{89}Zr Extracted as [^{89}Zr]Zr-phosphate

Phosphoric acid, also known as orthophosphoric acid or phosphoric (V) acid, is a mineral (inorganic) acid having the chemical formula H_3PO_4 where the molecules can combine with themselves to form a variety of compounds which are also referred to as phosphoric acids.

There are various kinds of phosphoric acids and phosphates. The phosphoric acids constitute the largest and most diverse group of the many phosphorus oxoacids.

The simplest phosphoric acid series begins with monophosphoric (orthophosphoric) acid, continues with many oligophosphoric acids such as diphosphoric (pyrophosphoric) acid and, finally, concludes with the polyphosphoric acids. However, phosphoric acid units can bind together into rings or cyclic structures, chains (catenas) or branched structures, with various combinations. Each of these can form phosphates (salts or esters). One of the commonest uses of phosphoric acid is for rust removal. It can also potentially be used for removal of ^{89}Zr from a hydroxamate resin column.

The first experiment involved using phosphoric acid as an extraction agent. The ^{89}Zr was separated from the dissolved target materials in the hydroxamate column using 2.5 mL 1.0 M of phosphoric acid as an extraction agent to form [^{89}Zr]Zr-phosphate. Firstly, the ^{89}Zr solution was loaded to the pre-washed hydroxamate resin column. The column was then washed with 6 mL 2 M HCl and 6 mL of sterile WFI and the ^{89}Zr activity was slowly eluted with 4 successive portions of 0.5 M phosphoric acid (4 x 0.5 mL) and each ^{89}Zr-phosphate vial was then measured in a dose calibrator as described in Chapter 2 (Section 2.2.1).

3.4.2 ^{89}Zr Extracted as [^{89}Zr]Zr-chloride

Hydrochloric acid (HCl) is a clear, colourless solution of hydrogen chloride in water. It is highly corrosive and also a strong mineral acid. HCl has many industrial uses and is found naturally in gastric acid. Meijs *et al.* (1994) [35] have described lengthy procedures for the production of [^{89}Zr]Zr-chloride from purified [^{89}Zr]Zr-oxalate, involving decarboxylation of the excess oxalic acid with H_2O_2 in 6 M HCl (aq) at

80°C followed by drying of the reaction mixture. Holland *et al.* (2009) found that $[Zr^{IV}(C_2O_4)_4]^{4-}$ can be removed from a solution with 100% efficiency by trapping on an activated a Sep-pak QMA strong anion exchange cartridge [34]. The majority (>99.8%) of the oxalic acid is then removed by washing the cartridge with a large volume of distilled water, and the activity eluted with 100% recovery of ^{89}Zr by chloride ion exchange with 300-500 μL of 1.0 M HCl (aq.). Standard 0.9% saline can also be used to elute the ^{89}Zr activity, but the recovery of activity was found to be less efficient. The oxalic acid can also be removed rapidly by boiling the eluate at 110°C under a continuous stream of argon, then reconstituted in 0.9% saline or 0.1 M HCl for further labelling studies. The time taken for the entire procedure of the formation of [^{89}Zr]Zr-chloride requires more than 1 hour.

Firstly, ^{89}Zr was separated from the dissolved target materials in the hydroxamate column using 2 mL 1.0M of oxalic acid as an extraction agent to form [^{89}Zr]Zr-oxalate. Following that, [^{89}Zr]Zr-oxalate solution was loaded onto an activated Sep-Pak Accell Plus QMA Plus Light cartridge. The cartridge was then washed with 40 mL of distilled water and finally, ^{89}Zr was eluted from the cartridge as [^{89}Zr]Zr-chloride with 0.5 mL, 1.0 M HCl solution. The [^{89}Zr]Zr-chloride in 1.0 M HCl was then further diluted to 0.1 M using H_2O.

3.4.3 Result

Following irradiation of ^{89}Y-foil targets (99.9%, 0.254 mm thick, American Elements) at low currents in a medical cyclotron (Oxford, 12 MeV), approximately 425 MBq ^{89}Zr was produced after 2.5 hours of irradiation. The bombarded target was

then left overnight for cooling and underwent gamma spectrum analysis that determined 511 keV and 909 keV energy peaks, indicating that ^{89}Zr had been successively produced.

Approximately 200 MBq each out of the overall amount of ^{89}Zr solution was loaded to two pre-washed hydroxamate resin columns to wash out as much of the impurities as possible in the resin, using 6 mL 2 M HCl and 6 mL of sterile WFI. The zirconium isotopes from each resin column were slowly eluted; the first resin column with 0.5 mL 1 M oxalic acid and the second resin column with 0.5 mL 1 M phosphoric acid for each fraction in 5 fractions. This finally resulted in having the ^{89}Zr radionuclide with a total of 2.5 mL in 1 mol/L phosphoric acid and oxalic acid, respectively. The radioactivity of each elution was then measured in the dose calibrator.

Extraction data are shown in Table 3.2 using either 1.0 M oxalic acid or 1.0 M phosphoric acid. The extraction data indicated that when using 1.0 M oxalic acid as an extraction agent, approximately average amount of 180.4 MBq ^{89}Zr was extracted from the hydroxamate resin column and average activity of 19.6 MBq ^{89}Zr was trapped in the column when 200 MBq ^{89}Zr was loaded to the column. The overall percentage of ^{89}Zr extracted from the hydroxamate resin column, when using 1 M oxalic acid as an extraction agent, was 90.2%. For the extraction of ^{89}Zr using 1.0 M phosphoric acid, approximately 140.2 MBq average amount of ^{89}Zr (70.1%) was extracted from the hydroxamate resin column of 200 MBq ^{89}Zr, where approximately 59.8 MBq average amount of ^{89}Zr was still trapped in the column. The ^{89}Zr was extracted as [^{89}Zr]Zr-phosphate. The average amount of ^{89}Zr radioactivity eluted

from the column is shown in a bar chart in Figure 3.2 and further calculation is shown in Appendix A.

As a result of the experiments that were undertaken for this study, it was ascertained that it is possible to use phosphoric acid as an alternative extraction agent for the separation and purification of ^{89}Zr.

Table 3.2

Extraction of ^{89}Zr using 1.0 M oxalic acid and 1.0 M phosphoric acid

^{89}Zr Extraction	Activity in the column	Activity extracted	Activity trapped in the column	% ^{89}Zr Extracted
1.0 M Oxalic Acid	200 MBq	180.4 MBq	19.6 MBq	90.2 %
0 M Phosphoric Acid	200 MBq	140.2 MBq	59.8 MBq	70.1 %

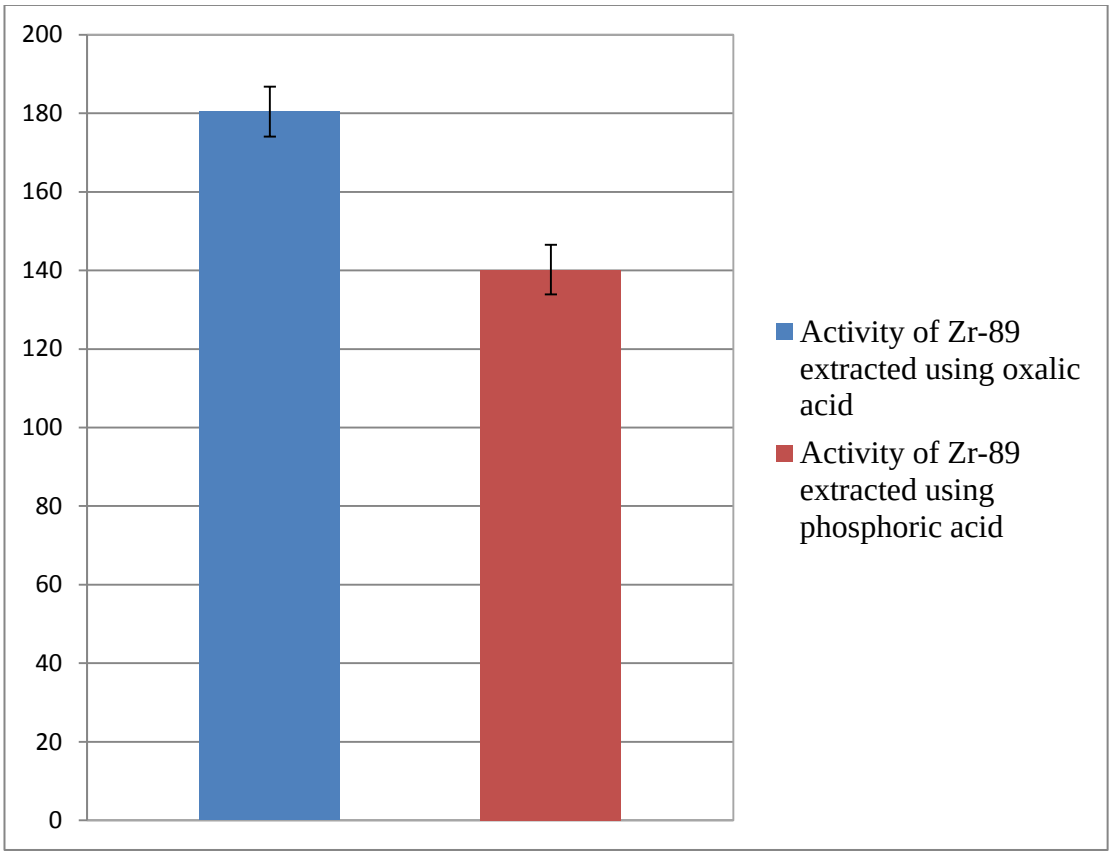

Figure 3.2 Amount of ^{89}Zr in MBq extracted from hydroxamate resin column using 1 M oxalic acid and 1.0 M phosphoric acid

Chapter 4: Radiolabelling of Zirconium-89

Over the past 20 years, attempts have been made to label proteins and antibodies with ^{89}Zr using DTPA derivatives and porphyrins as chelating agents [150, 167], as well as desferal (Df) conjugates [99, 100]. The process incorporates Df-groups onto monoclonal antibodies in a two-step procedure. Firstly, maleimide groups were incorporated into the protein with the assistance of succinimidyl-4-(*N*-maleimidomethyl) cyclohexane-1-carboxylate (SMCC). In the second step, the thioester of Df formed by conjugation to SATA was further converted to a free thiol with hydroxylamine to facilitate reaction with the maleimide groups of the antibody by subsequent radiolabelling with ^{89}Zr. The final purified product was obtained through gel filtration [99, 100]. This protocol was further modified by formation of *N*-succinyldesferrioxamine B of Df (N-SucDf) as an intermediate [36]. In this process, the hydroxamate groups of N-sucDf were temporarily blocked by formation of the Fe(III) complex, known as N-sucDf-Fe complex. It was then esterified and coupled to antibodies. Fe(III) was then removed by reduction to Fe(II) and transchelation to EDTA. Finally, the mAb-N-sucDf was radiolabelled with ^{89}Zr at pH 7.2-7.4 after 30 min incubation at room temperature [36]. Later in 2010, Perk *et al.* introduced the novel BFC *p*-isothiocyanatobenzyl-desferrioxamine B (Df-Bz-NCS) as a new bifunctional chelate for facile radiolabelling of monoclonal antibodies with ^{89}Zr for immuno-PET imaging [97]. Its performance was then compared in ^{89}Zr for immuno-PET with the reference bifunctional TFP-*N*-sucDf [36]. It was demonstrated that the novel Df-Bz-NCS allows efficient and easy preparation of optimally performing ^{89}Zr-labelled mAbs, thereby facilititating further exploration of ^{89}Zr-

immuno-PET as an imaging tool, with oxalic acid being used as an extraction agent to extract the ^{89}Zr from the hydroxamate resin column [97]. The step-by-step procedure was then described for the facile radiolabelling of mAbs or other proteins with ^{89}Zr using *p*-isothiocyanatobenzyl-desferrioxamine B (Df-Bz-NCS). First, Df-Bz-NCS is coupled to the lysine-NH_2 groups of a mAb and pH was adjusted to 9.0. Following that, the conjugation was purified using PD-10 desalting column gel filtration. The pre-modified mAb is then labelled at room temperature by the addition of ^{89}Zr-oxalic acid solution followed by purification using PD-10 column gel filtration to remove the unlabelled product and oxalic acid from the labelled compound. The achievements indicate that all reagents and procedures are in place to allow broad-scale clinical application of immuno-PET with ^{89}Zr labelled intact mAbs [32].

For a further experiment in radiolabelling, a high amount of ^{89}Zr activity was needed, hence yttrium foil was chosen as a target for bombardment on the 12 MeV medical cyclotron. Firstly, an aluminium target plate was cleansed with absolute ethanol and then 0.20 gram of ^{89}Y-foil starting material (0.1 mm, 100 % natural abundance) was cut and placed on the beaming area of the aluminium plate using a cello tape as a sticker. The copper plate was then covered by a piece of aluminium foil to make sure the yttrium foil would not become lost during bombardment. It was then irradiated in a 12 MeV medical cyclotron at 10 μA current for 2.5 hours. During irradiation, the target was placed in a holder and cooled with water. ^{89}Zr was produced via the ^{89}Y(*p*, *n*) ^{89}Zr transmutation reaction [34]. The ^{89}Zr produced was then left overnight for cooling.

After 24 h, the ^{89}Zr produced from yttrium foil was taken out from the target boat in the cyclotron and dissolved in 12 M HCl. The solution was then diluted with distilled water to ensure that the final concentration of ^{89}Zr was 2 M HCl. The ^{89}Zr solution was subsequently loaded to the pre-washed hydroxamate resin column. To ensure that as many impurities as possible were absent from the resin, the column was washed with 6 mL 2 M HCl and 6 mL of sterile WFI. Under these conditions, ^{89}Zr remained bound to the resin, whereas ^{89}Y and the other radionuclidic metal impurities were eluted. The zirconium isotopes were then slowly eluted with 2.5 mL of 1 mol/L oxalic acid. The activity of the elution was then measured in the dose calibrator and sent for spectrum analysis using MCA gamma counter.

4.1 Conjugation of Herceptin (Trastuzumab) with p-isothiocyanatobenzyl-desferrioxamine (Df-Bz-NCS)

Herceptin® (Trastuzumab) was conjugated with the novel bifunctional chelate *p*-isothiocyanatobenzyl-desferrioxamine B (Df-Bz-NCS) according to a modified procedure of Perk *et al.* [32, 97]. Firstly, Df–Bz–NCS is coupled to the lysine–NH_2 groups of Trastuzumab when a threefold molar excess of Df-Bz-NCS (in 20 µl DMSO) was added to the Trastuzumab (2–10 mg in 1 ml 0.1 M $NaHCO_3$ buffer, pH 9.0). The mixture was then incubated for 30 min at 37°C which finally produced the conjugated Df-Bz-NCS-Trastuzumab. Non-conjugated chelate was then removed by size exclusion chromatography using a PD-10 column (GE Healthcare Life Sciences) with 0.25 M sodium acetate or 0.9% sodium chloride 5 mg/mL (pH 5.0) as eluent for

purification purposes. The Df-Bz-NCS-Trastuzumab can be stored in the freezer at -20^{o}C until the day of radiolabelling for at least 2 weeks.

4.2 ^{89}Zr Radiolabelling with Df-Bz-NCS-Trastuzumab

The conjugated Df-Bz-NCS-Trastuzumab was labelled with ^{89}Zr according to the modified procedure of Perk *et al.* with a slight modification [32, 97]. Firstly, about 200 µL [^{89}Zr]Zr-oxalic acid solution was pipetted into a reaction vial, followed by the addition of 200 µL 1 M oxalic acid and 90 µL 2 M Na_2CO_3 into the vial. The vial was then incubated for 3 min at room temperature. Following that, 0.30 mL 0.5 M sodium acetate, 0.71 mL pre-modified Df-Bz-NCS-Trastuzumab and 0.70 mL 0.5 M sodium acetate was successively pipetted into the reaction vial. The pH of the labelling reaction should be in the range of 6.8-7.2 in order to give optimal labelling efficiency. The mixture was incubated for 1 h at room temperature while gently shaking the reaction vial which finally produced the radiolabelled ^{89}Zr-Df-Bz-NCS-Trastuzumab. Finally, ^{89}Zr-Df-Bz-NCS-Trastuzumab was purified by size exclusion chromatography using a PD-10 column (GE Healthcare Life Sciences) with 0.25 M sodium acetate (pH 5.0) as the mobile phase for purification purposes. To begin the ^{89}Zr-Df-Bz-NCS-Trastuzumab purification procedure through size exclusion chromatography, the following steps were undertaken. Firstly, the PD-10 column was rinsed with 20 mL of 0.25 M sodium acetate (pH 5.4-5.6). The radiolabelled reaction mixture was then pipetted into the column, discarding anything that passed through. A further 1.5 mL of 0.25 M sodium acetate (pH 5.4-5.6) was pipetted through, discarding anything further that passed through, with a final rinse of 2 mL

of 0.25 M sodium acetate (pH 5.4-5.6), this time collecting the purified ^{89}Zr-Df-Trastuzumab.

4.3 Quality Control Analyses

Radionuclidic and radiochemical purity was analysed using Thin Layer Chromatography (TLC) and High Performance Liquid Chromatography (HPLC) machines as shown in Figure 4.1. The TLC and HPLC system used for this study was a LC-10Avp Shimadzu model; Mobile phase: 0.1 M Phosphate Buffer pH 6.2-7.0, 0.87 % w/v NaCl, 0.065 % sodium azide; Column: Waters BioSuite 5u 125 HR SEC, 300 x 7.8 mm, 5µ; Temperature: Ambient; Flow rate: 0.65 mL/min; Detector: UV at 280 and 254 nm and scintillation Injection volume: 100 µL with run time of 30 minutes. The preparation of the mobile phase was 7.80 g $NaH_2PO_4.2H_2O$ and 8.90 g $Na_2HPO_4.2H_2O$ and 8.70 g NaCl and 0.65 g sodium azide to 1000 mL with Milli-Q water.

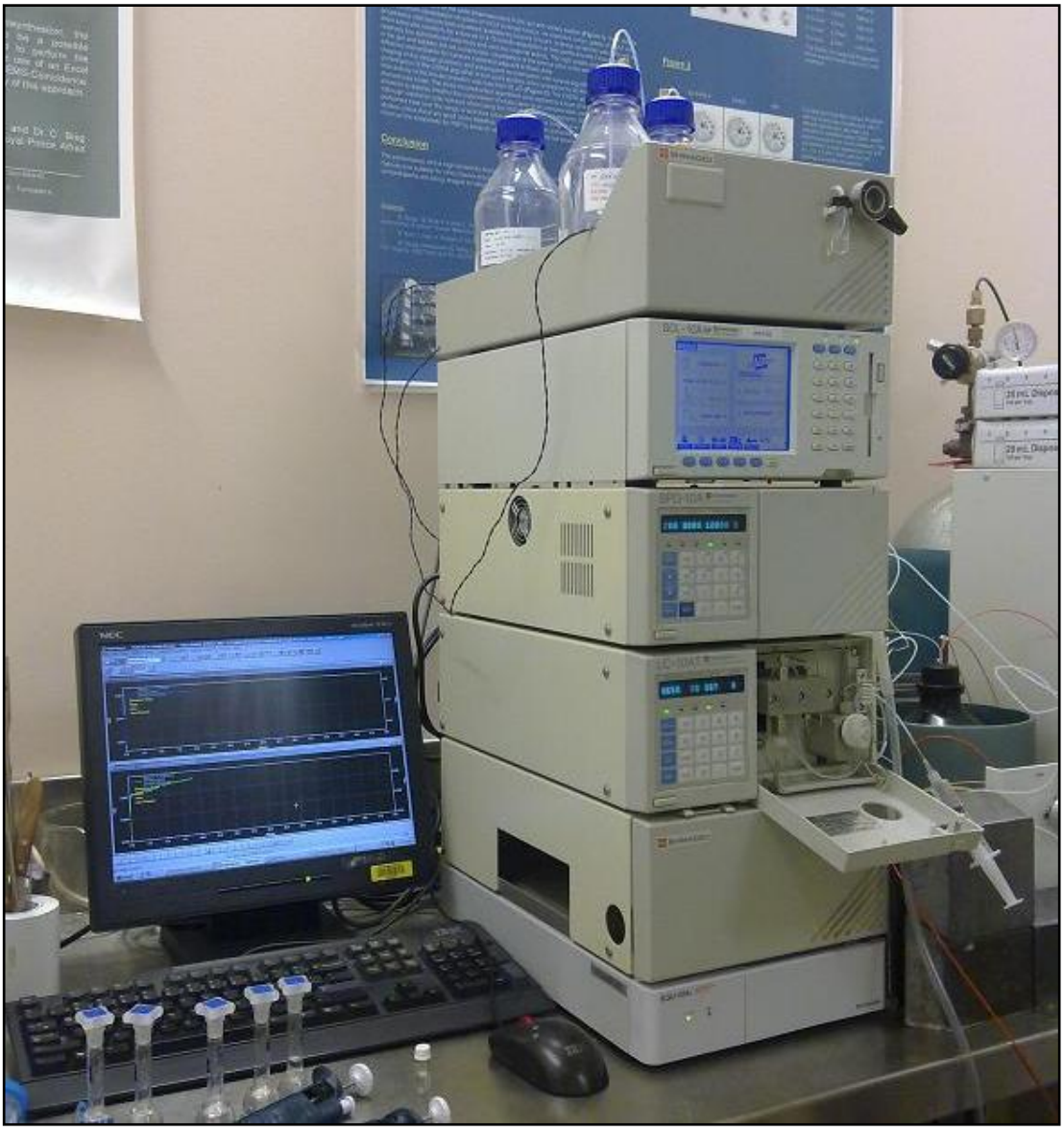

Figure 4.1 LC-10Avp Shimadzu model for TLC and HPLC Analyses

4.4 Result

4.4.1 Production and Purification of ^{89}Zr

^{89}Zr was produced from the ^{89}Y(p,n)^{89}Zr transmutation reaction by proton bombardment of commercially available, high purity (99.9%, 0.254 mm thick, American Elements) ^{89}Y-foil on the small cyclotron. A total yield of 400 MBq ^{89}Zr was produced after 2.5 hours of irradiation with proton beam energy of 12 MeV and 10 µA beam current. After the end of bombardment, the target was then left overnight for cooling and subsequently dissolved in 12 M HCl. Dissolution was complete within 10 min. About 200 MBq out of the overall amount of ^{89}Zr solution was loaded to the pre-washed hydroxamate resin column to wash out as many impurities as possible in the resin using 6 mL 2 M HCl and 6 mL of sterile WFI. The zirconium isotopes were slowly eluted with 0.5 mL of the oxalic acid for each fraction in 5 fractions, which finally resulted in a ^{89}Zr radionuclide totalling of 2.5 mL of 1 mol/L oxalic acid. The activity of the elution was then measured in the dose calibrator which showed that more than 85% of the ^{89}Zr radionuclide was eluted from the hydroxamate resin column.

4.4.2 Conjugation of Herceptin (Trastuzumab) with *p*-isothiocyanatobenzyl-desferrioxamine (Df-Bz-NCS)

Firstly, when the bifunctional chelate *p*-isothiocyanatobenzyl-desferrioxamine B (Df-Bz-NCS) was conjugated with Herceptin (Trastuzumab), Df-Bz-NCS was coupled to the lysine groups of a mAb. The condition of this conjugation step comprised the

addition of a three-fold molar excess of Df-Bz-NCS to the mAb solution, a reaction at pH 9.0, followed by incubation at 37°C for 30 min. The reaction after incubation resulted in a reproducible chelate:mAb substitution ratio of about 1.5:1. This was assessed by trace labeling with ^{89}Zr in a standard solution of Zr-oxalate. Figure 4.2 shows the HPLC analysis result with a high peak between 10 to 15 minutes in 280 nm UV length on the conjugated Df-Trastuzumab suggesting that the Df-Bz-NCS was successfully conjugated with Trastuzumab.

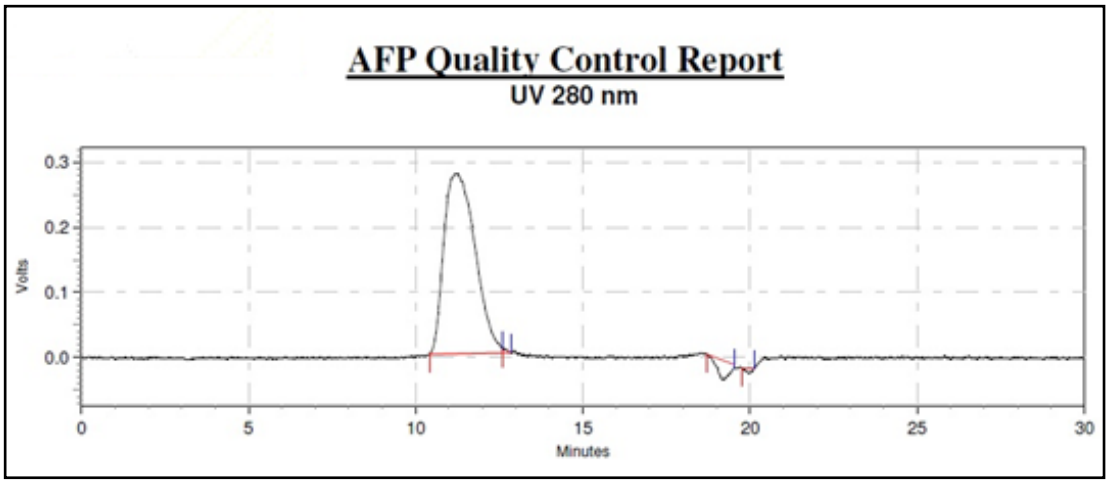

Figure 4.2 HPLC analysis result on conjugated Df-Trastuzumab

4.4.3 ^{89}Zr Radiolabelling with Df-Bz-NCS-Trastuzumab

In the next step, Df-Bz-NCS-mAbs were labelled with ^{89}Zr in 0.25 M HEPES buffer. After 60 min of incubation at room temperature at pH 6.8–7.2, the amount of ^{89}Zr

trans-chelated from oxalate to Df-Bz-NCSmAb was always more than 85% (mean, 91.9±4.6%). Labelling efficiency was distinctly higher at pH 6.8 and 7.2 than at pH 6.0, 6.2, and 7.4. The radiochemical purity was always >95% (mean, 97.5±0.7%; determined with ITLC and confirmed by HPLC) [97]. For radiolabeling analysis, a TLC test showed a high peak in the origin representing the labelled compound. A very low peak was observed in the solvent front representing the unlabelled compound (Figure 4.3). This would suggest that the mAb was sucessfully labelled with ^{89}Zr having a very high radiolabelling performance. For radiochemical analysis using HPLC test analysis, an overlapping peak was observed in both ^{89}Zr and trastuzumab between 10 to 15 minutes in 280 nm UV, indicating that the conjugated monoclonal antibody was successfully labelled with ^{89}Zr (Figure 4.4).

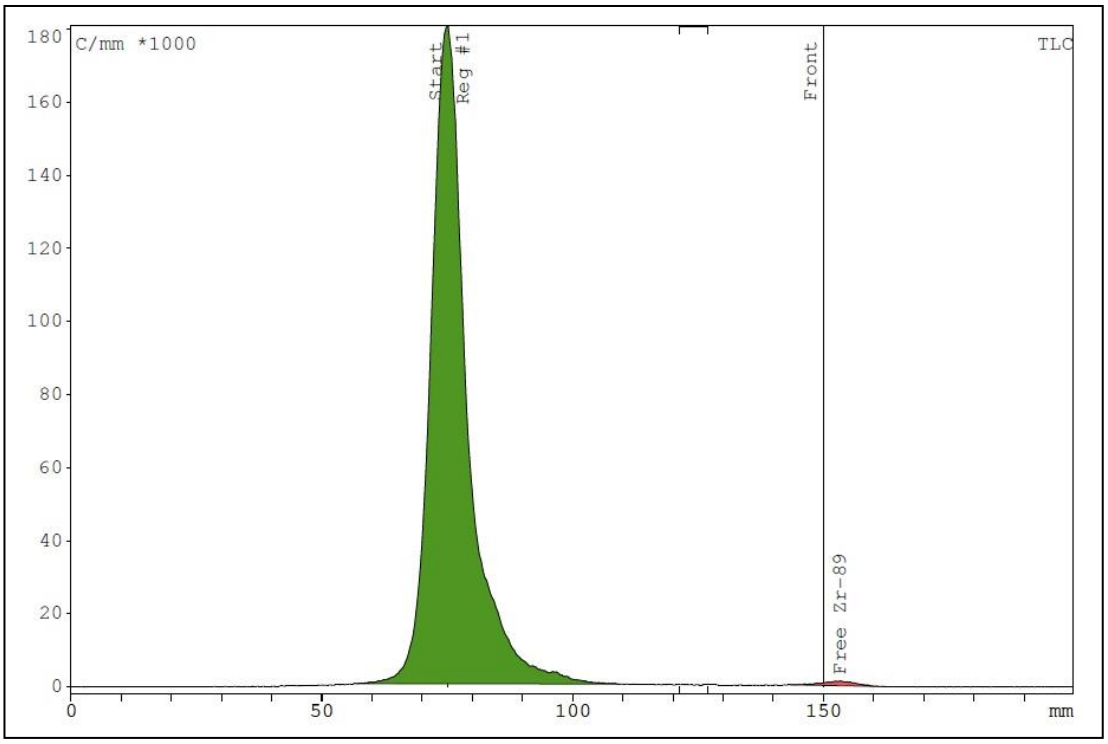

Figure 4.3 TLC analysis result of ^{89}Zr-Df-Trastuzumab

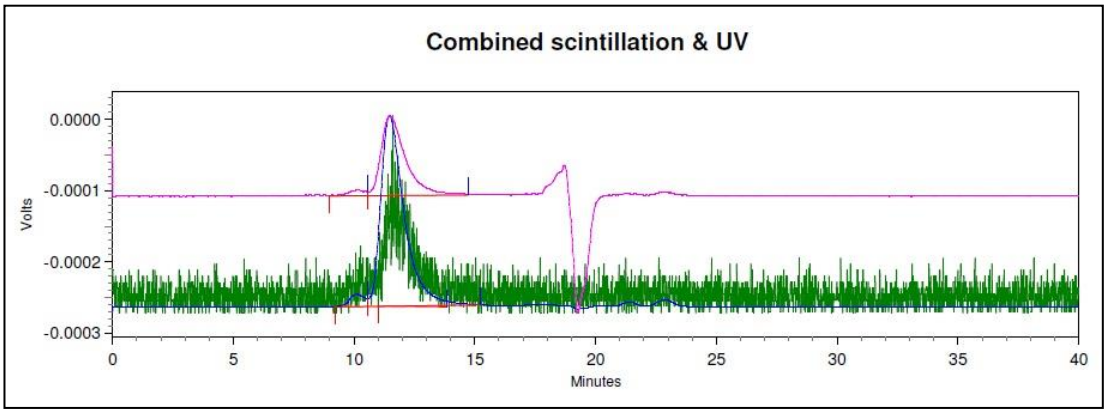

Figure 4.4 HPLC analysis result of ^{89}Zr-Df-Trastuzumab

Typically, total yields of 400 MBq ^{89}Zr were produced after 2.5 hours of irradiation with proton beam energy of 12 MeV and 10 μA beam current. After the end of bombardment, the target was then left overnight for cooling to allow for decay of the short-lived isomeric product, ^{89m}Zr [$t_{1/2}$=4.161(17) min] and other impurities. After 24 h, the ^{89}Zr produced from yttrium foil was taken out of the target boat in the cyclotron and dissolved in 12 M HCl. Dissolution was complete within 10 min but traces of a small black insoluble material were observed in the solution. This material is likely to be an insoluble form of yttrium chloride and was found not to contain any ^{89}Zr activity. Subsequently, the ^{89}Zr which was dissolved in 12 M HCl solution has to be diluted with distilled water down to 2 M of HCl concentration. This procedure has to be undertaken because the ^{89}Zr ions which were loaded to the pre-washed hydroxamate resin column were found to be sensitive to the concentration of HCl used. When using ≤ 2 M HCl concentration, the ^{89}Zr(IV) loading efficiency was found to be > 99.9 %. However, at higher HCl concentrations, (3-6 M), the binding affinity of ^{89}Zr to the hydroxamate resin decreases and at 6 M HCl, less than 26.0% of the activity was bound to the column. Higher concentrations of HCl were used to elute the ^{89}Zr from the hydroxamate resin column but the fact that they were unsuccessful indicates that the elution of ^{89}Zr from the hydroxamate resin column appears to be insensitive to acid concentration in contrast to resin loading [34].

Figure 4.5 shows the schematic representation of the conjugation involved in the conjugating process between Df-Bz-NCS and Trastuzumab [97]. This indicates that when the bifunctional chelate Df-Bz-NCS was conjugated with Trastuzumab, Df-Bz-NCS is coupled to the lysine groups of a mAb where the addition of a three-fold

molar excess of Df-Bz-NCS to the mAb solution had taken place to finally produce the conjugated monoclonal antibody.

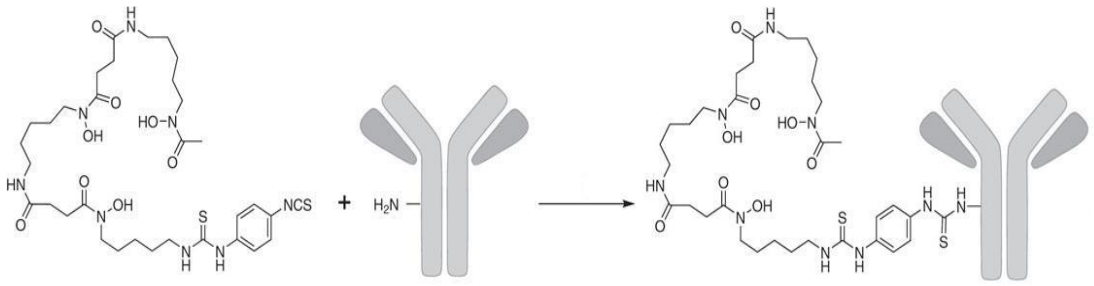

Figure 4.5 Schematic representation of monoclonal antibody (mAb) conjugation with a new bifunctional chelate Df-Bz-NCS [97]

Figure 4.6 shows the schematic representation of the radiolabelling process between the conjugated ^{89}Zr and Df-Trastuzumab. This demonstrates that when the ^{89}Zr was introduced to the conjugated monoclonal antibody, ^{89}Zr was bound to the hydroxamate group of the conjugated Df-Trastuzumab which finally produced the radiolabelled compound [97].

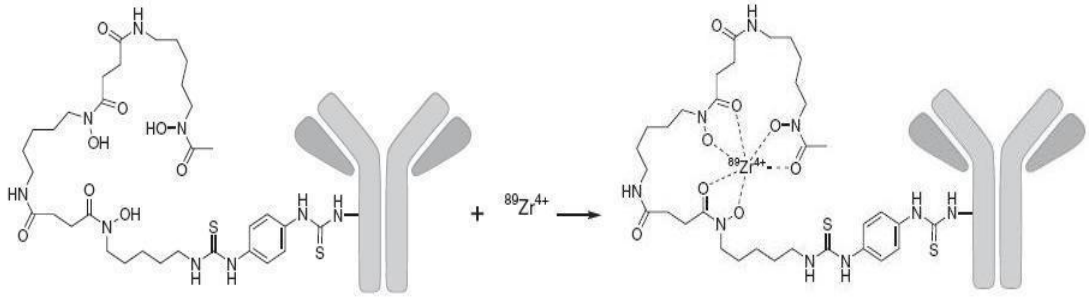

Figure 4.6 Schematic representation of labeling of conjugated mAb with ^{89}Zr [97]

Chapter 5: Zirconium-89 PET Imaging

After the monoclonal antibody had been successfully labelled with ^{89}Zr, the complex was studied for the effectiveness of the complex in binding with the specific tumours and the potential effectiveness of the complex in PET imaging for detection and monitoring of treatment responses.

It is essential to evaluate the effectiveness of the monoclonal antibody labelled with ^{89}Zr in animals before a targeted imaging technique can be used in humans in order to evaluate biodistribution, tumour concentration and PET detection capabilities. The radiopharmaceutical can then be assessed with *in vivo* studies [32, 36, 79, 88, 93, 108] using animals such as mice [36, 79, 93, 108] followed by human studies [21, 94]. In 2007, Sampath *et al.* used Balb/c nude mice, transplanted with the human breast cancer tumour cell line, SKBR-3, into the dorsal region of the mice left flank to investigate the biodistribution and concentration of the Trastuzumab-*N*-sucDf-^{89}Zr in the tumour site and the ability of the PET scanner to detect tumours using this complex. The tumour was grown to 0.5-0.8 cm in diameter and the mice were then injected via the tail vein with 200 µg of the ^{89}Zr labelled monoclonal antibody, Trastuzumab-*N*-sucDf-^{89}Zr and imaged right after injection, then 2 to 48 hours after injection [168]. The use of a mouse model is an important preliminary step in translating bench research into a means of identifying and perhaps subsequently treating cancer in human subjects.

Several preclinical immuno-PET from previous studies have been performed with ^{89}Zr-labelled mAbs as a prelude to clinical trials. These included, for example: the c-

mAb U36 [36], DN30 (anti-cMet), G250 [89], cetuximab [108], ibritumomab tiuxetan [94], rituximab, bevacizumab [90] and trastuzumab [169]. Also, for ^{89}Zr-labelled mAbs, sensitive tumour detection and accurate quantification with PET were demonstrated [44], while PET with ^{89}Zr-labelled mAbs appeared to be able to predict the biodistribution of ^{90}Y- or ^{177}Lu-labelled mAbs for RIT [44, 108]. Remarkably, the anti-VEGF mAb ^{89}Zr-bevacizumab also showed selective tumour uptake, possibly because of the proportion of human VEGF associated with extracellular matrix components [90]. Numerous clinical applications can be envisioned for this VEGF-specific tracer. Several other VEGF [170, 171] and VEGFR [172] PET imaging probes became available very recently. The introduction of an animal model allows the radionuclide to be assessed in the context of a full biological system.

A feasibility study has been performed in order to determine the optimal dosage and time of imaging of the monoclonal antibody ^{89}Zr-trastuzumab to enable PET imaging of human epidermal growth factor receptor 2 (HER2)-positive lesions. 14 patients with HER2-positive metastatic breast cancer received 37 MBq of ^{89}Zr-trastuzumab of one of three doses, namely; 10 or 50 mg for those who were trastuzumab-naive and 10 mg for those who were already on trastuzumab treatment. The patients were sent for at least two PET scans between days 2 and 5. The study showed that the best time for assessment of ^{89}Zr-trastuzumab uptake by tumours was 4–5 days after the injection [131]. The trastuzumab-naive patients required a 50 mg dose of ^{89}Zr-trastuzumab for optimal PET-scan results and patients already on trastuzumab treatment required only a 10 mg dose of ^{89}Zr-trastuzumab. The accumulation of ^{89}Zr-trastuzumab in lesions allowed PET imaging of most of the known lesions, as well as

some that had been undetected earlier. PET scanning after administration of ^{89}Zr-trastuzumab at appropriate doses allowed visualization and quantification of uptake in HER2-positive lesions in patients with metastatic breast cancer.

Several clinical trials with ^{89}Zr-labelled mAbs have recently taken place, including a study of ^{89}Zr-trastuzumab for the detection of HER-2–positive tumour lesions in breast cancer patients and for the quantification of HER-2 expression levels [169]. The highest uptake was found in HER2 positive tumours at 144 hours post injection (40% ID/g tissue for ^{89}Zr-trastuzumab and 47% ID/g for ^{111}In-ITC-DTPA-trastuzumab) compared to 8% ID/g tissue in HER2 negative control tumours. Liver uptake was low (8–12% ID/g tissue). Preliminary results from the first patients in that study showed excellent tumour tracer uptake and a resolution that was much better than that observed in previous SPECT studies with ^{111}In-trastuzumab [130].

In *in vivo* validation, a study where the ^{89}Zr-Df-trastuzumab localised in mice bodies was undertaken. The use of a mouse model is an important preliminary step in translating bench research into a means of identifying and perhaps subsequently treating cancer in human subjects.

5.1 Methodology

All experimental components of the methods were conducted at Peter MacCallum Cancer Centre, East Melbourne, Victoria, Australia. A small animal PET scanner (Philips Mosaic) was used to conduct PET imaging study of the radiolabelled compounds. The imaging aperture is 20 cm and the axial length is 12 cm. The system

has high spatial resolution (2 mm), with high sensitivity and large transverse imaging field-of-view of 12.8 cm.

5.1.1 Tumour Model

The labelled radiopharmaceuticals underwent *in vivo* testing in female Balb/c nude mice models that have a low immune system but no diseases, with LS174T (HER2-expressing) tumours. PET imaging was performed on them to determine if the label was successful *in vivo* in providing useful information from the images. A Balb/c nude mouse was injected subcutaneously on the right flank with the HER2 positive LS174T colorectal tumour. Two weeks later when the tumour reached a volume of approximately 180 mm^3, or the size of the tumours had grown to 0.5-0.8 cm in diameter, the imaging studies of ^{89}Zr-Df-Trastuzumab uptake were performed.

5.1.2 Preclinical Imaging of Tumour Model

The female Balb/c nude mouse with the HER2 positive LS174T colorectal tumour was injected via the tail vein with 200 µL of 1.85 MBq ^{89}Zr-Df-trastuzumab in saline solution. The mouse was then anaesthetised in 3% isofluorane in 50% oxygen in air and placed on the bed of a Philips Mosaic small animal PET scanner (Figure 5.1). Image data was acquired over 10 minutes; with corrected decay & randoms, and a 3-D RAMLA algorithm was used in reconstructing images [173]. The mouse was imaged by PET scanner at 24 hours post-injection.

Figure 5.1 Small Animal PET Facilities at Peter MacCallum Cancer Centre, Melbourne, Australia

5.2 Result

For PET imaging experiments, the PET images in Figure 5.2 show the *in vivo* behaviour of the ^{89}Zr-Df-Trastuzumab with phosphoric acid as an extraction agent in female Balb/c nude mice models, with LS174T (HER2-expressing) tumours. The images were taken at 24 and 48 hours post-injection. The tumour uptake of radiolabel at that time was noted. The quality of the image was limited by a low

activity of radiolabel. It appeared that most of the activity is localised in the liver. This could be due to its being ^{89}Zr-Df conjugation.

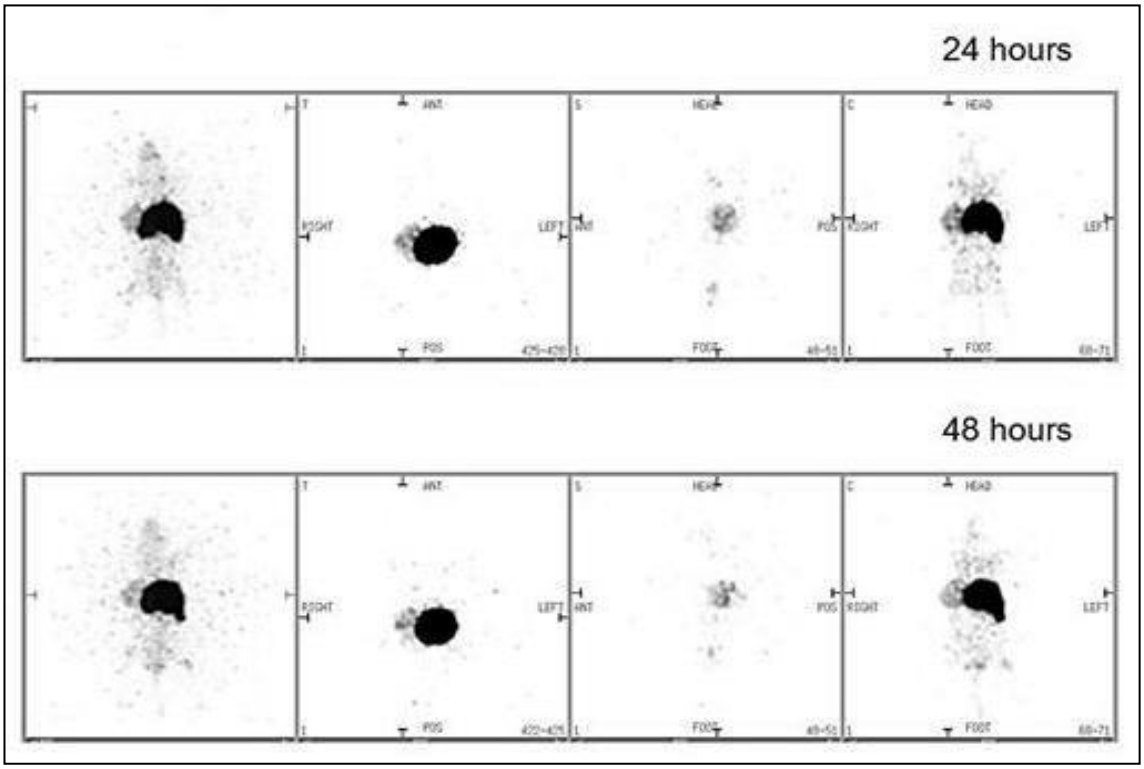

Figure 5.2 Small animal PET images using ^{89}Zr-Df with phosphoric acid as an extraction agent at 24 and 48 hours after injection

Figure 5.3 shows the PET images of the free ^{89}Zr in female Balb/c nude mice models, with LS174T (HER2-expressing) tumours, where the mouse was injected with 1.85 MBq (200 µL) of free ^{89}Zr. The images were taken at 1, 4 and 24 hours post-injection respectively. Following that, the skeletal uptake of free ^{89}Zr was noted at 24 hours post-injection and it was expected that free ^{89}Zr would be localised in the bone.

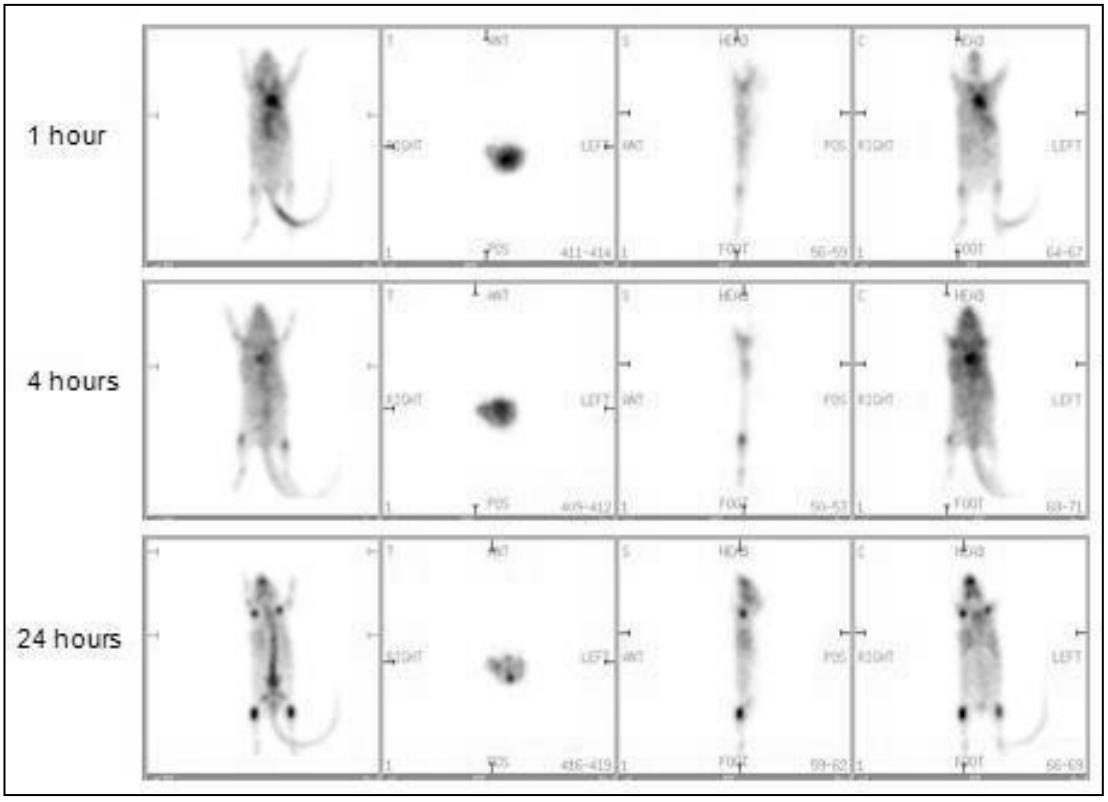

Figure 5.3 PET images using free ^{89}Zr, applied to a female Balb/c nude mouse model with subcutaneous LS174T tumour (HER2-expressing colorectal model) on the right flank

Next, the experiment on biodistribution and imaging of the female Balb/c nude mouse with the HER2 positive LS174T colorectal tumour, which was injected via the tail vein with 200 µL of 1.85 MBq ^{89}Zr-Df-trastuzumab in saline solution, showed a selective accumulation of ^{89}Zr-Df-Trastuzumab in tumour-bearing mice. The images at 24 hours show good tumour tracer uptake in the right flank, as well as cardiac uptake, which is a consequence of HER2 receptor expression on the heart suggesting that monoclonal antibody was successfully labelled with ^{89}Zr. (Figure 5.4).

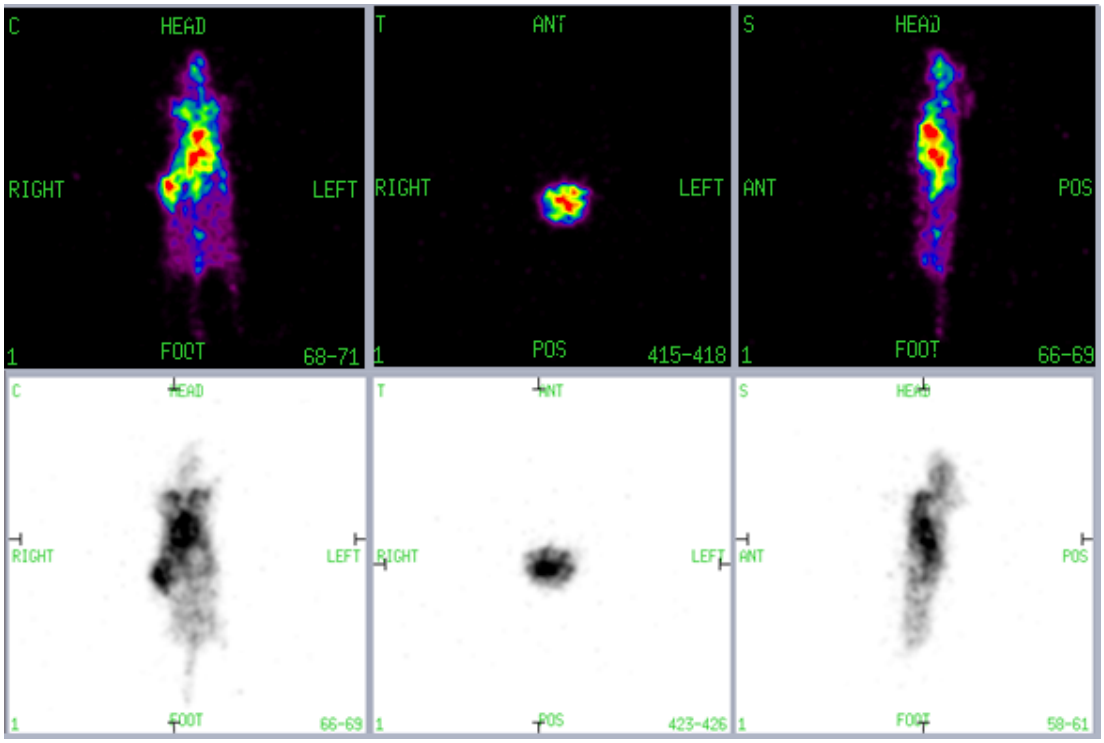

Figure 5.4 PET images using ^{89}Zr tracer bound to mAb as ^{89}Zr-Df-Trastuzumab, applied to a female Balb/c nude mouse model with subcutaneous LS174T tumour (HER2-expressing colorectal model) on the right flank

5.3 Discussion

HER2, which is a member of the ErbB tyrosine kinase receptor family, contributed in cell survival, metastasis, angiogenesis, differentiation, proliferation [109, 111, 129]. Overexpression of HER2 has been found in a wide variety of human cancers.

In our *in vivo* validation, a study where the ^{89}Zr-Df-trastuzumab was localised in mice bodies has been undertaken. PET imaging was performed on them to determine if the label was successful *in vivo* in providing useful information from the images. Experiments on PET imaging of the female Balb/c nude mouse with the HER2 positive LS174T colorectal tumour with ^{89}Zr-Df-trastuzumab were meant to validate the radiolabelled ^{89}Zr with monoclonal antibody (mAb). This disclosed the fact that radiolabelled ^{89}Zr with mAb showed an uptake to the targeted organ.

For the labelling of Df-Trastuzumab with [^{89}Zr]Zr-phosphate, the *in vivo* results following injection of the radioimmunoconjugate into female Balb/c nude mice models, with LS174T (HER2-expressing) tumours showed no uptake in the tumour that was located on the right flank at 24 and 48 hours respectively. The activity appears to have accumulated in the liver, suggesting that the label has denatured *in vivo* forming ^{89}Zr-Df conjugation.

For the labeling of Df-Trastuzumab with [^{89}Zr]Zr-chloride, there was no uptake of the ^{89}Zr-Df-Trastuzumab to the tumour, suggesting that the monoclonal antibody was not labelled with ^{89}Zr. However, skeletal uptake of the tracer was noted at 24 hours post-injection, suggesting that free ^{89}Zr was localised in the bone.

For immuno-PET, there are two common methods of excretion and/or degradation of the radiotracer, namely: demetalation/ligand dissociation and hydrolysis of the linker group between the mAb and the metallo-chelate. For these situations, PET imaging data would demonstrate that high liver accumulation may be expected if ^{89}Zr ions are lost from potential [^{89}Zr]Zr-Df-mAb immune-PET conjugates *via* demetalation. On the other hand, rapid renal excretion may be anticipated if the [^{89}Zr]Zr-Df-mAb complex remains intact, which would then decrease background tissue accumulation and enhance image contrast [34].

For the labeling of Df-Trastuzumab with [^{89}Zr]Zr-oxalate, the result showed a selective accumulation of ^{89}Zr-Df-Trastuzumab in tumour-bearing mice, where the images at 24 hours show good tumour tracer uptake in the right flank. Apart from that, there was also an indication of cardiac uptake, a consequence of HER2 receptor expression on the heart, in accordance with the known pharmacokinetics of trastuzumab [174]. The image was a little noisy but considering the injected dose, delayed imaging and the low positron yield for ^{89}Zr, the quality of PET image was acceptable. Options for other reconstruction algorithms more suited to low counts might reduce noise in the image if needed. The selective and accumulation uptake of the compound to the tumour, as well as cardiac uptake, demonstrated that monoclonal antibody was labelled with ^{89}Zr.

Essentially, the exact mechanisms underlying such dose-dependent pharmacokinetics of ^{89}Zr-trastuzumab are unknown; but one possible explanation is that it involves rapid but saturable elimination of low doses from the circulation during the first elimination phase, which has a half-life of ~4 days. Another mechanism that may

play a role in increasing ^{89}Zr-trastuzumab clearance in trastuzumab-naive is the presence of high plasma levels of extracellular domains shed by HER2. In this instance, the resulting complex of ^{89}Zr-trastuzumab with extracellular domains is cleared by the liver and excreted into the intestines [131].

The ability of ^{89}Zr-trastuzumab PET to quantify the alternations in HER2 expression level after treatment with a heat shock protein 90 (Hsp90) inhibitor has been investigated [33]. PET imaging revealed a significant decrease of tracer uptake in the tumour, indicating that ^{89}Zr-trastuzumab PET can be employed for non-invasive quantification of HER2 down-regulation after treatment. Related discoveries were also perceived in a separate study using a differently labelled ^{89}Zr-trastuzumab and a different Hsp90 inhibitor [79]. Recently, site-specific labelling of engineered trastuzumab (through cysteine residues) with ^{89}Zr was reported [101]. The resulting tracers were stable in serum and showed PET imaging properties comparable to conventionally prepared ^{89}Zr-trastuzumab, where labelling was achieved through the lysine residues.

Chapter 6: Hydroxamate Resin for Gallium-68 Generator

My next series of experiments are intended to study the potential of hydroxamate resin column (which was successfully being used as a column separator in our previous series of ^{89}Zr purification and extraction experiments), to be used in Gallium generator for ^{68}Ga elution and radiolabelling. From my previous experience in trapping the ^{89}Zr in hydroxamate resin column, it is believed that the column can also be used to trap ^{68}Ga, purify and extract the radionuclide from hydroxamate resin column and finally be labelled to conjugated monoclonal antibody to produce ^{68}Ga radiopharmaceutical for PET imaging study.

6.1 Radionuclide generators

Radionuclide generator systems continue to play an important role in providing both diagnostic and therapeutic radionuclides for various applications in nuclear medicine and oncology. A major turning point in the way radionuclides are produced was the invention of the ^{99}Molybdenum/^{99m}Technetium (^{99}Mo/^{99m}Tc) radionuclide generator for clinical use. ^{99m}Tc is the most common radionuclide used and current Nuclear Medicine departments employ on-site ^{99m}Tc generators for easy and cost-effective production [175, 176].

Generator systems involve long-lived parent radionuclides which naturally decay to produce shorter-lived daughter radionuclides. Both radionuclides are contained in a chromatography system which allows separation and extraction of the desired daughter radionuclide, through a process referred to as elution. Extraction through

elution is possible in a generator, as the parent and daughter radionuclides are two separate elements and therefore, do not have similar chemical properties. The parent is chemically attached to the column matrix; the daughter radionuclide forms a chemical bond with the eluting solution and is removed from the generator system. Once removed from the generator, the daughter radionuclide can be replaced through constant radioactive decay from the parent radionuclide in the system. The shelf life of individual generator systems is dependent on the physical half-life of the parent radionuclide and, therefore, length of clinical use of each generator type varies [175, 176].

The most widely used radionuclide generator for clinical applications is the ^{99}Mo/^{99m}Tc generator system. However, in recent years, there has been an enormous increase in the use of generators to provide therapeutic radionuclides. This has contributed to the development of complementary technologies for targeting agents for therapy and in the general increased interest in the use of unsealed therapeutic radioactive sources. The invention of the ^{99}Mo/^{99m}Tc generator reduced the need for other types of Nuclear Medicine generators. However, as molecular imaging undergoes continuous growth, other generator types such as the ^{68}Germanium/^{68}Gallium (^{68}Ge/^{68}Ga) generator are gaining acceptance in the field for use in PET [177, 178]. To date, the investigations into other generator types appear promising with the successful construction of the ^{82}Strontium/^{82}Rubidium generator, ^{113}Tin/^{113}Indium generator, and the ^{68}Ge/^{68}Ga generator. With the invention of generators that produce specific radionuclides, PET imaging is expected to become a

more cost-effective imaging modality, independent of constant cyclotron access [179].

6.2. Gallium-68 generators

^{68}Ga is a generator-produced isotope with a half-life of 68 min. ^{68}Ga decays from Germanium-68 by positron emission via electron capture with 511 keV annihilation radiation [38, 40]. The photon abundance is 178% [41]. The ^{68}Ga electrochemistry consists of 3 available valence electrons. In general, the generator is made up of alumina loaded in a plastic or glass column. The commercially available ^{68}Ge/^{68}Ga generators operate on similar concepts to the ^{99m}Tc generator, despite the many more complex processes involved [180]. Current sources of ^{68}Ge, used in ^{68}Ge/^{68}Ga generators, are produced by proton bombardment in a cyclotron and must be chemically attached to the column matrix for generator construction [181, 182]. ^{68}Ge has a strong affinity for metal oxides as well as organic materials [183, 184]. Carrier free ^{68}Ge in HCl is neutralized in EDTA solution and absorbed on the column. ^{68}Ga is eluted from the column with 0.05 M EDTA solution. Alternatively, ^{68}Ge is absorbed on a stannous dioxide column and ^{68}Ga is eluted with 1 M HCl. ^{68}Ge/^{68}Ga generator can be eluted quite frequently since maximum yield is obtained in a few hours. Due to the long half-life (271 days) of ^{68}Ge, the ^{68}Ge/^{68}Ga generator can be used for 1–2 years which allows PET imaging at facilities without the on-site cyclotron. The half-life of ^{68}Ga is long enough to permit multiple-step radiotracer syntheses and data requisition over longer periods. With properly designed radiotracers, ^{68}Ga could become the radionuclide as useful for PET imaging as for

^{99m}Tc for planar and SPECT imaging. There are a lack of efficient production methods for ^{68}Ge, thus ^{68}Ga is often considered the most cost-prohibitive radionuclide for PET imaging [185, 186]. A major advantage of the ^{68}Ge/^{68}Ga generators is the long shelf life of greater than one year which is a direct result of the 270 day half-life of ^{68}Ge, the parent radionuclide [179, 180]. This long lifespan is of great importance as it reduces dependence on constant cyclotron access, thereby increasing the likelihood of the expansion of PET to more rural areas where cyclotrons are less common [177, 179, 181].

^{68}Ga radiopharmaceutical labelling largely depends on obtaining a pure and useable form of the ^{68}Ga. Proposed purification methods involve minimizing the undesired presence of metal ions through the insertion of a post elution purification. As current generator systems solely use inorganic materials for matrix construction, organic polymers for use in matrix construction would appear to overcome some current disadvantages such as contaminants which arise from matrix composition [181].

1,4,7,10-tetraazacyclododecane-1,4,7,10-tetraacetic acid (DOTA) is increasingly being used as a versatile chelator that binds a large number of main group and transition metal ions as well as Ga with high stability constants [187]. Classes of biomolecules to which DOTA may be conjugated include macromolecules such as antibodies [188] or antibody fragments, small peptides, peptidomimetics or nonpeptide receptor ligands [189].

The most interesting DOTA-based ^{68}Ga radiotracer, i.e. ^{68}Ga-DOTATOC, is clearly superior to the other DOTA somatostatin analogs as well as Octreoscan^{TM} as indicated by its uniquely high tumour-to non-target tissue ratio [190]. In particular,

radiogallium isotopes labelled with somatostatin analogues may give us the opportunity for diagnosis and therapy of somatostatin receptor (SSTR) positive tumours. Other ^{68}Ga small molecules have been prepared and used for their possible diagnostic value [144, 191].

6.3 Elution Tests of ^{68}Ga from Hydroxamate Resin Column

^{68}Ga was eluted from the ^{68}Ga generator using 0.5 M of hydochloric acid (HCl) and the level of radioactivity was measured using an ionization chamber. Sodium hydroxide (NaOH) was then added to the ^{68}Ga solution to turn it into alkaline with a pH range of 8-9. In the meantime, the experimental setup for the elution test was rinsed with 4 M HCl and distilled water. After that, hydroxamate resin is suspended in 0.9% NaCl before being packed into the column. Thereafter, the column is rinsed with 5 mL MeCN, 10 mL 0.9% NaCl and 2 mL 2 M HCl.

When the experimental setup for the elution test was rinsed and ready, Approximately 200 MBq out of the overall amount of ^{68}Ga solution was then loaded to the pre-washed hydroxamate resin column. Under these conditions, ^{68}Ga remained bound to the resin and the column was washed with 6 mL of sterile WFI where the ^{68}Ga was trapped. Following that, various buffers at pH 4 including acetate and citrate and HCl itself were used to elute the ^{68}Ga from the column, respectively (Figure 6.1). The activity of each elution was then measured in a dose calibrator.

Figure 6.1 Elution of ^{68}Ga from hydroxamate resin column

6.4 Gamma spectroscopy of ^{68}Ga

The ^{68}Ga produced from the elution was verified through its decay mode, emission energies and half-life. After the elution, the samples were measured for their level of radioactivity. Radionuclidic purity was determined by measuring the energy peaks using a multi-channel analyser. The presence of gamma energies in the sample can be analysed by gamma spectroscopy, showing the presence of radioactive isotopes. A

gamma spectroscopy test with MCA gamma counter was undertaken for ^{68}Ga verification by measuring the peak at 511 keV in ^{68}Ga. It was then compared to a known amount of ^{18}F as well as ^{89}Zr in the same region of interest (ROI) where quantification is possible. The ROI consisted of 21 channels (495-526 keV) around the peak of 511 keV. In this relative quantification, the contribution from background activity is (within a very good approximation) assumed to be equal.

6.5 Df-Trastuzumab Conjugation

Trastuzumab was conjugated with the novel bifunctional chelate *p*-isothiocyanatobenzyl-desferrioxamine B (Df-Bz-NCS) where Df–Bz–NCS is coupled to the lysine–NH2 groups of Trastuzumab. To begin the conjugation procedure, a threefold molar excess of Df-Bz-NCS (in 20 μl DMSO) was added to the Trastuzumab (2–10 mg in 1 ml 0.1 M $NaHCO_3$ buffer, pH 9.0), and incubated for 30 min at 37°C. This process finally produced the conjugated Df-Bz-NCS-Trastuzumab. Nonconjugated chelate was then removed by size exclusion chromatography using a PD-10 column (GE Healthcare Life Sciences) with 0.25 M sodium acetate or 0.9% sodium chloride 5 mg/ml (pH 5.0) as eluent for purification purposes. The Df-Bz-NCS-Trastuzumab can be stored in the freezer at -20^{o}C until the day of radiolabelling for at least 2 weeks. Figure 6.2 shows the experiment conducted on the conjugation of Trastuzumab with *p*-isothiocyanatobenzyl-desferrioxamine (Df-Bz-NCS).

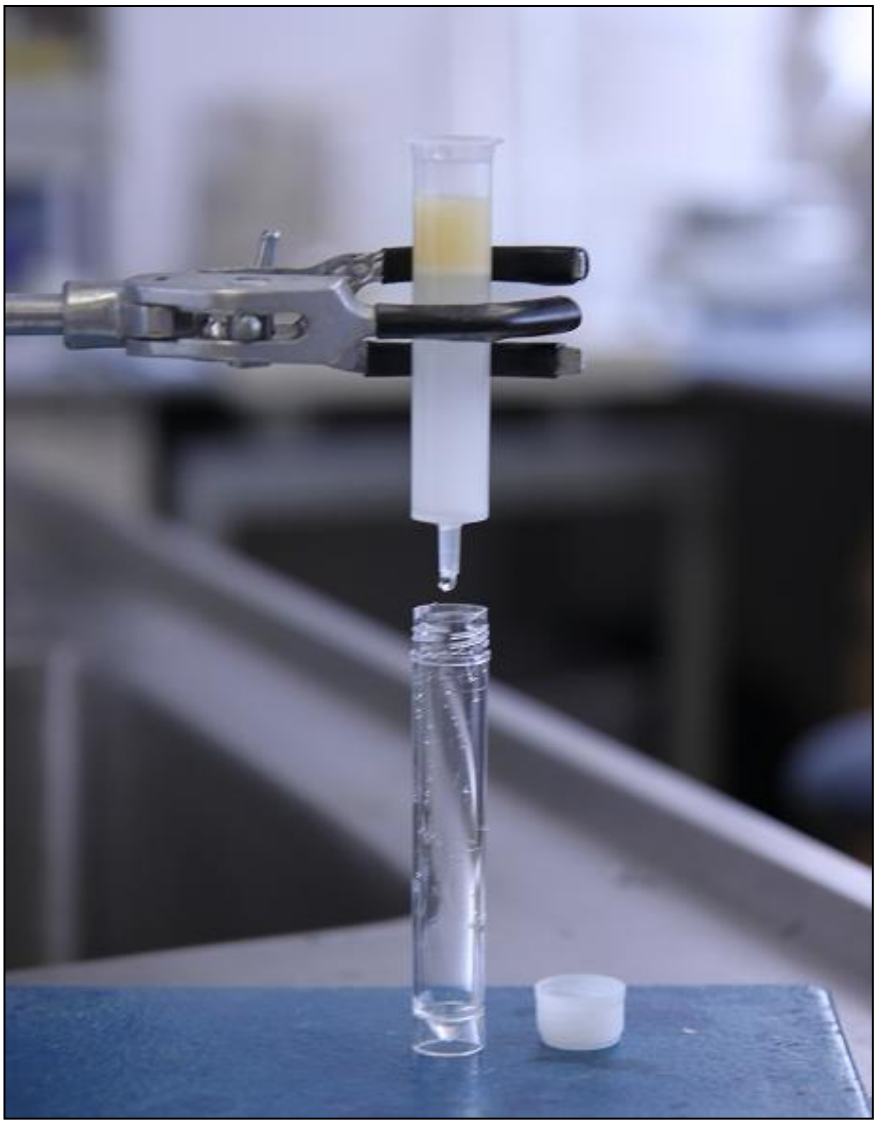

Figure 6.2 Conjugation of Trastuzumab with Df-Bz-NCS

6.6 ^{68}Ga radiopharmaceutical Labelling

6.6.1 ^{68}Ga-Df-Trastuzumab Direct Labelling

To begin with, ^{68}Ga was eluted from the ^{68}Ga generator using 0.5 M HCl, and 5 mL of it was added to 2.6 mL 1 M NaOH in order to achieve the final pH around 8 to 9 (alkaline solution). The sample was then loaded to the hydroxamate resin column and washed with 6 mL of H_2O. The ^{68}Ga was eluted with 2.5 mL of 0.1 M sodium citrate. Finally, 2 mL of Df-Trastuzumab was slowly added to the ^{68}Ga and incubated for 30 min before quality control was performed. The quality control method to test this was TLC and HPLC for radiolabelling performance and radiochemical analysis, respectively.

6.6.2 ^{68}Ga-Pentetreotide Labelling

5 mL of ^{68}Ga in 0.5 HCl was added to 2.6 mL 1 M NaOH in order to have the final pH around 8 to 9 (alkaline solution). The sample was then loaded to the hydroxamate resin column and washed with 6 mL of H_2O. The ^{68}Ga was eluted with pentetreotide in 0.1 M citrate form. The sample eluted was then sent for TLC and HPLC test analyses.

6.7 Result

Table 6.1 shows the average amount and percentage of ^{68}Ga eluted from 50 mg, 100 mg and 200 mg of hyrdoxamate resin respectively using 0.01 M, 0.05 M and 0.1 M of citrate buffer. The table indicated that for the elution of ^{68}Ga from 50 mg of hydoxamate resin using 0.01 M citrate buffer, 170 MBq (85 %) of the ^{68}Ga radioactivity was to be eluted from the column and decreased to 120 MBq (60 %) for 100 mg and 132 MBq (66 %) for 200 mg, respectively. For the elution of ^{68}Ga using 0.05 M citrate buffer, when using 50 mg of hydoxamate resin, 185.6 MBq (92.8 %) of the ^{68}Ga radioactivity was eluted from the column and decreased to 130 MBq (65 %) for 100 mg, but increased to 160 MBq (80 %) for 200 mg, respectively. Finally, for the elution test using 0.1 M citrate buffer, 195.6 MBq (97.8 %) of the ^{68}Ga radioactivity was eluted from the column and then decreased to 148 MBq (74 %) for 100 mg, but increased to 184 MBq (92 %) for 200 mg, respectively. Figure 6.3 shows the bar chart of the ^{68}Ga average amount eluted from 50 mg, 100 mg and 200 mg of hydroxamate resin respectively using 0.01 M, 0.05 M and 0.1 M of citrate buffer. Further calculation is shown in Appendix B.

Table 6.1

Average amount and percentage of ^{68}Ga eluted from 50, 100 and 200 mg hydroxamate resin column using Citrate Buffer at pH 4

Concentration of Citrate Buffer	50 mg Hydroxamate Resin (MBq)	% Eluted	100 mg Hydroxamate Resin (MBq)	% Eluted	200 mg Hydroxamate Resin (MBq)	% Eluted
0.01 M	170	85	120	60	132	66
0.05 M	185.6	92.8	130	65	160	80
0.1 M	195.6	97.8	148	74	184	92

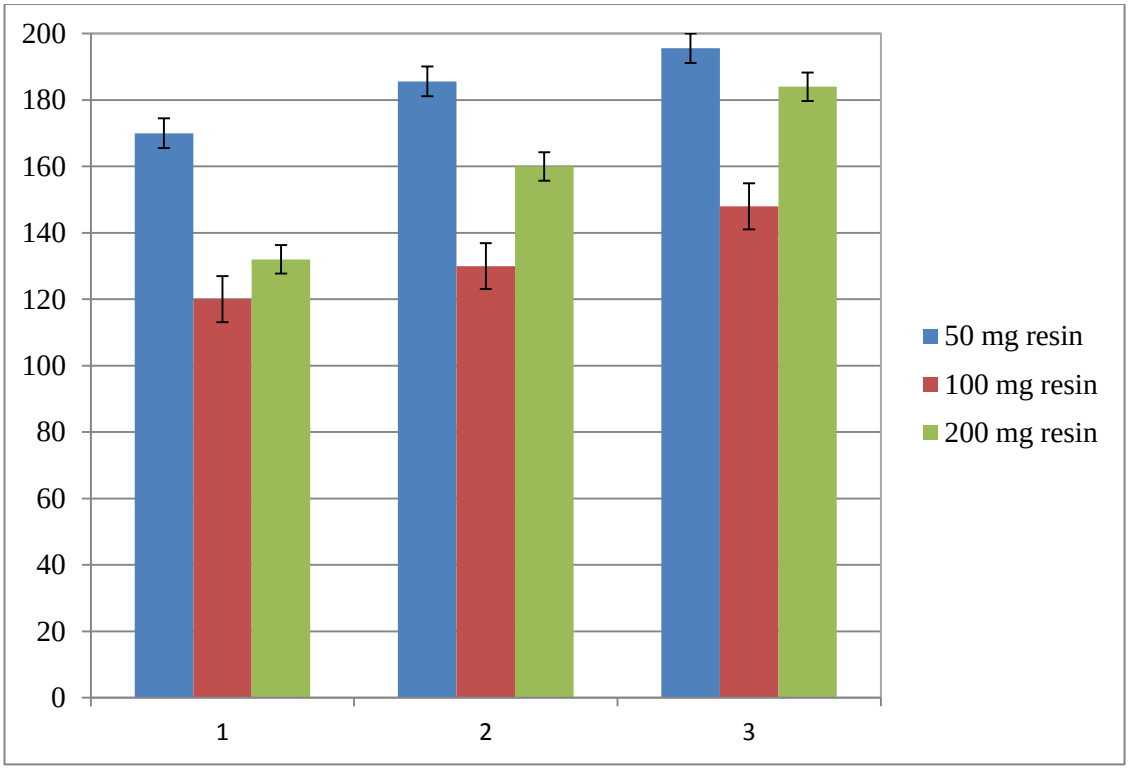

Figure 6.3 Average amount of ^{68}Ga in MBq eluted from 50, 100 and 200 mg hydroxamate resin column using 0.01, 0.05 and 0.1 M Citrate Buffer at pH 4

Table 6.2 shows the average amount and elution percentage of ^{68}Ga eluted from 50 mg hydroxamate resin column using 0.01, 0.05 and 0.1 M of HCl, respectively. The table indicated that when using 0.01 M HCl concentration to elute the ^{68}Ga from the column, approximately 12.8 MBq (6.4 %) of ^{68}Ga was eluted. For the elution of ^{68}Ga using 0.05 M HCl, approximately 81.4 MBq (40.7 %) of the ^{68}Ga radioactivity was eluted from the column and increased to 154.8 MBq (77.4 %) for 0.1 M HCl, respectively. Figure 6.4 shows the bar chart of the ^{68}Ga average amount eluted from 50 mg hydroxamate resin respectively using 0.01 M, 0.05 M and 0.1 M of HCl. Further calculation is shown in Appendix C.

Table 6.2

Elution of ^{68}Ga from 50 mg hydroxamate resin column using HCl

HCl Concentration	^{68}Ga Eluted (MBq)	% ^{68}Ga Eluted
0.01 M	12.8	6.4 %
0.05 M	81.4	40.7 %
0.1 M	154.8	77.4 %

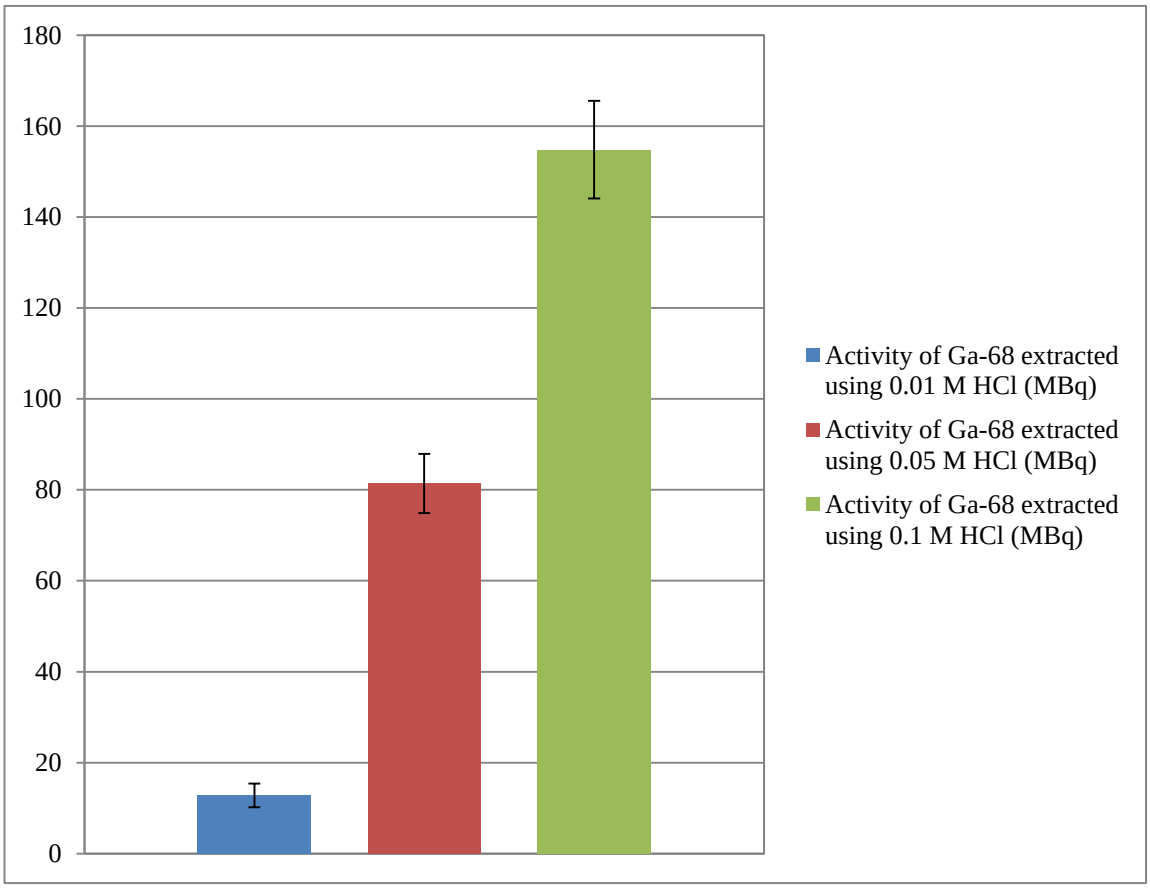

Figure 6.4 Average amount of ^{68}Ga eluted from 50 mg hydroxamate resin using 0.01, 0.05 and 0.1 M of HCl

Table 6.3 indicates the ^{68}Ga elution test from hydroxamate resin column using various buffers including acetate and citrate, citrate in HCl with different concentration and eluting with HCl itself. The table shows that 0.1 M Citrate Buffer eluted more than 60% (121.2 MBq) of ^{68}Ga from the hydroxamate resin column for the first 0.5 ml fraction compared to other solutions. 1 M Na Citrate in 0.5 M HCl was comparable with 0.5 M HCl with each of them extracting approximately 55.5 % (111 MBq) and 55.2 % (110.4 MBq) ^{68}Ga from the hydroxamate column, respectively. The amount of ^{68}Ga eluted from the column is shown in Figure 6.5 and further calculation is shown in Appendix D.

Table 6.3

Average amount and percentage of ^{68}Ga extracted from hydroxamate resin column using various solutions

^{68}Ga Extraction from Hydroxamate Resin Column	Amount of ^{68}Ga extracted (MBq)	% ^{68}Ga extracted from the column
1 M Na Citrate in 0.5 M HCl	111	55.5 %
0.5 M Na Citrate in 0.25 M HCl	89	44.5 %
0.2 M Na Citrate in 0.1 M HCl	51.4	25.7 %
0.1 M Na Citrate + 0.05 M HCl	44.8	22.4 %
0.1 M Citrate Buffer at pH 4	121.2	60.6 %
1 M Na Citrate + 1 M Citric Acid	101.4	50.7 %
0.5 M HCl	110.4	55.2 %
0.1 M HCl	52.8	26.4 %
0.01 M Citrate Buffer at pH 4	73.4	36.7 %
1 M Acetate Buffer at pH 4	0	0 %

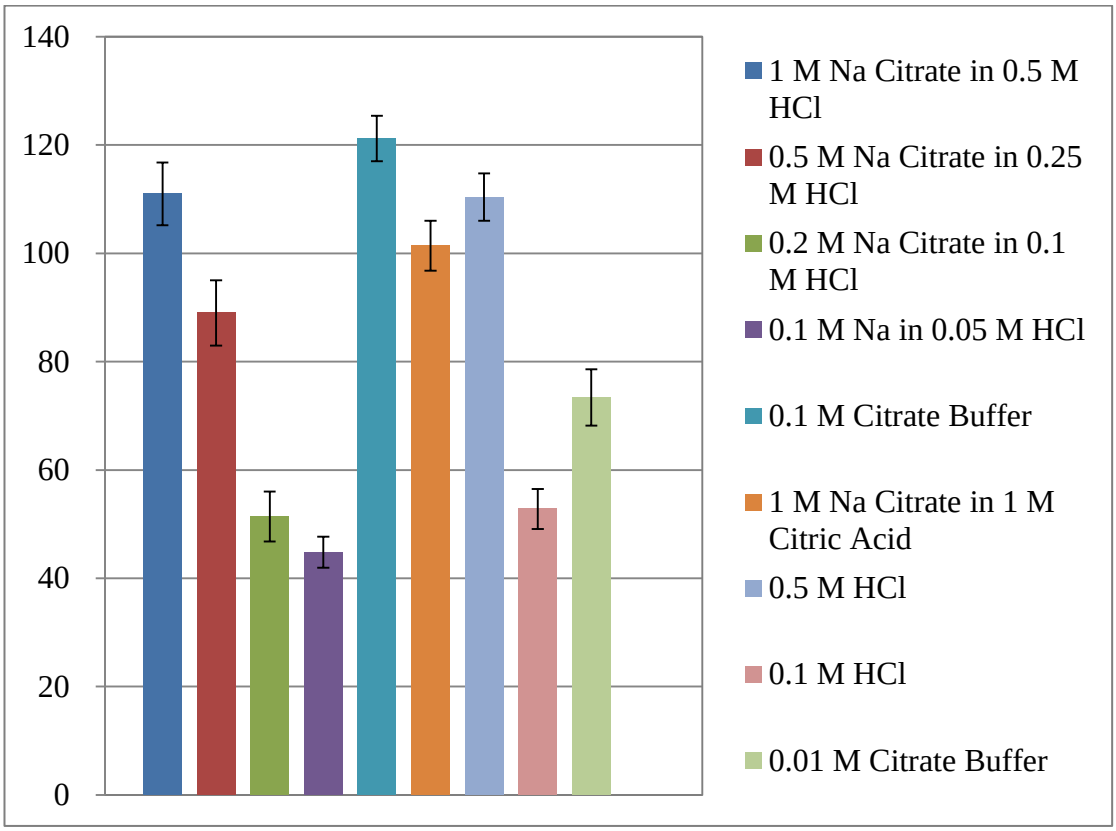

Figure 6.5 Average amount of ^{68}Ga in MBq extracted from hydroxamate resin column using various solutions

For ^{68}Ga-Df-Trastuzumab radiolabelling performance analysis, the TLC test showed a very high peak in the origin (Figure 6.6).

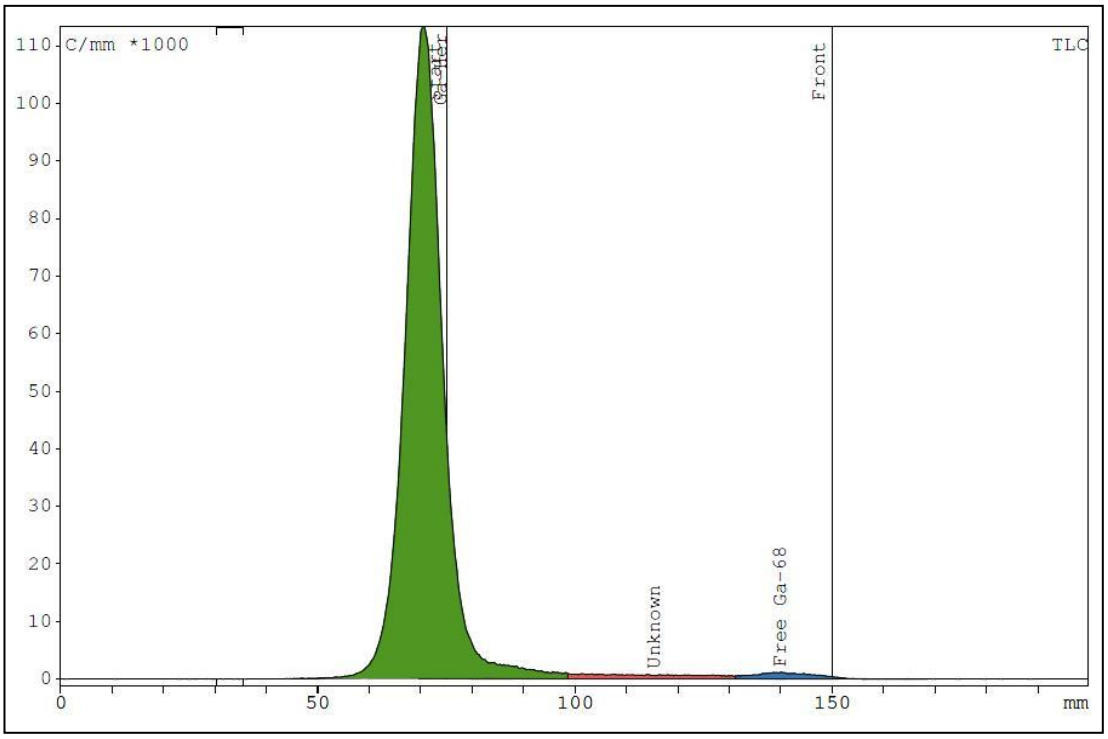

Figure 6.6 TLC analysis result of ^{68}Ga-Df-Trastuzumab

Figure 6.7 shows the HPLC analysis result on free ^{68}Ga. The figure indicated that a high peak of free ^{68}Ga was shown between 15 to 20 minutes in 280 nm UV.

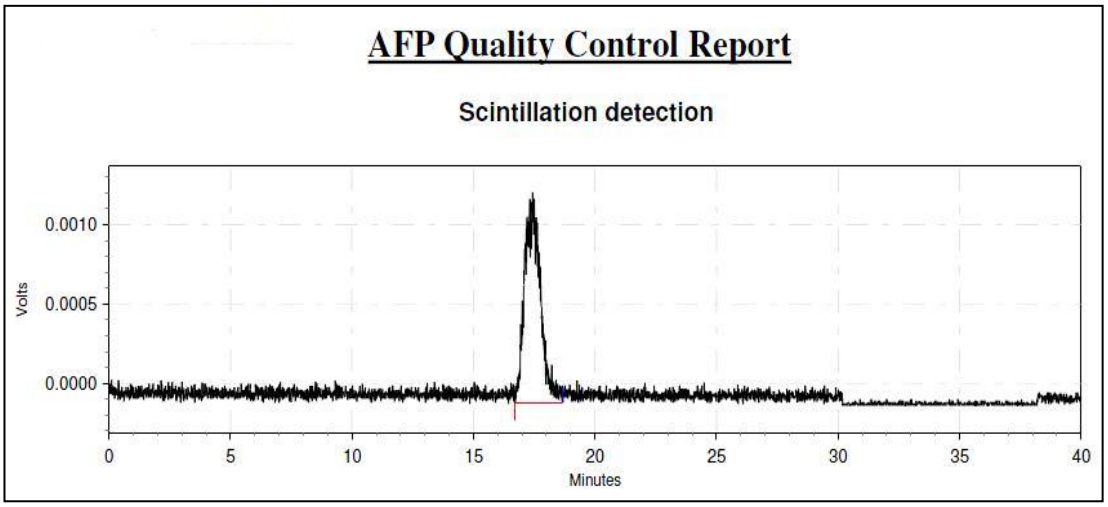

Figure 6.7 HPLC analysis result of free ^{68}Ga

For radiochemical analysis, the HPLC test showed the overlapping labelled peak in both ^{68}Ga and Df-Trastuzumab as between 10 to 15 minutes in 280 nm UV (Figure 6.8).

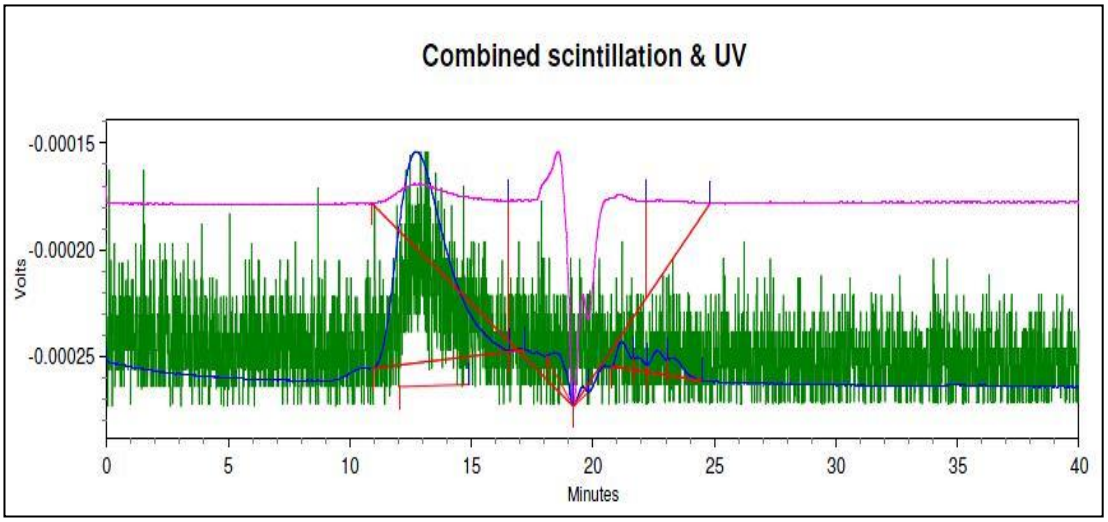

Figure 6.8 HPLC analysis result of ^{68}Ga-Df-Trastuzumab

For ^{68}Ga-Pentetreotide radiolabelling analysis, the TLC test showed a high peak in the origin (Figure 6.9). Apart from that, there are also two peaks observed in the solvent front.

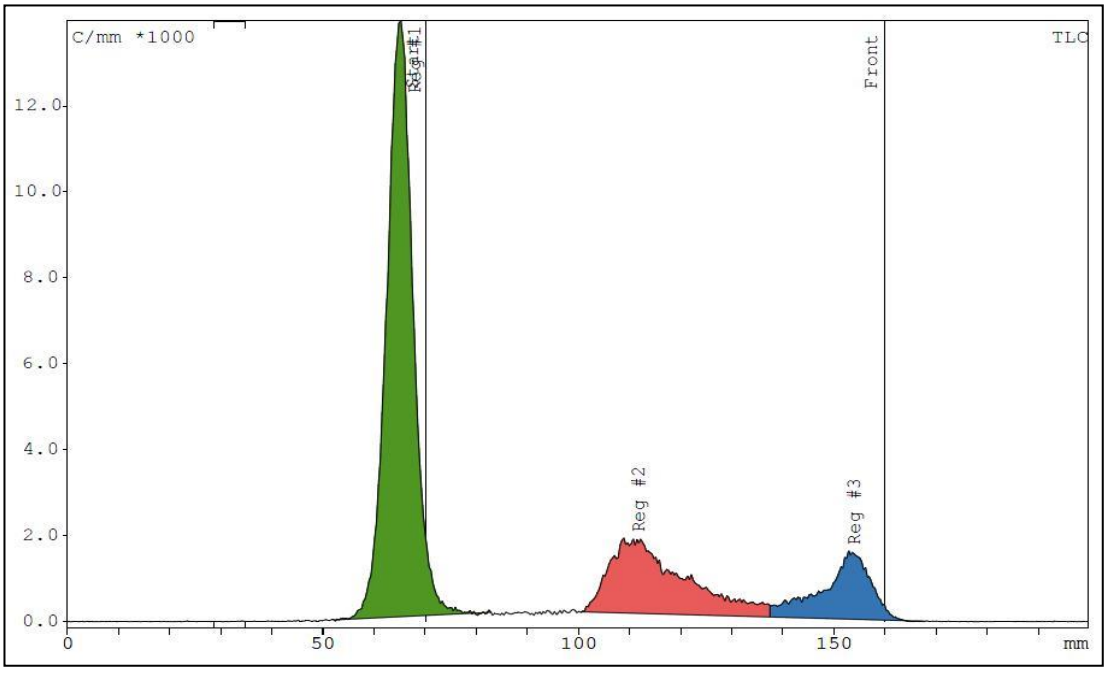

Figure 6.9 TLC analysis result of ^{68}Ga-Pentetreotide

For radiochemical analysis, the HPLC test showed the overlapping peaks in both ^{68}Ga and Pentetreotide between 10 to 15 minutes and free ^{68}Ga between 16 to 20 minutes in 280 nm UV, respectively (Figure 6.10). There were also overlapping peaks found in 280 nm UV between 24 to 27 minutes.

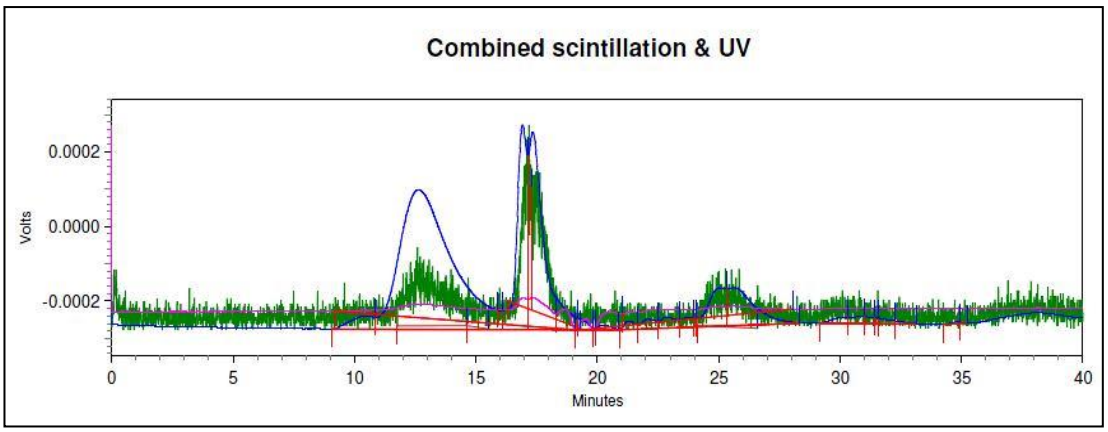

Figure 6.10 HPLC analysis result of ^{68}Ga-Pentetreotide

6.8 Discussion

The first experiment of this study sought to determine whether different hydroxamate resin quantities of 50 mg, 100 mg and 200 mg respectively affect the extraction and to determine different concentrations of 0.01 M, 0.05 M and 0.1 M of citrate buffer for evaluating the appropriate citrate buffer concentration for ^{68}Ga elution from hydroxamate resin column. Results from the experiments indicated that, when using 0.01 M citrate buffer at pH 4 as an extraction agent, the highest amount of ^{68}Ga radionuclide (85 %) was found to be eluted from 50 mg hydroxamate resin when compared with 100 mg (60 %) and 200 mg (66 %) in terms of the percentage (Table 6.1). The similar result was found in another two ^{68}Ga elution experiments using 0.05 M and 0.1 M citrate buffer, where the ^{68}Ga elution percentage of 92.8 % and 97.8 % from 50 mg hydroxamate resin, which demonstrated that 50 mg of the resin was suitable for the optimum extraction of the ^{68}Ga radionuclide. The experiment, which was also carried out to find the appropriate concentration of citrate buffer to elute ^{68}Ga from the hydroxamate resin column, indicated that 0.1 M citrate buffer provided the highest elution percentage of ^{68}Ga radionuclide (97.8 %) compared to 0.05 M (92.8 %) and 0.01 M (85 %) of citrate buffer concentration, respectively.

Second experiment was conducted to determine the appropriate concentration of HCl needed to elute the ^{68}Ga from 50 mg hydroxamate resin column. Results showed the elution percentage of ^{68}Ga from 50 mg hydroxamate resin column using 0.01, 0.05 and 0.1 M of HCl, respectively and concluded that 0.1 M HCl was able to elute the highest amount of ^{68}Ga radionuclide (77.4%).

Third experiment involved the ^{68}Ga elution test from hydroxamate resin column, using various buffers including: acetate and citrate, citrate in HCl with different concentration and eluting with HCl itself. These series of experiments were undertaken to determine the suitable buffer for ^{68}Ga elution, which showed that 0.1 M citrate buffer eluted more than 60 % of ^{68}Ga from the hydroxamate resin column for the first 0.5 ml fraction compared to other solutions. This indicated that a 0.1 M citrate buffer was suitable for ^{68}Ga elution from hydroxamate resin column. Citrate buffer was chosen in this series of experiments because citrate with appropriate pH has the advantage of perhaps being an easier environment in which to label radiopharmaceuticals compared to HCl.

The next series of experiments were the ^{68}Ga radiopharmaceutical radiolabelling where two sets of experiments were undertaken; one was ^{68}Ga-Df-Trastuzumab radiolabelling and the other one was ^{68}Ga-Pentetreotide radiolabelling. For ^{68}Ga-Df-Trastuzumab radiolabelling analysis, the TLC test showed a very high peak in the origin indicating that ^{68}Ga was successfully labelled to Df-Trastuzumab. Another radiochemical analysis test was undertaken using HPLC test analysis which showed the overlapping peaks in both ^{68}Ga and Df-Trastuzumab between 10 to 15 minutes in 280 nm UV, indicating the successful radiolabelling of the compound.

TLC test analysis for ^{68}Ga-Pentetreotide radiolabelling showed a high peak in the origin. However, there are also two peaks observed at the solvent front which indicated that the radiolabelling efficiency between ^{68}Ga and Pentetreotide was weak. Further testing on radiochemical analysis showed the overlapping peaks in both ^{68}Ga and Pentetreotide between 10 to 15 minutes and free ^{68}Ga between 16 to 20 minutes

in 280 nm UV. In addition, there was also an overlapping peak found in 280 nm UV, of between 24 to 27 minutes, suggesting a weak radiolabelling efficiency of the ^{68}Ga-Pentetreotide labelling.

Chapter 7: Conclusions and Future Directions

The set of experiments and observations presented in this thesis represent the production of ^{89}Zr using five different types of ^{89}Y solid target by a process of cyclotron bombardment with ^{89}Y(p, n)^{89}Zr reaction in a 12 MeV medical cyclotron at 10 µA beam current. ^{89}Zr was then purified and separated from the starting materials and other impurities using a hydroxamate resin column. The experiments continued on with radiolabelling of monoclonal antibodies with ^{89}Zr using the novel *p*-isothiocyanatobenzyl-desferrioxamine B (Df-Bz-NCS) as a bifunctional chelating agent. Herceptin® (Trastuzumab) was the monoclonal antibody of interest for these series of experiments as it showed a stable conjugation with the chelating agent.

This thesis also studied and discussed the experiments on the PET imaging studies of ^{89}Zr-labelled with monoclonal antibodies. These were conducted in order to examine the *in vivo* behaviour of ^{89}Zr-Df-Trastuzumab using female Balb/c nude mice models that have a low immune system but no diseases, with LS174T (HER2-expressing) tumours. PET imaging was performed on them to determine if the ^{89}Zr-labelled with trastuzumab was successful *in vivo* in providing useful information from the images at 24 hours after injection of ^{89}Zr-Df-Trastuzumab radiopharmaceutical.

Furthermore, the experiments on the potential of phosphoric acid to be used as ^{89}Zr extraction agent from hydroxamate resin column (thus labelling it with Df-Bz-NCS-Trastuzumab) have been discussed.

In addition, in Chapter 6, this thesis established and discussed the series of experiments on the elution of ^{68}Ga from hydroxamate resin column, followed by a study on the experiments on ^{68}Ga-labelled with Trastuzumab and Pentetreotide using hydroxamate resin column as an ion exchanger.

7.1 Production of ^{89}Zr

There are five different types of ^{89}Y solid targets that were successfully prepared as starting materials for ^{89}Zr production. These are, specifically: yttrium foil, yttrium nitrate, electrodeposited yttrium nitrate using two different methods of preparation and yttrium sputtering technique. The two different methods used in preparing electrodeposited yttrium nitrate include: electrodeposition of yttrium in aqueous bath (diluted nitric acid) and electrodeposition of yttrium in non-aqueous bath (ethanol), respectively.

According to the experiments, the amount of yttrium nirate used for yttrium nitrate compacting technique was 0.45g with 10 minutes preparation time. Preparation time on both aqueous and non-aqueous electrodeposition took up to 1 hour at room temperature during the electrodeposition process, with approximately 0.05 and 0.03 g respectively of the deposited ^{89}Y onto the copper target plate. For the yttrium sputtering technique, the final amount of yttrium produced after 10 minutes of sputtering process was 0.01 g, which was the lowest yield of ^{89}Y produced compared to other techniques. The easiest yttrium target preparation was the preparation of yttrium foil target plate where the preparation time took around 10 minutes and was usually for a layer of placement. Up to 0.20 g can be placed directly on the

aluminium target plate and up to 3 layers with altogether 0.6 g of yttrium foil can be placed on the aluminium plate to obtain a higher yield of the ^{89}Zr radioisotope produced after bombardment in the cyclotron which can provide approximately 400 MBq after the end of bombardment.

Five types of yttrium solid targets were bombarded, which successfully produced ^{89}Zr in a 12 MeV medical cyclotron. Yttrium foil produced the highest amount of ^{89}Zr radioactivity after bombardment compared to the other types of yttrium solid targets. As high amount of ^{89}Zr activity is needed for successful labelling with monoclonal antibody; yttrium foil was selected to be used as a starting material in the production of ^{89}Zr for radiolabelling and PET imaging study.

7.2 Purification of ^{89}Zr

The successfully produced ^{89}Zr radioisotopes using a 12 MeV medical cyclotron were loaded to the hydroxamate resin column and result indicated that 1.0 M of oxalic acid extracted more than 80% of ^{89}Zr radioactivity from the hydroxamate resin column. Usually, purification of ^{89}Zr involved a two-step procedure which involves the separation process of ^{89}Zr radionuclide from its impurities and starting materials, followed by extraction of the radionuclide from the retention column and hydroxamate resin column. This procedure has been widely used for separating ^{89}Zr which is embedded in the metal yttrium target, where ^{89}Zr can be separated from the target by ion exchange chromatography with an overall yield of ~80% [35, 151].

There was concern over the ability of zirconium in oxalate complexes to tran-chelate to Df [35]. However, a study has shown that chelation efficacy is not impaired by

oxalate since the oxalate can be removed and replaced by chloride on an anion exchange column [34]. Meanwhile, another study recommended that the chloride form is objectionable due to hypochlorite formation from radiolysis [36]. Later in 2010, a new bifunctional chelate was introduced for facile radiolabeling of monoclonal antibodies with ^{89}Zr, which is also able to remove the oxalate from the complex [97].

7.2.1 Alternative ^{89}Zr Extraction Agent

The significance of this study, by refining the separation and labelling techniques for ^{89}Zr-Trastuzumab and then validating the product through subsequent *in vivo* testing in mice, a simpler, safer and more effective immuno-PET imaging agent will be available to allow delayed imaging of specific tumours. These are important in any pre-radioimmunotherapy work-up to determine the following: if the patient is likely to respond to the therapy, to provide quantifiable information that can be used to calculate the radiation dose that will be delivered during therapy, and to help determine which are the dose-limiting organs [16]. It is anticipated that this can be achieved without the use of oxalic acid as an extraction agent, which is known to be highly toxic but is currently being widely used in ^{89}Zr extraction from hydroxamate resin column.

From the experiment, it has been determined that it is possible to use phosphoric acid as an alternative extraction agent for separating and purifying ^{89}Zr. It is also possible to label ^{89}Zr-phosphate to Df-Bz-NCS-Trastuzumab. However, further research needs to be undertaken, especially with regard to its *in vivo* behaviour. Oxalate from

^{89}Zr-oxalate can be removed and replaced by chloride using an activated Waters Sep-pak Light QMA strong anion exchange cartridge. However, another study recommended that the chloride form is undesirable due to hypochlorite formation from radiolysis [36]. Presently, oxalic acid is still the most successful agent for the separation and purification of ^{89}Zr used in labelling ^{89}Zr-Df-Trastuzumab. Although oxalic acid is toxic, it can be removed from the product via purification chromatography [32].

7.3 ^{89}Zr Radiolabelling

A high amount of ^{89}Zr activity was needed in order to be labelled with monoclonal antibody; hence yttrium foil was chosen as a target for bombardment on the 12 MeV medical cyclotron. It has been shown that yttrium foil provided a high amount of ^{89}Zr activity after bombardment. Approximately 400 MBq ^{89}Zr was produced after two and a half hours of irradiation with proton beam energy of 12 MeV and 10 μA beam current after the end of bombardment.

Herceptin (Trastuzumab) was conjugated with the novel bifunctional chelate *p*-isothiocyanatobenzyl-desferrioxamine B (Df-Bz-NCS) and finally the conjugated Df-Bz-NCS-Trastuzumab was labelled with ^{89}Zr to form ^{89}Zr-Df-Trastuzumab.

Results on the HPLC analysis on the conjugated Df-Trastuzumab suggest that the Df-Bz-NCS was successfully conjugated with Trastuzumab and the radiolabelling performance; while TLC analysis showed the highest peak of ^{89}Zr in the origin suggesting the mAb was successfully labelled with ^{89}Zr. For radiochemical analysis, HPLC test results showed the overlapping labelled peak in both ^{89}Zr and mAb at

between 10 to 15 minutes in 280 nm UV length suggesting that the mAb was successfully labelled with ^{89}Zr.

7.4 ^{89}Zr PET Imaging

Experiments on biodistribution and PET imaging of the female Balb/c nude mice with the HER2 positive LS174T colorectal tumour were undertaken to validate the successful radiolabelling procedure between ^{89}Zr and monoclonal antibody using ^{89}Zr produced in a 12 MeV medical cyclotron in preclinical condition. PET images at 24 hours showed a selective accumulation of ^{89}Zr-Df-Trastuzumab in tumour-bearing mice with good tumour uptake in the right flank (Figure 5.4). Tumour uptake of ^{89}Zr-Df-Trastuzumab was also observed in the cardiac (which having HER2 receptor expression on the heart), demonstrated that the conjugated monoclonal antibody was successfully labelled with ^{89}Zr.

Experiments on PET imaging of the radiolabelled ^{89}Zr-Df-Trastuzumab validated the successful radiolabelling between ^{89}Zr and monoclonal antibody using ^{89}Zr produced in a 12 MeV medical cyclotron and in preclinical conditions.

Nowadays, varieties of mAbs have been labelled with ^{89}Zr and several of these radiolabelled ^{89}Zr-mAbs have entered clinical studies with promising results. With the availability of ^{89}Zr and simpler radiolabelling techniques, it is expected that more ^{89}Zr PET tracers will be developed commercially in the future.

7.5 ^{68}Ga Elution from Hydroxamate Resin Column

Early and specific tumour detection, as well as therapy selection and response evaluation, are some challenges of improved medicine which usually involve high sensitive and specific molecular imaging such as positron emission tomography (PET). The use of peptides for PET molecular imaging has unquestionable advantages, including: the possibility of targeting through interaction of peptide-receptor, small size and low-molecular weight recommending good penetration in the tissue or at cellular level with low toxicity and no antigenicity, and also the possibility of a wide variety of choices for radiolabeling [192]. Among β^+-emitter radioelements, ^{68}Ga is a very attractive positron-emitter compared with carbon-11 or fluorine-18, taking into account its easy production via a ^{68}Ge/^{68}Ga generator and well-established radiochemistry. ^{68}Ga chemistry is based on well-defined coordination complexes with macrocycle or chelates having strong properties of binding which are suitable for linking peptides that allow resistance to in vivo transchelation of the metal ion. Understanding the mechanism of specific and nonspecific molecular in oncogenesis is one major key to developing new molecular imaging tools. The recent review focuses on peptide signalling involved in different oncogenic pathways. The signalization might be common for tumoural and non-tumoural processes, or could be indicative of an oncological process. Furthermore, the review describes gallium chemistry and different ^{68}Ga-radiolabelled peptides already in use or under development, aiming at developing molecular PET imaging of different oncological processes.

The first series of experiments on different quantity of hydroxamate resin column indicated that 50 mg of the resin was suitable for the optimum extraction of the ^{68}Ga radionuclide. The next series of experiments in finding the appropriate concentration of citrate buffer to elute ^{68}Ga from the hydroxamate resin column revealed that the highest elution percentage of ^{68}Ga radionuclide was eluted by 0.1 M citrate buffer, compared to 0.05 M and 0.01 M citrate buffer, respectively. The subsequent series of experiments in determining the suitable concentration of HCl to elute the ^{68}Ga from 50 mg hydroxamate resin column concluded that 0.1 M HCl was able to elute the highest amount of ^{68}Ga radionuclide.

A series elution test of ^{68}Ga from hydroxamate resin column using various buffers including: acetate and citrate, citrate in HCl with different concentration and eluting with HCl itself, indicated that 0.1 M citrate buffer at pH 4 was suitable for ^{68}Ga elution and comparable to 0.5 M HCl which is currently being used in ^{68}Ga elution from ^{68}Ge/^{68}Ga generator. The advantage of citrate having appropriate pH may result in an easier environment in which to label radiopharmaceuticals compared to HCl.

7.6 ^{68}Ga Radiolabelling

Experiments on the ^{68}Ga radiopharmaceutical radiolabelling concluded that ^{68}Ga-Df-Trastuzumab radiolabelling was successful according to TLC and HPLC analysis results. As for ^{68}Ga-Pentetreotide radiolabelling, TLC analysis results showed a high peak in the origin. However, there were also two peaks observed at the solvent front indicating that the radiolabelling efficiency between ^{68}Ga and Pentetreotide was weak. Further HPLC radiochemical analysis test results showed the overlapping

peaks in both ^{68}Ga-Pentetreotide, between 10 to 15 minutes and free ^{68}Ga, between 16 to 20 minutes in 280 nm UV. In addition, an unknown overlapping peak was found in 280 nm UV between 24 to 27 minutes, suggesting a weak radiolabelling efficiency of the ^{68}Ga-Pentetreotide labelling.

7.6 General Conclusion

The observations of this thesis have led to new suggestions concerning the production, purification, labelling and imaging of ^{89}Zr for targeted positron emission tomography (PET) radiopharmaceuticals.

Over the last several years, PET imaging with ^{89}Zr-based agents has been a highly dynamic research area. Presently, the majority of agents that have been labelled with ^{89}Zr are mAbs, since the decay half-life of ^{89}Zr matches very well with the biological half-life of antibodies.

Currently, labelling of ^{89}Zr is primarily through desferrioxamine B, which serves as the chelator where the ^{89}Zr-Df conjugate is quite stable for in vivo applications. Hence, the key to in vivo stability of ^{89}Zr-based tracers lies in the linkage between Df and the antibody or the nanoparticle. Although site-specific labeling of ^{89}Zr will not compromise the immunoreactivity of the resulting antibody conjugate, the requirement of protein engineering expertise will limit the wide-spread adoption of such site-specific labelling strategy.

There is currently significantly simplified radiochemistry such as the 2-step method, increased commercial available of the ^{89}Zr isotope supply and chelating agents

for ^{89}Zr radiopharmaceutical labelling, as well as successful proof-of-principle in pilot human studies. As a result, PET imaging of ^{89}Zr-based tracers is expected to be a constantly evolving and highly vibrant field for the next decade. Therefore, further efforts are needed to accelerate the translation of more promising ^{89}Zr-based tracers into clinical use.

In conclusion, the field of radioimmunoimaging with longer-lived positron-emitting radionuclides is believed to hold significant promise. However, several scientific and nonscientific challenges have to be conquered before realising the true potential of PET radioimmunoimaging with intact antibodies. This study is by definition a part of Nuclear Medicine aimed as a reference by which researchers can produce ^{89}Zr radionuclide in a medical cyclotron to be labelled to various types of proteins, monoclonal antibodies and peptides so that it could be safely used in a clinical environment.

7.7 Future Directions

The successful production of ^{89}Zr in a medical cyclotron demonstrated all the characteristics necessary for translation of ^{89}Zr radioisotopes to be labelled with monoclonal antibodies as PET agents into the clinical setting. This study has presented preliminary data on the preparation of ^{89}Y solid target as a starting material in the production of ^{89}Zr using a 12 MeV medical cyclotron. Subsequently, the study on the production, purification, labelling and imaging of ^{89}Zr for targeted positron emission tomography (PET) radiopharmaceuticals has also been presented.

The next stage of further investigations should be related to the mass production of ^{89}Zr so that ^{89}Zr radioisotope can be easily available in order to be used for further study on the radiolabelling process with various proteins and peptides. For this reason, ^{89}Zr production using yttrium foil in a medical cyclotron with increased irradiation time of 4 to 6 hours is suggested so that a higher yield of ^{89}Zr can be produced in a clinical condition. This can then be used to further the studies on PET imaging of radiolabelled compounds.

References

1. Pillai, M.R.A. and M. Haji-Saeid, *Cyclotron Produced Radionuclides : Principles and Practice*, in *Technical reports series* 2008, International Atomic Energy Agency.
2. Harbert, J. and A.F.G. Da Roche, eds. *Textbook of Nuclear Medicine*. Basic Science. Vol. 1. 1984, Lea and Febiger, Philadelphia, PA
3. Sorenson, J.A., Phelps, M.E., ed. *Physics in Nuclear Medicine*. Vol. 2nd edn. 1987, Grune and Stratton, New York
4. Saha, G.B., *Fundamentals of Nuclear Pharmacy.* Springer-Verlag, Berlin, 1979: p. 95 - 112.
5. Eckelman, W.C., *The status of radiopharmaceutical research.* Int. J. Radiat. Appl. Instrum. B, 1991. **18**: p. iii-vi.
6. Ruth, T.J., *The Production of Radionuclides for Radiotracers in Nuclear Medicine.* Reviews of Accelerator Science and Technology, 2009. **2**(1): p. 17-33.
7. Wrenn, F.R., M.L. Good, and P. Handler, *The use of positron-emitting radioisotopes for the localization of brain tumors.* Science, 1951. **113**: p. 525-7.
8. Anger, H.O., *Radioisotope camera Instrumentation in Nuclear Medicine.* ed G J Hine (New York: Academic), 1967. **I**: p. 485-552.
9. Aronow, S., *Positron scanning Instrumentation in Nuclear Medicine.* ed GJ Hine (NewYork: Academic), 1967. **I**: p. 461-83.
10. Phelps, M.E., et al., *Application of annihilation coincidence detection to transaxial reconstruction tomography.* J. Nucl. Med., 1975. **16**: p. 210-4.
11. Hans Lundqvist, M.L. and V. Tolmachev, *Positron Emission Tomography.* Eur. J. Nucl. Med., 1998. **19**: p. 537-52.

12. Szabo, Z., J. Xia, and W.B. Mathews, *Radiopharmaceuticals for Renal Positron Emission Tomography Imaging.* Seminars in Nuclear Medicine, 2008. **38**(1): p. 20-31.

13. Workman, R.B., et al., *Fundamentals of PET and PET/CT Imaging*, in *PET/CT*. 2006, Springer New York. p. 1-22.

14. Phelps, M.E., *Molecular Imaging and Its Biological Applications.* European Journal of Nuclear Medicine and Molecular Imaging, 2004. **31**(11): p. 1544.

15. Wernick, M.N. and J.N. Aarsvold, *Emission Tomography: The Fundamentals of PET and SPECT.* Elsevier Inc., 2004: p. 179-81.

16. Verel, I., G.W.M. Visser, and G.A. van Dongen, *The Promise of Immuno-PET in Radioimmunotherapy.* J Nucl Med, 2005. **46**(1_suppl): p. 164S-171.

17. Blokland, J.A.K., et al., *Positron emission tomography: a technical introduction for clinicians.* European Journal of Radiology, 2002. **44**(1): p. 70-75.

18. Lee, F.T. and A.M. Scott, *Immuno-PET for tumor targeting.* J Nucl Med, 2003. **44**: p. 1282-3.

19. Boswell, C.A. and M.W. Brechbiel, *Development of radioimmunotherapeutic and diagnostic antibodies: an inside-out view.* Nuclear Medicine and Biology, 2007. **34**(7): p. 757-78.

20. Goldenberg, D.M., et al., *Antibody pretargeting advances cancer radioimmunodetection and radioimmunotherapy.* J Clin Oncol, 2006. **24**(5): p. 823-34.

21. van Dongen, G.A.M.S., et al., *Immuno-PET: A Navigator in Monoclonal Antibody Development and Applications.* Oncologist, 2007. **12**(12): p. 1379-89.

22. Strijckmans, K., *Charged particle accelerators.* Chemical analysis by nuclear methods, 1994: p. 64-74.

23. Strijckmans, K., *The isochronous cyclotron: principles and recent developments.* Computerized Medical Imaging and Graphics, 2001. **25**(2): p. 69-78.

24. Pillai, M.R.A. and M. Haji-Saeid, *Cyclotron Produced Radionuclides: Physical Characteristics and Production Methods*, in *Technical Reports series No. 468,* . 2009, International Atomic Energy Agency.

25. Schlyer, D.J., *Laboratory and cyclotron requirements for PET research.*, A.N. Chemists' Views of Imaging Centers (EMRAN, Ed.), Editor. 1993. p. 123-131.

26. Haji-Saeid, M., *Directory of Cyclotrons Used for Radionuclide Production in Member States: 2006 Update*. 2006, International Atomic Energy Agency.

27. Pagani, M., et al., *Alternative positron emission tomography with non-conventional positron emitters: effects of their physical properties on image quality and potential clinical applications.* Eur. J. Nucl. Med., 1997. **24**: p. 1301-27.

28. Nayak, T.K. and M.W. Brechbiel, *Radioimmunoimaging with Longer-Lived Positron-Emitting Radionuclides: Potentials and Challenges.* Bioconjugate Chemistry, 2009. **20**(5): p. 825-841.

29. Dutta, B., M. Maiti, and S. Lahiri, *Production of ^{88,89}Zr by proton induced activation of natY and separation by SLX and LLX*. Journal of Radioanalytical and Nuclear Chemistry, 2009. **281**(3): p. 663-667.

30. Lewis Jason, S., K. Singh Rajendra, and J. Welch Michael, *Long Lived and Unconventional PET Radionuclides*, in *Molecular Imaging in Oncology*. 2008. p. 283-292.

31. Perk, L.R., et al., *Quantitative PET imaging of Met-expressing human cancer xenografts with ^{89}Zr-labelled monoclonal antibody DN30.* Eur. J. Nucl. Med. Mol. Imaging, 2008. **35**(10): p. 1857-67.

32. Vosjan, M.J.W.D., et al., *Conjugation and radiolabeling of monoclonal antibodies with zirconium-89 for PET imaging using the bifunctional chelate*

p-isothiocyanatobenzyl-desferrioxamine. Nat. Protocols, 2010. **5**(4): p. 739-743.

33. Oude Munnink, T.H., et al., *^{89}Zr-trastuzumab PET visualises HER2 downregulation by the HSP90 inhibitor NVP-AUY922 in a human tumour xenograft.* European Journal of Cancer, 2010. **46**(3): p. 678-684.

34. Holland, J.P., Y. Sheh, and J.S. Lewis, *Standardized methods for the production of high specific-activity zirconium-89.* Nuclear Medicine and Biology, 2009. **36**(7): p. 729-739.

35. Meijs, W.E., et al., *Production of highly pure no-carrier added ^{89}Zr for the labelling of antibodies with a positron emitter.* Applied Radiation and Isotopes, 1994. **45**(12): p. 1143-1147.

36. Verel, I., et al., *^{89}Zr Immuno-PET: Comprehensive Procedures for the Production of ^{89}Zr-Labeled Monoclonal Antibodies.* J Nucl Med, 2003. **44**(8): p. 1271-1281.

37. Aerts, H., et al., *Disparity Between In Vivo EGFR Expression and ^{89}Zr-Labeled Cetuximab Uptake Assessed with PET.* The Journal of Nuclear Medicine, 2009. **50**(1): p. 123-131.

38. Ruth, T.J., et al., *Radionuclide production for biosciences.* Nucl. Med. Biol., 1989. **16**: p. 323-336.

39. Miller, M.J., *Syntheses and therapeutic potential of hydroxamic acid based siderophores and analogs.* Chemical Reviews, 1989. **89**(7): p. 1563-1579.

40. Karelin, Y.A. and Y.G. Toporov, *RIAR reactor produced radionuclides.* Applied Radiation and Isotopes, 1998. **49**(4): p. 299-304.

41. Liu, S., *Bifunctional coupling agents for radiolabeling of biomolecules and target-specific delivery of metallic radionuclides.* Advanced Drug Delivery Reviews, 2008. **60**(12): p. 1347-1370.

42. Kandil, S., et al., *A comparative study on the separation of radiozirconium via ion-exchange and solvent extraction techniques, with particular reference*

to the production of ^{88}Zr and ^{89}Zr in proton induced reactions on yttrium. Journal of Radioanalytical and Nuclear Chemistry, 2007. **274**(1): p. 1-8.

43. Shure, K.M.D., *Radiations from Zr-89.* Physical Review, 1951. **82**(1): p. 122.

44. Verel, I., et al., *Quantitative ^{89}Zr Immuno-PET for In Vivo Scouting of ^{90}Y-Labeled Monoclonal Antibodies in Xenograft-Bearing Nude Mice.* J Nucl Med, 2003. **44**(10): p. 1663-1670.

45. Kinzler, K.W.V., Bert, *The genetic basis of human cancer* New York: McGraw-Hill, Medical Pub. Division., 2002. **2**: p. 5.

46. Toikkanen, S., et al., *Prognostic significance of HER-2 oncoprotein expression in breast cancer: a 30-year follow-up.* J Clin Oncol, 1992. **10**: p. 1044-8.

47. King, C.R., M.H. Kraus, and S.A. Aaronson, *Amplification of a novel v-erbB related gene in human mammary carcinoma.* Science, 1985. **229**: p. 974-76.

48. Pegram, M.D., D. Baly, and C. Wirth, *Antibody dependent cell-mediated cytotoxicity in breast cancer patients in phase III clinical trials of humanized anti-HER-2 antibody.* Proc Am Assoc Cancer Res, 1997. **38**: p. 602.

49. Bilous, M., et al., *Predicting the HER2 status of breast cancer from basic histopathology data: an analysis of 1500 breast cancers as part of the HER2000 International Study.* The Breast, 2003. **12**: p. 92-98.

50. Slamon, D.J., et al., *Human breast cancer: correlation of relapse and survival with amplification on Her-2/neu oncogene.* Science, 1987. **235**: p. 177-182.

51. Ditsch, N., et al., *Trastuzumab (HERCEPTIN): monoclonal antibody in the treatment of HER2/neu-overexpressing breast cancer in the metastatic and (neo)adjuvant situation.* Breast Care, 2006. **1**(2): p. 78-84.

52. Paudyal, P., et al., *Imaging and biodistribution of Her2/neu expression in non-small cell lung cancer xenografts with ^{64}Cu-labeled trastuzumab PET.* Cancer Science, 2010. **101**(4): p. 1045-1050.

53. Dejesus, O.T. and R.J. Nickles, *Production and purification of ^{89}Zr, a potential PET antibody label.* International Journal of Radiation Applications and Instrumentation. Part A. Applied Radiation and Isotopes, 1990. **41**(8): p. 789-790.

54. Meijs, W.E., et al., *Evaluation of desferal as a bifunctional chelating agent for labeling antibodies with Zr-89.* International Journal of Radiation Applications and Instrumentation. Part A. Applied Radiation and Isotopes, 1992. **43**(12): p. 1443-1447.

55. Carter, P.J., *Potent antibody therapeutics by design.* Nat Rev Immunol, 2006. **6**(5): p. 343-357.

56. Reichert, J.M.V.-A., V.E., *Development trends for monoclonal antibody cancer therapeutics.* Nat. Rev. Drug Discov., 2007. **6**: p. 349-356.

57. Wu, A.M., *Antibodies and Antimatter: The Resurgence of Immuno-PET.* Journal of Nuclear Medicine, 2009. **50**(1): p. 2-5.

58. van Dongen, G. and M. Vosjan, *Immuno-Positron Emission Tomography: Shedding Light on Clinical Antibody Therapy.* Cancer Biotherapy & Radiopharmaceuticals, 2010. **25**(4): p. 375.

59. Stacy, S.L., *Billion dollar babies-biotech drugs as blockbusters.* Nat Biotechnol, 2007. **25**(4): p. 380-382.

60. Stern, M. and R. Herrmann, *Overview of monoclonal antibodies in cancer therapy: present and promise.* Critical Reviews in Oncology/Hematology, 2005. **54**(1): p. 11-29.

61. Adams, G.P. and L.M. Weiner, *Monoclonal antibody therapy of cancer.* Nat Biotech, 2005. **23**(9): p. 1147-1157.

62. Zafir-Lavie, I., Y. Michaeli, and Y. Reiter, *Novel antibodies as anticancer agents.* Oncogene, 2007. **26**(25): p. 3714-33.

63. Albanell, J., et al., *Node-negative breast cancers with p53(-)/HER2-neu(-) status may identify women with very good prognosis.* Anticancer Research, 1996. **16**: p. 1027-1032.

64. Valabrega, G., F. Montemurro, and M. Aglietta, *Trastuzumab: mechanism of action, resistance and future perspectives in HER2-overexpressing breast cancer.* Ann Oncol, 2007. **18**(6): p. 977-84.

65. Badache, A. and N.E. Hynes, *A new therapeutic antibody masks ErbB2 to its partners.* Cancer Cell, 2004. **5**: p. 299-301.

66. Agus, D.B., et al., *Phase I clinical study of pertuzumab, a novel HER dimerization inhibitor, in patients with advanced cancer.* J Clin Oncol, 2005. **23**(11): p. 2534-2543.

67. Weiner, L.M. and G.P. Adams, *New approaches to antibody therapy.* Oncogene, 2000. **19**(53): p. 6144-51.

68. Clynes, R.A., et al., *Inhibitory Fc receptors modulate in vivo cytotoxicity against tumor targets.* Nat Med, 2000. **6**(4): p. 443-6.

69. Gennari, R., et al., *Pilot study of the mechanism of action of preoperative trastuzumab in patients with primary operable breast tumors overexpressing HER2.* Clinical Cancer Research, 2004. **10**(17): p. 5650-5655.

70. Disis, M.L., et al., *Generation of T-cell immunity to the HER-2/neu protein after active immunization with HER-2/neu peptide-based vaccines.* J Clin Oncol, 2002. **20**(11): p. 2624-32.

71. Milenic, D.E. and M.W. Brechbiel, *Targeting of radio-isotopes for cancer therapy.* Cancer Biol Ther, 2004. **3**(4): p. 361-70.

72. Petit, A.M., et al., *Neutralizing antibodies against epidermal growth factor and ErbB-2/neu receptor tyrosine kinases down-regulate vascular endothelial growth factor production by tumor cells in vitro and in vivo: angiogenic implications for signal transduction therapy of solid tumors.* Am J Pathol, 1997. **151**(6): p. 1523-30.

73. Viloria-Petit A, C.T., Jothy S, et al., *Acquired resistance to the antitumor effect of epidermal growth factor receptorblocking antibodies in vivo: a role for altered tumor angiogenesis.* Cancer Research, 2001. **61**: p. 5090-5101.

74. Kumar, R. and R. Yarmand-Bagheri, *The role of HER2 in angiogenesis.* Semin Oncol, 2001. **28**(5 Suppl 16): p. 27-32.

75. Pegram, M.D. and D.M. Reese, *Combined biological therapy of breast cancer using monoclonal antibodies directed against HER2/neu protein and vascular endothelial growth factor.* Semin Oncol, 2002. **29**(3 Suppl 11): p. 29-37.

76. Martin, M., et al., *Phase II study of bevacizumab in combination with trastuzumab and capecitabine as first-line treatment for HER-2-positive locally recurrent or metastatic breast cancer.* Oncologist, 2012. **17**(4): p. 469-75.

77. Thijs, H.O.M., et al., *^{89}Zr-trastuzumab PET visualises HER2 downregulation by the HSP90 inhibitor NVP-AUY922 in a human tumour xenograft.* European journal of cancer (Oxford, England : 1990), 2009. **46**(3): p. 678-684.

78. Molina, M.A., et al., *Trastuzumab (Herceptin), a Humanized Anti-HER2 Receptor Monoclonal Antibody, Inhibits Basal and Activated HER2 Ectodomain Cleavage in Breast Cancer Cells.* Cancer Res, 2001. **61**(12): p. 4744-4749.

79. Holland, J.P., et al., *Measuring the Pharmacodynamic Effects of a Novel Hsp90 Inhibitor on HER2/neu Expression in Mice Using ^{89}Zr-DFO-Trastuzumab.* PLoS ONE, 2010. **5**(1).

80. Hudis, C.A., *Trastuzumab - Mechanism of Action and Use in Clinical Practice.* New England Journal of Medicine, 2007. **357**(1): p. 39-51.

81. Norenberg, J.P., et al., *213Bi-[DOTA0, Tyr3]octreotide peptide receptor radionuclide therapy of pancreatic tumors in a preclinical animal model.* Clin Cancer Res, 2006. **12**(3 Pt 1): p. 897-903.

82. Chinn, P., et al., *Antibody therapy of non-Hodgkin's B-cell lymphoma.* Cancer Immunol Immunother, 2003. **52**(5): p. 257-80.

83. Li, L., et al., *A novel antiangiogenesis therapy using an integrin antagonist or anti-Flk-1 antibody coated 90Y-labeled nanoparticles.* Int J Radiat Oncol Biol Phys, 2004. **58**(4): p. 1215-27.

84. Packard, A.B., J.F. Kronauge, and M.W. Brechbiel, *Metalloradiopharmaceuticals II, Diagnosis and Therapy*. 1999: Clarke, MJ.; Sadler, PJ., editors. Springer; New York. 45-116.

85. Brechbiel, M.W., *Bifunctional chelates for metal nuclides.* Q J Nucl Med Mol Imaging, 2008. **52**(2): p. 166-73.

86. Martell, A.S., RM. , *Critical Stability Constants*. Vol. 1. 1974, New York: Plenum.

87. Pritchard, J.H., et al., *Indium-III-labeled Antibody Heavy Metal Chelate Conjugates: A Potential Alternative to Radioiodination.* Proc Soc Expt Biol Med., 1976. **151**: p. 297-302.

88. Iris, V., et al., *Long-Lived Positron Emitters Zirconium-89 and Iodine-124 for Scouting of Therapeutic Radioimmunoconjugates with PET*. Cancer Biotherapy & Radiopharmaceuticals, 2003. **18**(4): p. 655-61.

89. Brouwers, A., et al., *PET radioimmunoscintigraphy of renal cell cancer using ^{89}Zr-labeled cG250 monoclonal antibody in nude rats.* . Cancer Biother. Radiopharm., 2004. **19**: p. 155-63.

90. Nagengast, W.B., et al., *In vivo VEGF imaging with radiolabeled bevacizumab in a human ovarian tumor xenograft.* J Nucl Med, 2007. **48**(8): p. 1313-9.

91. Borjesson, P., Jauw, Y., de Bree, R., Roos, J., Castelijns, J., Leemans, C., van Dongen, G., & Boellaard, R.. , *Radiation Dosimetry of ^{89}Zr-Labeled Chimeric Monoclonal Antibody U36 as Used for Immuno-PET in Head and Neck Cancer Patients.* The Journal of Nuclear Medicine, 2009. **50**(11): p. 1828-36.

92. Borjesson, P.K.E., et al., *Performance of Immuno-Positron Emission Tomography with Zirconium-89-Labeled Chimeric Monoclonal Antibody*

U36 in the Detection of Lymph Node Metastases in Head and Neck Cancer Patients. Clinical Cancer Research, 2006. **12**(7): p. 2133-2140.

93. Dijkers, E.C.F., et al., *Development and Characterization of Clinical-Grade ^{89}Zr-Trastuzumab for HER2/neu ImmunoPET Imaging.* J Nucl Med, 2009. **50**(6): p. 974-981.

94. Perk, L., et al., *Preparation and evaluation of ^{89}Zr-Zevalin for monitoring of ^{90}Y-Zevalin biodistribution with positron emission tomography.* European Journal of Nuclear Medicine and Molecular Imaging, 2006. **33**(11): p. 1337-1345.

95. Zalutsky, M.R., *Potential of Immuno-Positron Emission Tomography for Tumor Imaging and Immunotherapy Planning.* Clinical Cancer Research, 2006. **12**(7): p. 1958-1960.

96. Herscheid, J.D., A. Hoekstra, and C.M. Vos, *N-Succinyldesferrioxamine B: a potential radiopharmaceutical for assessing renal function.* Eur J Nucl Med, 1984. **9**(11): p. 508-10.

97. Perk, L., et al., *p-Isothiocyanatobenzyl-desferrioxamine: a new bifunctional chelate for facile radiolabeling of monoclonal antibodies with zirconium-89 for immuno-PET imaging.* European Journal of Nuclear Medicine and Molecular Imaging, 2010. **37**(2): p. 250-259.

98. Chakrabarti, M.C., et al., *Prevention of radiolysis of monoclonal antibody during labeling.* J Nucl Med, 1996. **37**(8): p. 1384-8.

99. Meijs, W.E., et al., *Zirconium-Labeled Monoclonal Antibodies and Their Distribution in Tumor-Bearing Nude Mice.* J Nucl Med, 1997. **38**(1): p. 112-118.

100. Meijs, W.E., et al., *A facile method for the labeling of proteins with zirconium isotopes.* Nuclear Medicine and Biology, 1996. **23**(4): p. 439-448.

101. Tinianow, J.N., et al., *Site-specifically ^{89}Zr-labeled monoclonal antibodies for ImmunoPET.* Nucl Med Biol, 2010. **37**(3): p. 289-97.

102. Zhang, Y., H. Hong, and W. Cai, *PET tracers based on Zirconium-89.* Curr Radiopharm, 2011. **4**(2): p. 131-9.

103. Bowen, H., *The Biogeochemistry of the Elements*, in *Trace Elements in Biochemistry*. 1966, Academic Press, London. p. 173-239.

104. O'Donnell, R.T., et al., *Radioimmunotherapy with (111)In/(90)Y-2IT-BAD-m170 for metastatic prostate cancer.* Clin Cancer Res, 2001. **7**(6): p. 1561-8.

105. Wong, J.Y., et al., *A phase I trial of (90)Y-DOTA-anti-CEA chimeric T84.66 (cT84.66) radioimmunotherapy in patients with metastatic CEA-producing malignancies.* Cancer Biother Radiopharm, 2006. **21**(2): p. 88-100.

106. Lovqvist, A., et al., *PET imaging of (86)Y-labeled anti-Lewis Y monoclonal antibodies in a nude mouse model: comparison between (86)Y and (111)In radiolabels.* J Nucl Med, 2001. **42**(8): p. 1281-7.

107. Palm, S., et al., *Pharmacokinetics and Biodistribution of (86)Y-Trastuzumab for (90)Y dosimetry in an ovarian carcinoma model: correlative MicroPET and MRI.* J Nucl Med, 2003. **44**(7): p. 1148-55.

108. Lars, R.P., et al., *^{89}Zr as a PET Surrogate Radioisotope for Scouting Biodistribution of the Therapeutic Radiometals ^{90}Y and ^{177}Lu in Tumor-Bearing Nude Mice After Coupling to the Internalizing Antibody Cetuximab.* The Journal of Nuclear Medicine, 2005. **46**(11): p. 1898-906.

109. Cai, W., G. Niu, and X. Chen, *Multimodality imaging of the HER-kinase axis in cancer.* Eur J Nucl Med Mol Imaging, 2008. **35**(1): p. 186-208.

110. Normanno, N., et al., *Epidermal growth factor receptor (EGFR) signaling in cancer.* Gene, 2006. **366**(1): p. 2-16.

111. Gross, M.E., R.L. Shazer, and D.B. Agus, *Targeting the HER-kinase axis in cancer.* Semin Oncol, 2004. **31**(1 Suppl 3): p. 9-20.

112. Mitsudomi, T. and Y. Yatabe, *Epidermal growth factor receptor in relation to tumor development: EGFR gene and cancer.* FEBS J, 2010. **277**(2): p. 301-8.

113. Herbst, R.S. and D.M. Shin, *Monoclonal antibodies to target epidermal growth factor receptor-positive tumors: a new paradigm for cancer therapy.* Cancer, 2002. **94**(5): p. 1593-611.

114. Goldstein, N.I., et al., *Biological efficacy of a chimeric antibody to the epidermal growth factor receptor in a human tumor xenograft model.* Clin Cancer Res, 1995. **1**(11): p. 1311-8.

115. Pines, G., W.J. Kostler, and Y. Yarden, *Oncogenic mutant forms of EGFR: lessons in signal transduction and targets for cancer therapy.* FEBS Lett, 2010. **584**(12): p. 2699-706.

116. Yeh, H.H., et al., *Molecular imaging of active mutant L858R EGF receptor (EGFR) kinase-expressing nonsmall cell lung carcinomas using PET/CT.* Proc Natl Acad Sci U S A, 2011. **108**(4): p. 1603-8.

117. Cai, W. and X. Chen, *Multimodality imaging of vascular endothelial growth factor and vascular endothelial growth factor receptor expression.* Front Biosci, 2007. **12**: p. 4267-79.

118. Ellis, L.M. and D.J. Hicklin, *VEGF-targeted therapy: mechanisms of anti-tumour activity.* Nat Rev Cancer, 2008. **8**(8): p. 579-91.

119. Middleton, G. and D.V. Lapka, *Bevacizumab (Avastin).* Clin J Oncol Nurs, 2004. **8**(6): p. 666-9.

120. Nagengast, W.B., et al., *^{89}Zr-bevacizumab PET of early antiangiogenic tumor response to treatment with HSP90 inhibitor NVP-AUY922.* J Nucl Med, 2010. **51**(5): p. 761-7.

121. Webb, D.S., et al., *LFA-3, CD44, and CD45: physiologic triggers of human monocyte TNF and IL-1 release.* Science, 1990. **249**(4974): p. 1295-7.

122. Jacobson, K., et al., *Redistribution of a major cell surface glycoprotein during cell movement.* J Cell Biol, 1984. **99**(5): p. 1613-23.

123. Nestor, M., K. Andersson, and H. Lundqvist, *Characterization of ^{111}In and ^{177}Lu-labeled antibodies binding to CD44v6 using a novel automated radioimmunoassay.* J Mol Recognit, 2008. **21**(3): p. 179-83.

124. Mulder, J.W., et al., *Colorectal cancer prognosis and expression of exon-v6-containing CD44 proteins.* Lancet, 1994. **344**(8935): p. 1470-2.

125. Heider, K.H., et al., *CD44v6: a target for antibody-based cancer therapy.* Cancer Immunol Immunother, 2004. **53**(7): p. 567-79.

126. Colnot, D.R., et al., *Phase I Therapy Study of ^{186}Re-Labeled Chimeric Monoclonal Antibody U36 in Patients with Squamous Cell Carcinoma of the Head and Neck.* Journal of Nuclear Medicine, 2000. **41**(12): p. 1999-2010.

127. Colnot, D.R., et al., *Reinfusion of unprocessed, granulocyte colony-stimulating factor-stimulated whole blood allows dose escalation of ^{186}Re labeled chimeric monoclonal antibody U36 radioimmunotherapy in a phase I dose escalation study.* Clin Cancer Res, 2002. **8**(11): p. 3401-6.

128. de Bree, R., et al., *Selection of monoclonal antibody E48 IgG or U36 IgG for adjuvant radioimmunotherapy in head and neck cancer patients.* Br J Cancer, 1997. **75**(7): p. 1049-60.

129. Niu, G., W. Cai, and X. Chen, *Molecular imaging of human epidermal growth factor receptor 2 (HER-2) expression.* Front Biosci, 2008. **13**: p. 790-805.

130. Perik, P.J., et al., *Indium-111–Labeled Trastuzumab Scintigraphy in Patients With Human Epidermal Growth Factor Receptor 2–Positive Metastatic Breast Cancer.* Journal of Clinical Oncology, 2006. **24**(15): p. 2276-2282.

131. Dijkers, E.C., et al., *Biodistribution of ^{89}Zr-trastuzumab and PET Imaging of HER2-Positive Lesions in Patients With Metastatic Breast Cancer.* Clin Pharmacol Ther, 2010. **87**(5): p. 586-592.

132. Oude Munnink, T.H., et al., *Trastuzumab pharmacokinetics influenced by extent human epidermal growth factor receptor 2-positive tumor load.* J Clin Oncol, 2010. **28**(21): p. 355-357.

133. Olson, W.C., W.D. Heston, and A.K. Rajasekaran, *Clinical trials of cancer therapies targeting prostate-specific membrane antigen.* Rev Recent Clin Trials, 2007. **2**(3): p. 182-90.

134. Manyak, M.J., *Indium-111 capromab pendetide in the management of recurrent prostate cancer.* Expert Rev Anticancer Ther, 2008. **8**(2): p. 175-81.

135. Holland, J.P., et al., *^{89}Zr-DFO-J591 for immunoPET of prostate-specific membrane antigen expression in vivo.* J Nucl Med, 2010. **51**(8): p. 1293-300.

136. Ruggiero, A., et al., *Cerenkov luminescence imaging of medical isotopes.* J Nucl Med, 2010. **51**(7): p. 1123-30.

137. Swietach, P., et al., *New insights into the physiological role of carbonic anhydrase IX in tumour pH regulation.* Oncogene, 2010. **29**(50): p. 6509-21.

138. Hoeben, B.A., et al., *PET of hypoxia with ^{89}Zr-labeled cG250-F(ab')$_2$ in head and neck tumors.* J Nucl Med, 2010. **51**(7): p. 1076-83.

139. Heskamp, S., et al., *ImmunoSPECT and immunoPET of IGF-1R expression with the radiolabeled antibody R1507 in a triple-negative breast cancer model.* J Nucl Med, 2010. **51**(10): p. 1565-72.

140. Cai, W. and X. Chen, *Nanoplatforms for targeted molecular imaging in living subjects.* Small, 2007. **3**(11): p. 1840-54.

141. Hong, H., T. Gao, and W. Cai, *Molecular Imaging with Single-Walled Carbon Nanotubes.* Nano Today, 2009. **4**(3): p. 252-261.

142. Ruggiero, A., et al., *Imaging and treating tumor vasculature with targeted radiolabeled carbon nanotubes.* Int J Nanomedicine, 2010. **5**: p. 783-802.

143. Herscheid, J.D.M., C.M. Vos, and A. Hoekstra, *Manganese-52m for direct application: A new ^{52}Fe/^{52m}Mn generator based on a hydroxamate resin.* The International Journal of Applied Radiation and Isotopes, 1983. **34**(6): p. 883-886.

144. Al-Nahhas, A., et al., *What can gallium-68 PET add to receptor and molecular imaging?* European Journal of Nuclear Medicine and Molecular Imaging, 2007. **34**(12): p. 1897-1901.

145. Wang, Z., et al., *Biotinylation, pharmacokinetics, and extracorporeal adsorption of humanized MAb 111In-MN14 using an avidin-affinity column in rats.* Cancer Biother Radiopharm, 2003. **18**(3): p. 365-75.

146. Kasbollah, A., et al., *Review on Production of ^{89}Zr in a Medical Cyclotron for PET Radiopharmaceuticals.* Journal of Nuclear Medicine Technology, 2013. **41**(1): p. 35-41.

147. Nathan, L., et al., *Positron emission tomography (PET), immuno-PET and radioimmunotherapy in renal cell carcinoma: a developing diagnostic and therapeutic relationship.* BJU International, 2006. **97**(5): p. 916-922.

148. Severin, G.W., et al., *^{89}Zr radiochemistry for positron emission tomography.* Med Chem, 2011. **7**(5): p. 389-94.

149. Lee, J.Y. and Y.S. Tak, *The Preparation of Yttrium Oxide Film Deposited by Electrochemical Method.* Journal of Industrial and Engineering Chemistry, 1999. **5**(2): p. 139-142.

150. Link, J.M., et al., *^{89}Zr for antibody labelling and positron tomography.* Journal of Labelled Compounds and Radiopharmaceuticals, 1986. **23**(10-12): p. 1296-1297.

151. Zweit, J., S. Downey, and H.L. Sharma, *Production of no-carrier-added zirconium-89 for positron emission tomography.* International Journal of Radiation Applications and Instrumentation. Part A. Applied Radiation and Isotopes, 1991. **42**(2): p. 199-201.

152. Matsuda, Y., et al., *Formation of yttrium oxide by electrodeposition in organic electrolyte.* Journal of Alloys and Compounds, 1993. **193**(1-2): p. 277-279.

153. Reischl, G., F. Rosch, and H.J. Machulla, *Electrochemical separation and purification of yttrium-86.* Radiochimica Acta, 2002. **90**(4): p. 225-228.

154. Kumbhar, P.P. and C.D. Lokhande, *Electrodeposition of yttrium from a nonaqueous bath.* Metal Finishing, 1995. **93**(4): p. 28-28.

155. Sadeghi, M., T. Kakavand, and M. Taghilo, *Targetry of Y_2O_3 on a copper substrate for the non-carrier-added ^{89}Zr production via $^{89}Y(p, n)$ ^{89}Zr reaction.* Kerntechnik, 2010. **75**(5): p. 298-302.

156. Snook, D.E., et al., *Preparation and in vivo study of ^{124}I-labelled monoclonal antibody H17E2 in a human tumour xenograft model. A prelude to positron emission tomography (PET).* Br J Cancer Suppl, 1990. **10**: p. 89-91.

157. Pentlow, K.S., et al., *Quantitative imaging of I-124 using positron emission tomography with applications to radioimmunodiagnosis and radioimmunotherapy.* Med Phys, 1991. **18**(3): p. 357-66.

158. Bakir, M.A., et al., *c-erbB2 protein overexpression in breast cancer as a target for PET using iodine-124-labeled monoclonal antibodies.* J Nucl Med, 1992. **33**(12): p. 2154-60.

159. Hohn, A., et al., *Production and separation of "non-standard" PET nuclides at a large cyclotron facility: the experiences at the Paul Scherrer Institute in Switzerland.* Q J Nucl Med Mol Imaging, 2008. **52**(2): p. 145-50.

160. Saha, G.B., N.T. Porile, and L. Yaffe, *(p, xn) and (p, pxn) Reactions of Yttrium-89 with 5-85-MeV Protons.* Physical Review, 1966. **144**(3): p. 962-71.

161. Scharli, R.K., et al., *Establishing reliable production of the PET isotope ^{89}Zr for research use: From target fabrication to preclinical imaging.* American Institute of Physics Conference Proceedings, 2012. **1509**(1): p. 101-107.

162. Taghilo, M., et al., *Cyclotron production of ^{89}Zr: A potent radionuclide for positron emission tomography.* International Journal of Physical Sciences, 2012. **7**(9): p. 1321-5.

163. Sadeghi, M., M. Enferadi, and M. Bakhtiari, *Accelerator production of the positron emitter zirconium-89.* Annals of Nuclear Energy, 2012. **41**(0): p. 97-103.

164. Dabkowski, A.M., K. Probst, and C. Marshall, *Cyclotron production for the radiometal Zirconium-89 with an IBA cyclone 18/9 and COSTIS solid target*

system (STS). American Institute of Physics Conference Proceedings, 2012. **1509**(1): p. 108-113.

165. Hong, H., et al., *Positron emission tomography imaging of CD105 expression with 89Zr-Df-TRC105.* Eur J Nucl Med Mol Imaging, 2012. **39**(1): p. 138-48.

166. Allen J. Bard, R.P., and Joseph Jordan, *Standard potentials in aqueous solution*. Monographs in electroanalytical chemistry and electrochemistry. 1985, New York, USA: Marcel Dekker.

167. Ali, S.A. and E.G. Shankland, *Radiochemical synthesis of ^{89}Zr-porphyrin for positron label of monoclonal antibodies.* J. Labelled Compd. Radiopharm., 1991. **30**: p. 326.

168. Sampath, L., et al., *Dual-labeled trastuzumab-based imaging agent for the detection of human epidermal growth factor receptor 2 overexpression in breast cancer.* J Nucl Med, 2007. **48**(9): p. 1501-10.

169. Dijkers, E., et al., *Characterization of ^{89}Zr-trastuzumab for clinical HER2 immunoPET imaging.* Journal of Clinical Oncology, 2007. **25**(18S): p. 3508.

170. Jayson, G.C., et al., *Molecular Imaging and Biological Evaluation of HuMV833 Anti-VEGF Antibody: Implications for Trial Design of Antiangiogenic Antibodies.* Journal of the National Cancer Institute, 2002. **94**(19): p. 1484-1493.

171. Collingridge, D.R., et al., *The Development of [^{124}I]Iodinated-VG76e.* Cancer Research, 2002. **62**(20): p. 5912-9.

172. Cai, W., et al., *PET of Vascular Endothelial Growth Factor Receptor Expression.* Journal of Nuclear Medicine, 2006. **47**(12): p. 2048-2056.

173. Cullinane, C., et al., *Differential ^{18}F-FDG and 3'-deoxy-3'-^{18}F-fluorothymidine PET responses to pharmacologic inhibition of the c-MET receptor in preclinical tumor models.* J Nucl Med, 2011. **52**(8): p. 1261-7.

174. Slamon, D.J., et al., *Use of chemotherapy plus a monoclonal antibody against HER2 for metastatic breast cancer that overexpresses HER2.* N Engl J Med, 2001. **344**(11): p. 783-92.

175. Peacock, K., et al., *^{99m}Tc-stannous colloid white cell scintigraphy in childhood inflammatory bowel disease.* J Nucl Med, 2004. **45**(2): p. 261-5.

176. Vinberg, N. and K. Kristensen, *Fission MO-99/Tc-99m Generators -- a study of their performance and quality.* Eur J Nucl Med, 1980. **5**(5): p. 435-8.

177. Tsang, B.W., C.J. Mathias, and M.A. Green, *A gallium-68 radiopharmaceutical that is retained in myocardium: ^{68}Ga[(4,6-MeO2sal)2BAPEN]$^{+}$*. J Nucl Med, 1993. **34**(7): p. 1127-31.

178. Rosch, F., *(68)Ge/ (68)Ga generators: past, present, and future.* Recent Results Cancer Res, 2013. **194**: p. 3-16.

179. Azhdarinia, A., et al., *Infrared-based module for the synthesis of ^{68}Ga-labeled radiotracers.* Nucl Med Biol, 2007. **34**(1): p. 121-7.

180. Maecke, H.R., M. Hofmann, and U. Haberkorn, *^{68}Ga-Labeled Peptides in Tumor Imaging.* Journal of Nuclear Medicine, 2005. **46**(1 suppl): p. 172S-178S.

181. Nakayama, M., et al., *A new ^{68}Ge/^{68}Ga generator system using an organic polymer containing N-methylglucamine groups as adsorbent for ^{68}Ge.* Applied Radiation and Isotopes, 2003. **58**(1): p. 9-14.

182. Roesch, F., *Maturation of a key resource - the germanium-68/gallium-68 generator: development and new insights.* Curr Radiopharm, 2012. **5**(3): p. 202-11.

183. Boros, E., et al., *Acyclic Chelate with Ideal Properties for ^{68}Ga PET Imaging Agent Elaboration.* Journal of the American Chemical Society, 2010. **132**(44): p. 15726-15733.

184. Ehrhardt, G.J. and M.J. Welch, *A New Germanium-68/Gallium-68 Generator.* Journal of Nuclear Medicine, 1978. **19**(8): p. 925-929.

185. M.J. Welch, T.J.M., *The potential role of generator-produced radiopharmaceuticals in clinical PET.* J. Nucl. Med., 2000. **41**: p. 315-317.

186. Rosch, F., *Past, present and future of 68Ge/68Ga generators.* Appl Radiat Isot, 2013. **76**: p. 24-30.

187. Li, M. and C.F. Meares, *Synthesis, metal chelate stability studies, and enzyme digestion of a peptide-linked DOTA derivative and its corresponding radiolabeled immunoconjugates.* Bioconjug Chem, 1993. **4**(4): p. 275-83.

188. Jalilian, A.R., et al., *Preparation, quality control and biodistribution studies of [67Ga]-DOTA-anti-CD20.* Radiochimica Acta, 2008. **96**(3): p. 167-174.

189. Liu, S. and D.S. Edwards, *Bifunctional chelators for therapeutic lanthanide radiopharmaceuticals.* Bioconjug Chem, 2001. **12**(1): p. 7-34.

190. Froidevaux, S., et al., *Preclinical comparison in AR4-2J tumor-bearing mice of four radiolabeled 1,4,7,10-tetraazacyclododecane-1,4,7,10-tetraacetic acid-somatostatin analogs for tumor diagnosis and internal radiotherapy.* Endocrinology, 2000. **141**(9): p. 3304-12.

191. Al-Nahhas, A., et al., *Gallium-68 PET: a new frontier in receptor cancer imaging.* Anticancer Res, 2007. **27**(6B): p. 4087-94.

192. Morgat, C., et al., *Gallium-68: Chemistry and Radiolabeled Peptides Exploring Different Oncogenic Pathways.* Cancer Biotherapy & Radiopharmaceuticals, 2013. **28**(2): p. 85-97.

Appendix A. Amount of ^{89}Zr in MBq extracted from hydroxamate resin column using 1.0 M oxalic acid and 1.0 M phosphoric acid as extraction agents

Amount of ^{89}Zr in MBq extracted from hydroxamate resin column using 1 M oxalic acid and 1 M phosphoric acid as extraction agents

	Activity of Zr-89 extracted using oxalic acid (MBq)	Activity of Zr-89 extracted using phophoric acid (MBq)
Activity in the column	200	200
Elution 1	179.4	146.6
Elution 2	173.2	138.4
Elution 3	182.8	143.5
Elution 4	176.8	130.2
Elution 5	189.8	142.3
Average:	180.4	140.2
Std Dev:	6.32	6.31

Appendix B. Amount of ^{68}Ga in MBq eluted from 50, 100 and 200 mg hydroxamate resin column using 0.01, 0.05 and 0.1 M Citrate Buffer at pH 4

Amount of ^{68}Ga in MBq eluted from 50 mg hydroxamate resin column using 0.01, 0.05 and 0.1 M Citrate Buffer at pH 4

	50 mg hydroxamate resin, 0.01 M Citrate Buffer (MBq)	50 mg hydroxamate resin, 0.05 M Citrate Buffer (MBq)	50 mg hydroxamate resin, 0.1 M Citrate Buffer (MBq)
Activity in the column	200	200	200
Elution 1	170	187	197
Elution 2	176	184	193
Elution 3	168	179	196
Elution 4	164	188	197
Elution 5	172	190	195
Average:	170	185.6	195.6
Std Dev:	4.47	4.28	1.67

Amount of ^{68}Ga in MBq eluted from 100 mg hydroxamate resin column using 0.01, 0.05 and 0.1 M Citrate Buffer at pH 4

	100 mg hydroxamate resin, 0.01 M Citrate Buffer (MBq)	100 mg hydroxamate resin, 0.05 M Citrate Buffer (MBq)	100 mg hydroxamate resin, 0.1 M Citrate Buffer (MBq)
Activity in the column	200	200	200
Elution 1	126	137	143
Elution 2	120	131	156
Elution 3	118	136	147
Elution 4	120	125	153
Elution 5	116	121	141
Average:	120	130	148
Std Dev:	3.742	6.928	6.403

Amount of ^{68}Ga in MBq eluted from 200 mg hydroxamate resin column using 0.01, 0.05 and 0.1 M Citrate Buffer at pH 4

	200 mg hydroxamate resin, 0.01 M Citrate Buffer (MBq)	200 mg hydroxamate resin, 0.05 M Citrate Buffer (MBq)	200 mg hydroxamate resin, 0.1 M Citrate Buffer (MBq)
Activity in the column	200	200	200
Elution 1	136	149	181
Elution 2	133	165	178
Elution 3	124	161	186
Elution 4	129	159	187
Elution 5	138	166	188
Average:	132	160	184
Std Dev:	5.612	6.782	4.301

Appendix C. Amount of ^{68}Ga in MBq eluted from 50 mg hydroxamate resin column using 0.01, 0.05 and 0.1 M HCl

Amount of ^{68}Ga in MBq eluted from 50 mg hydroxamate resin column using 0.01, 0.05 and 0.1 M HCl

	0.01 M HCl (MBq)	0.05 M HCl (MBq)	0.1 M HCl (MBq)
Activity in the column	200	200	200
Elution 1	16	86	165
Elution 2	12	73	167
Elution 3	15	82	143
Elution 4	10	89	152
Elution 5	11	77	147
Average:	12.8	81.4	154
Std Dev:	2.588	6.504	10.33

Appendix D. Amount of ^{68}Ga in MBq eluted from hydroxamate resin column using various solutions

Amount of ^{68}Ga in MBq eluted from hydroxamate resin column using various solutions

	Activity of Ga-68 extracted using 1 M Na Citrate in 0.5 M HCl (MBq)	Activity of Ga-68 extracted using 0.5 M Na Citrate in 0.25 M HCl (MBq)	Activity of Ga-68 extracted using 0.2 M Na Citrate in 0.1 M HCl (MBq)
Activity in the column	200	200	200
Elution 1	103	96	55
Elution 2	109	85	53
Elution 3	115	83	47
Elution 4	118	95	56
Elution 5	110	86	46
Average:	111	89	51.4
Std Dev:	5.788	6.042	4.615

Amount of ^{68}Ga in MBq eluted from hydroxamate resin column using various solutions

	Activity of Ga-68 extracted using 0.1 M Na Citrate in 0.05 M HCl (MBq)	Activity of Ga-68 extracted using 0.1 M Citrate Buffer (MBq)	Activity of Ga-68 extracted using 1 M Na Citrate in 1 M Citric Acid (MBq)
Activity in the column	200	200	200
Elution 1	47	127	98
Elution 2	43	124	107
Elution 3	41	118	105
Elution 4	45	120	96
Elution 5	48	117	101
Average:	44.8	121.2	101.4
Std Dev:	2.864	4.207	4.615

Amount of ^{68}Ga in MBq eluted from hydroxamate resin column using various solutions

	Activity of Ga-68 extracted using 0.5 M HCl (MBq)	Activity of Ga-68 extracted using 0.1 M HCl (MBq)	Activity of Ga-68 extracted using 0.01 M Citrate Buffer (MBq)	Activity of Ga-68 extracted using 1 M Acetate Buffer (MBq)
Activity in the column	200	200	200	200
Elution 1	115	48	77	0
Elution 2	104	51	69	0
Elution 3	109	54	67	0
Elution 4	110	53	79	0
Elution 5	114	58	75	0
Average:	110.4	52.8	73.4	0
Std Dev:	4.393	3.701	5.177	0.000

Appendix E. PET images using ^{89}Zr-Df with phosphoric acid as an extraction agent, applied to a female Balb/c nude mouse model with subcutaneous LS174T tumour (HER2-expressing colorectal model) on the right flank.

PET images using ^{89}Zr-Df applied to a female Balb/c nude mouse model with subcutaneous LS174T tumour (HER2-expressing colorectal model) on the right flank at 24 h and 4h h post injection (Mouse #1).

24 hours

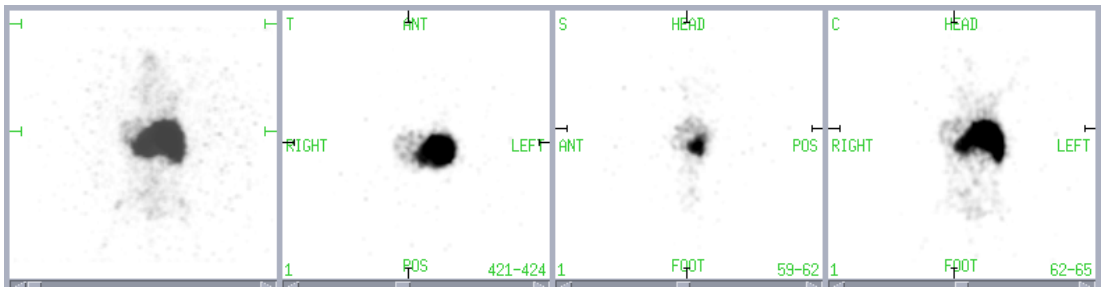

48 hours

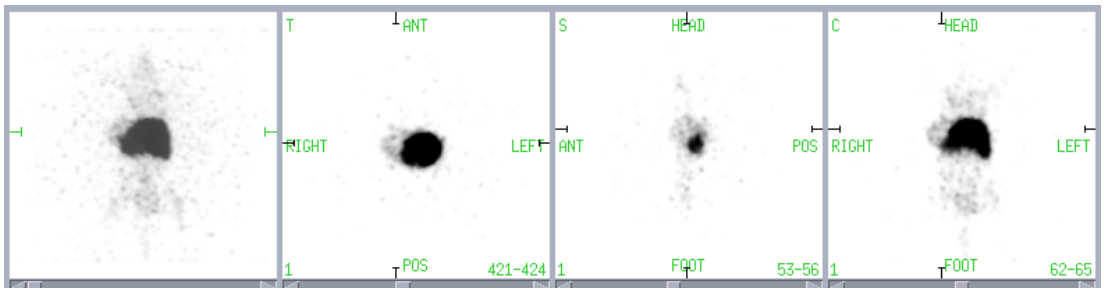

PET images using ^{89}Zr-Df applied to a female Balb/c nude mouse model with subcutaneous LS174T tumour (HER2-expressing colorectal model) on the right flank at 24 h and 4h h post injection (Mouse #2).

24 hours

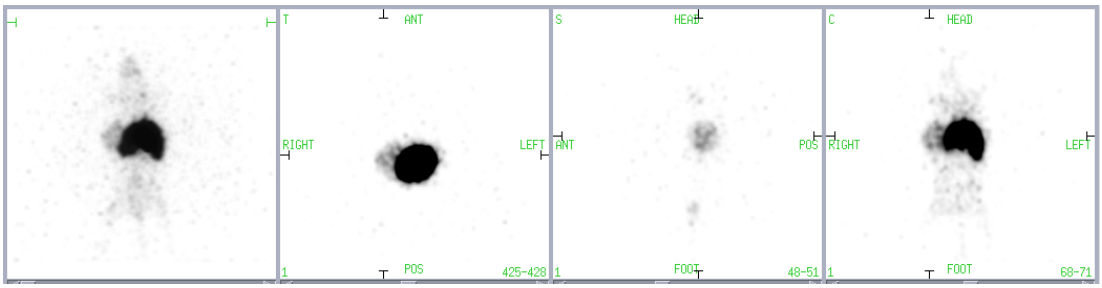

48 hours

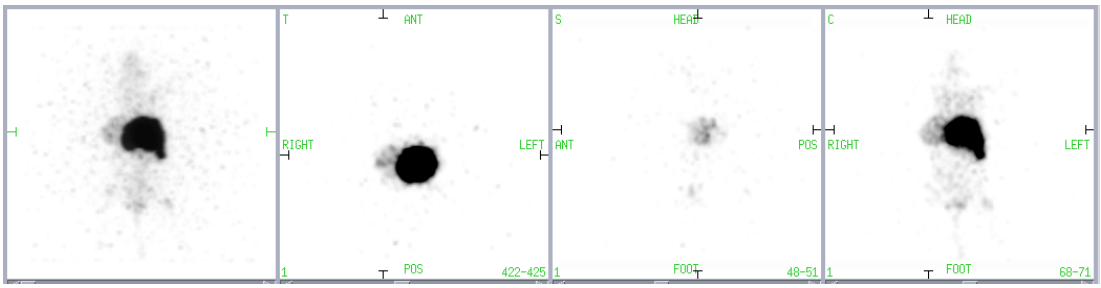

Appendix F. PET images using free ^{89}Zr, applied to a female Balb/c nude mouse model with subcutaneous LS174T tumour (HER2-expressing colorectal model) on the right flank.

PET images at 1, 4 and 24 h post injection (Mouse #1).

1 hour

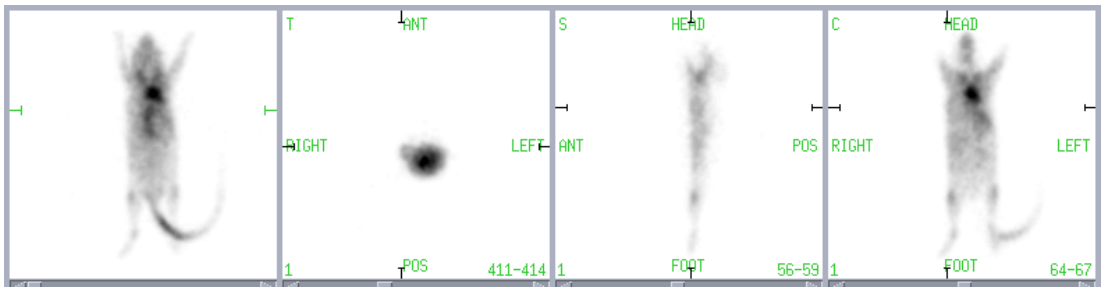

4 hours

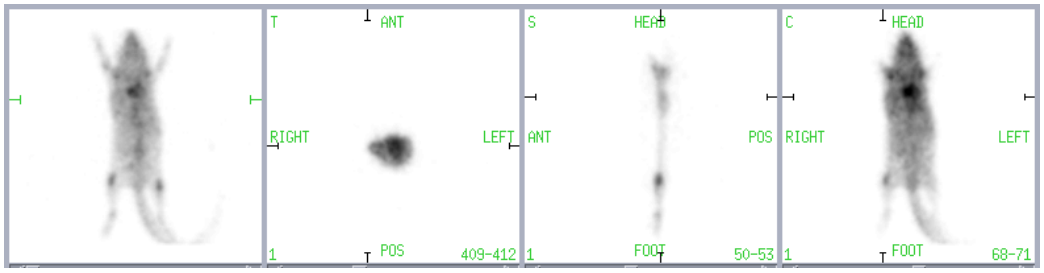

24 hours

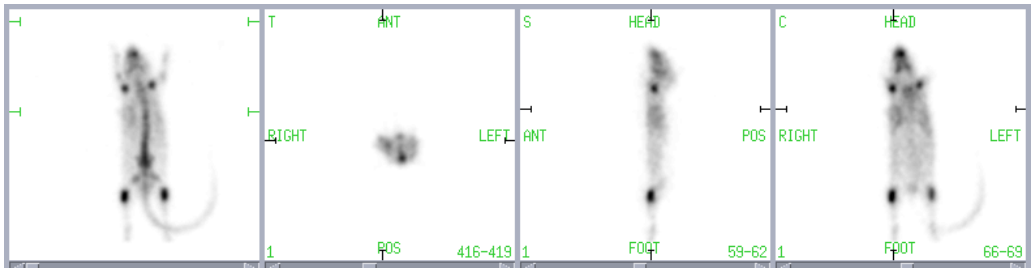

PET images at 1, 4 and 24 h post injection (Mouse #2).

1 hour

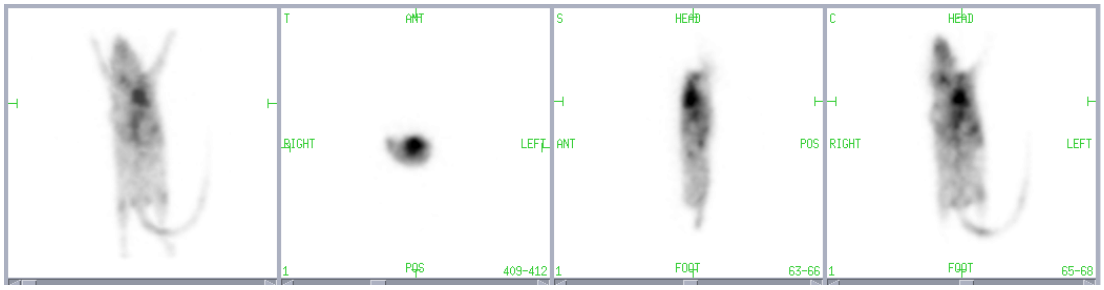

4 hours

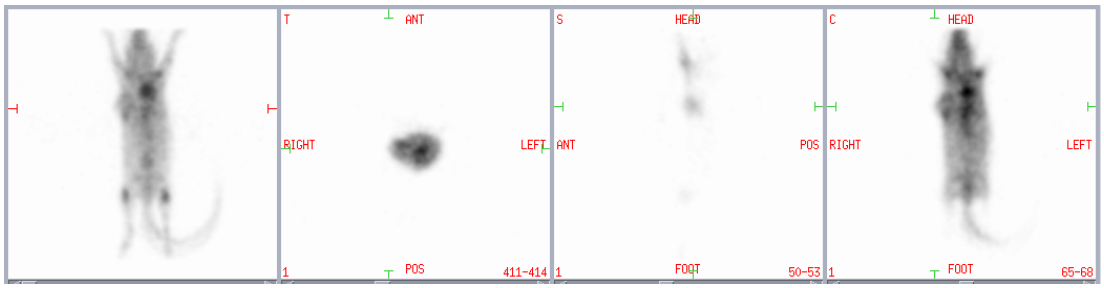

24 hours

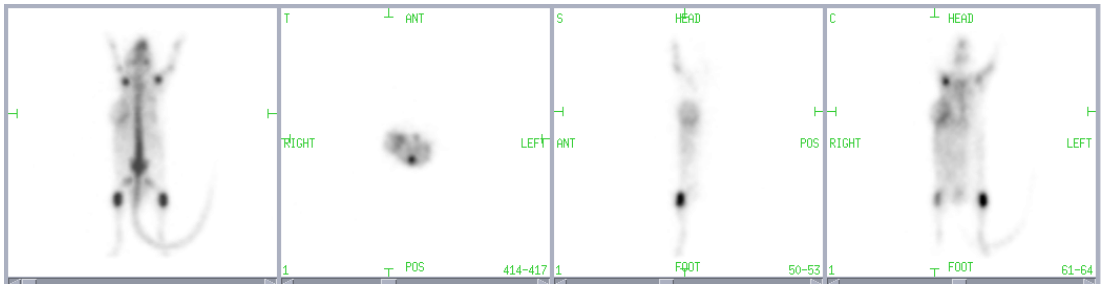

Appendix G. PET images using ^{89}Zr tracer bound to mAb as ^{89}Zr-Df-Trastuzumab, applied to a female Balb/c nude mouse model with subcutaneous LS174T tumour (HER2-expressing colorectal model) on the right flank.

PET images using ^{89}Zr-Df-Trastuzumab, applied to a female Balb/c nude mouse model with subcutaneous LS174T tumour (HER2-expressing colorectal model) on the right flank at 24 h post injection (Mouse #1).

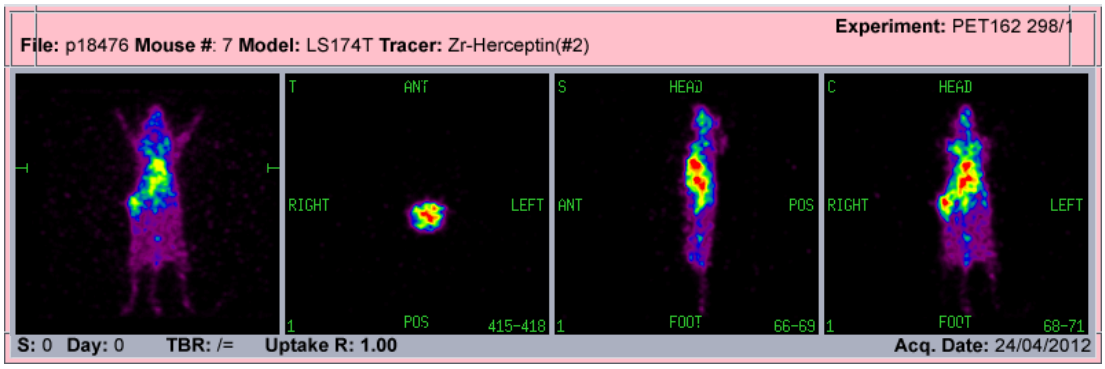

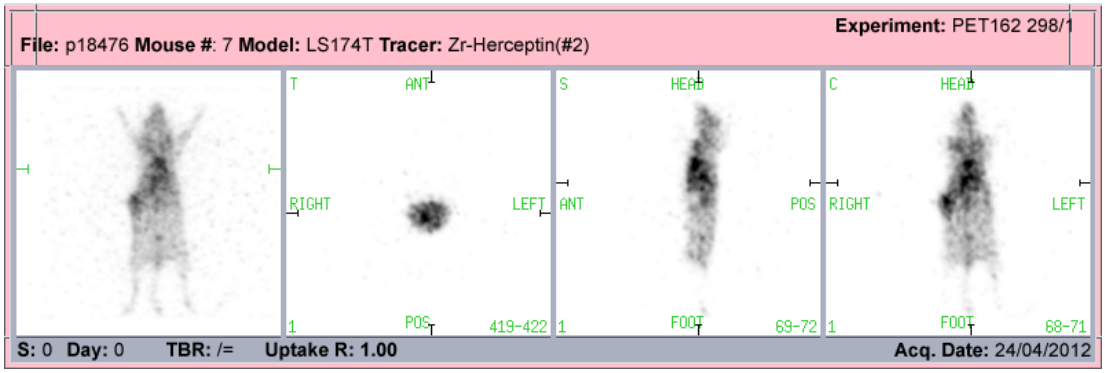

PET images using ^{89}Zr-Df-Trastuzumab, applied to a female Balb/c nude mouse model with subcutaneous LS174T tumour (HER2-expressing colorectal model) on the right flank at 24 h post injection (Mouse #2).

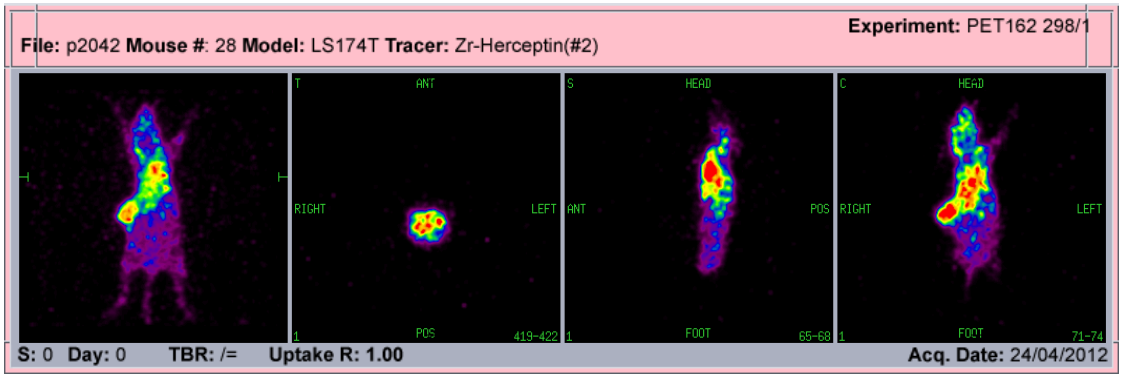

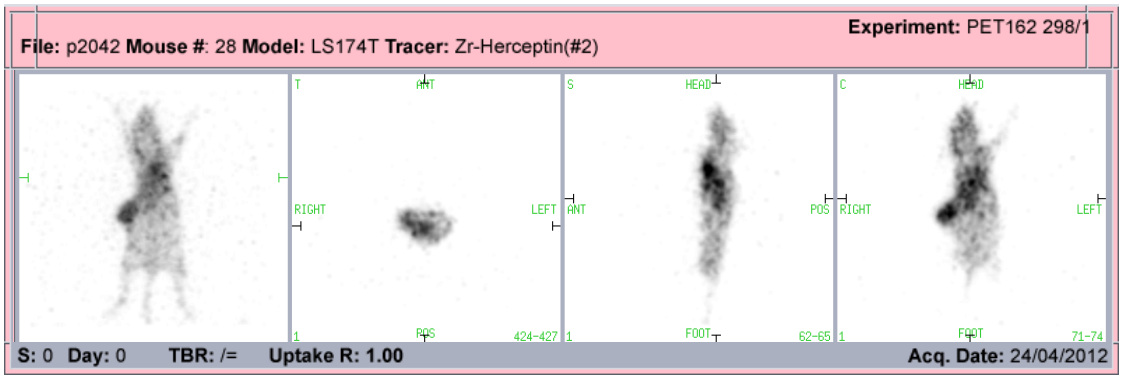

PET images using ^{89}Zr-Df-Trastuzumab, applied to a female Balb/c nude mouse model with subcutaneous LS174T tumour (HER2-expressing colorectal model) on the right flank at 24 h post injection (Mouse #3).

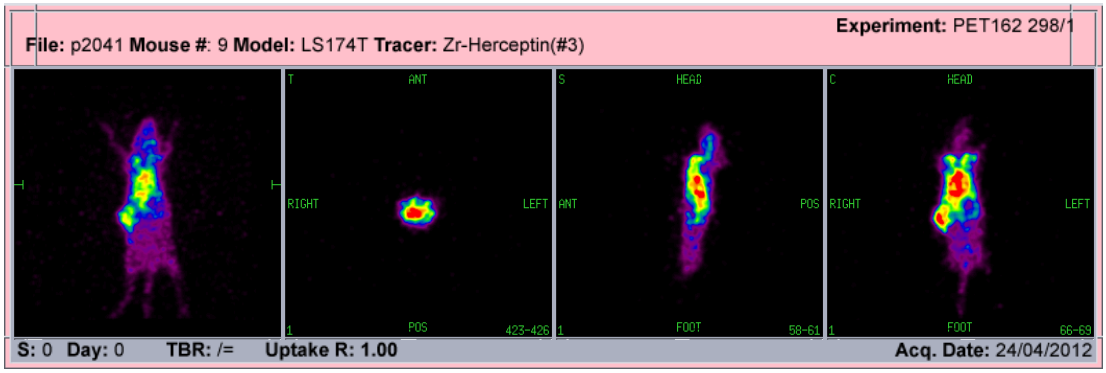

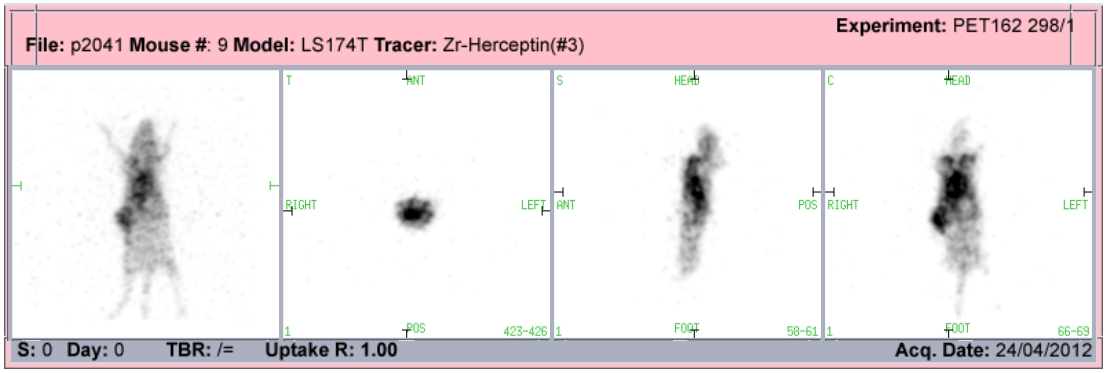

PET images using ^{89}Zr-Df-Trastuzumab, applied to a female Balb/c nude mouse model with subcutaneous LS174T tumour (HER2-expressing colorectal model) on the right flank at 24 h post injection (Mouse #4).

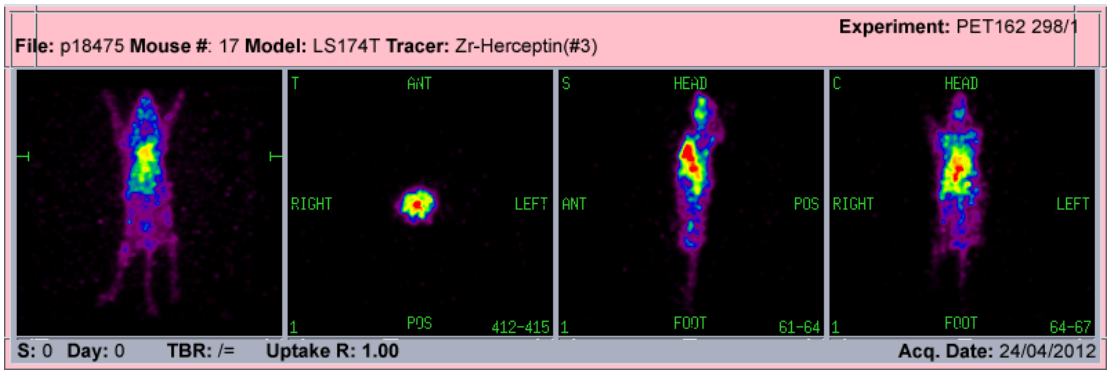

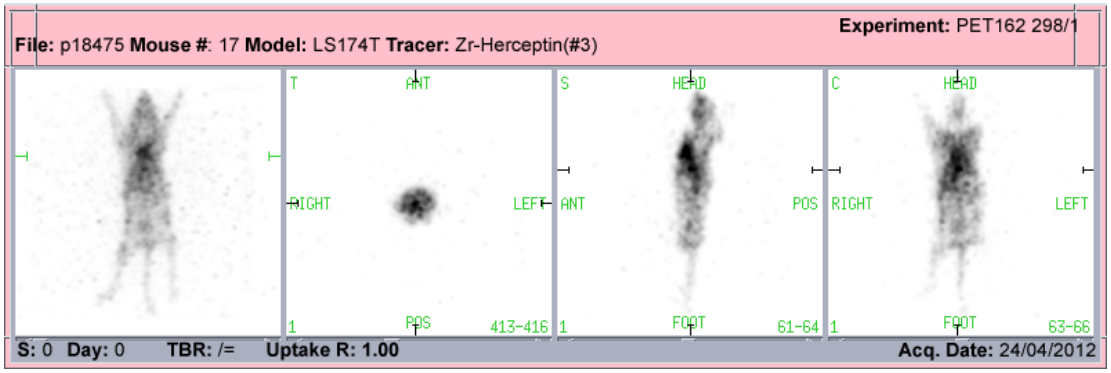

Appendix H. Publications and Conference Presentations

Publications:

Kasbollah, A., Eu, P., Cowell, S., Deb, P., Review on Production of ^{89}Zr in a Medical Cyclotron for PET Radiopharmaceuticals. Journal of Nuclear Medicine Technology, 2013. 41(1): p. 35-41.

Scharli, R. K., R. I. Price, Cullinane, C., Eu, P., **Kasbollah, A.**, et al. (2012). Establishing reliable production of the PET isotope ^{89}Zr for research use: From target fabrication to preclinical imaging. AIP Conference Proceedings 1509(1): 101-107.

Publication submitted:

Kasbollah, A., Eu, P., Cullinane, C. (Submitted) Production of ^{89}Zr-Trastuzumab for PET Radiopharmaceutical Imaging. Biomedical Imaging and Intervention Journal.

Online Published Abstract:

a. Internal Medicine Journal 2012; 42 (Suppl. 3): 18–52

http://onlinelibrary.wiley.com/doi/10.1111/j.1445-5994.2012.02873.x/pdf

1. P99: The Preparation of Yttrium-89 Target via Electroplating Technique for Production of Zirconium-89. K Keo, **A Kasbollah**, S Cowell, RMIT, Melbourne; P Eu, Peter MacCallum Cancer Centre, Melbourne

2. P102: Investigation of Yttrium Solid Targets for the Production of Zirconium-89. **A Kasbollah**, S Cowell, RMIT, Melbourne; P Eu, Peter MacCallum Cancer Centre, Melbourne

3. P103: A Potential New Column for a Gallium-68 Generator. **A Kasbollah**, RMIT, Melbourne; P Eu, Peter MacCallum Cancer Centre, Melbourne

b. Internal Medicine Journal 2011; 41 (Suppl. 3): 1–48

http://onlinelibrary.wiley.com/doi/10.1111/j.1445-5994.2011.02531.x/pdf

P36: Hydroxamate Column construction for Preliminary Assessment of Viability for ^{89}Zr Purification: The ^{68}Ga Test. A Livori, **A Kasbollah**, S Cowell, RMIT, Melbourne; P Eu, Peter MacCallum Cancer Centre, Melbourne

Conference Presentations:

Kasbollah A, Eu P (2012). Production, Purification and Radiolabelling of Zirconium-89 for Positron Emission Tomography (PET) Radiopharmaceuticals. 25th Annual Congress of European Association of Nuclear Medicine (EANM), 27-31 October 2012.

Kasbollah A, Eu P (2012). Production and Purification of Zirconium-89 for PET Radiopharmaceuticals. Annual Higher Degree Research Student Conference, RMIT University Bundoora West Campus, 19th October 2012.

Carey A, Kasbollah A, Eu P (2012). Determining an Alternative to Oxalic Acid as an Extractor for the Purification of Zirconium-89 to be labelled with Monoclonal Antibodies. 5th Annual Nuclear Medicine Symposium, RMIT University, 6th September 2012.

Kasbollah A, Eu P (2012). A Potential of New Column for a Gallium-68 Generator. 42nd Annual Scientific Meeting of the Australian and New Zealand Society of Nuclear Medicine (ANZSNM 2012), 27-30 April 2012.

Kasbollah A, Eu P, Cowell SF (2011). Investigation of Yttrium Targets for the Production of Zirconium-89. 42nd Annual Scientific Meeting of the Australian and New Zealand Society of Nuclear Medicine (ANZSNM 2012), 27-30 April 2012.

Keo K, Kasbollah A, Eu P, Cowell SF (2011). The Preparation of Yttrium-89 Target via Electroplating Technique for Production of Zirconium-89. 42nd Annual Scientific Meeting of the Australian and New Zealand Society of Nuclear Medicine (ANZSNM 2012), 27-30 April 2012.

Kasbollah A, Eu P, Cowell SF (2011). Investigation of Yttrium Targets for the Production of Zirconium-89 Radionuclide in a Medical Cyclotron. Higher Degrees by Research Student Conference, RMIT University Bundoora West Campus, 21st October 2011

Keo K, Kasbollah A, Eu P, Cowell SF (2011). The Preparation of Yttrium-89 Target via Electroplating Technique for Production of Zirconium-89. 4th Annual Nuclear Medicine Symposium, RMIT University, 7th September 2011.

Livori, A, Kasbollah A, Eu P, Cowell SF (2011). Hydoxomate column construction for preliminary assessment of viability for Zirconium-89 purification: The Ga68 test. Australian & New Zealand Society of Nuclear Medicine, Darwin, 14-18 July 2011.

Kasbollah A, Bansal V, Eu P, Cowell SF (2010). An Improved Target for the Production of Zirconium-89 in a Medical Cyclotron. Annual Higher Degree Research Student Conference, RMIT University, 20th October 2010.

Livori A, Kasbollah A, Eu P, Cowell SF (2010). Hydroxamate column construction for preliminary assessment of viability for Zirconium 89 purification: The Gallium 68 test. 3rd Annual Nuclear Medicine Symposium, RMIT University, 15th September 2010.

Appendix I. Review on Production of ^{89}Zr in a Medical Cyclotron for PET Radiopharmaceuticals

Review on Production of ^{89}Zr in a Medical Cyclotron for PET Radiopharmaceuticals

Azahari Kasbollah[1,2], Peter Eu[3], Simon Cowell[1], and Pradip Deb[1]

[1]Discipline of Medical Radiations, School of Medical Sciences, RMIT University, Victoria, Australia; [2]Malaysian Nuclear Agency, Ministry of Science, Technology and Innovation (MOSTI), Putrajaya, Malaysia; and [3]Peter MacCallum Cancer Centre, Victoria, Australia

This article is intended to provide an overview of the production and application of ^{89}Zr for the professional development of nuclear medicine technologists. It outlines the cyclotron targeting, separation and labeling options, and techniques for the preparation of the radionuclide ^{89}Zr (half-life, 78.4 h [3.3 d]) used in PET. Unlike the commonly used ^{18}F-FDG, with a 109.7-min half-life, the longer half-life of ^{89}Zr makes it possible to use high-resolution PET/CT to localize and image tumors with monoclonal antibody radiopharmaceuticals and thus potentially expand the use of PET. **Methods:** This paper briefly reviews the cyclotron technique of ^{89}Zr production and outlines the range and preparation techniques available for making ^{89}Y targets as a starting material. It then discusses how cyclotron-produced ^{89}Zr can be separated, purified, and labeled to monoclonal antibodies for PET/CT of specific tumors. **Results:** We argue that knowledge and understanding of this long-lived PET radionuclide should be part of the professional development of nuclear medicine technologists because it will lead to better patient outcomes and potentially increase the pool of collaborators in this field of research.

Key Words: positron emission tomography (PET); monoclonal antibodies; yttrium solid target; ^{89}Zr radionuclide; radiolabeling

J Nucl Med Technol 2013; 41:35–41
DOI: 10.2967/jnmt.112.111377

The Nobel Prize in Chemistry won by George de Hevesy in 1943 for the development of the tracer principle used in nuclear medicine is possibly one of the most significant achievements of the 20th century (*1*). The introduction of cyclotron and PET technology into clinical medicine greatly improved the management of patients with cancer and other diseases, and the development of combined imaging with PET/CT has substantially improved the effectiveness of this modality (*2*). A radiopharmaceutical (radiotracer) is a radioactive compound used for the diagnosis and therapeutic treatment of human diseases. It is composed of 2 parts: a radionuclide, which is a radioactive isotope that can be injected safely into the body, and a pharmaceutical, which acts as a carrier molecule delivering the isotope to the area to be treated or examined within the body. For a radiotracer to be used safely in humans, for imaging or therapy, it must meet high standards for quality that include chemical and radiochemical purity, sterility, and freedom from pyrogenic material. For functional nuclear medicine imaging, there are few ideal radiopharmaceuticals (*3*). Table 1 outlines the ideal diagnostic radiopharmaceutical for imaging. The ability to measure regional biochemical function requires a careful design process with these principles in mind. However, in reality it is not possible to meet all of these criteria. For example, all decay processes involve the emission of particles, as in the case of the pure γ-emitters, which have Auger electrons emitted during some fraction of the decays. Thus, in addition to the quest for an ideal radiopharmaceutical in the development of a biochemical probe, the following 3 factors must be considered (*4*): the radiotracer must be able to bind preferentially to a specific site, the radiotracer must be sensitive to minor changes in biochemistry, and if possible, the specific biochemical change should be a function of a specific disease that matches that sensitivity.

Many radiotracers have been synthesized to probe metabolic turnover such as oxygen consumption, glucose utilization, and amino acid synthesis. Enzymatic activity, neurotransmission, receptor density, and occupancy have all been measured through appropriately designed radiotracers. It should be emphasized that the development of radiotracers for PET fundamentally violates rule 2(a) in Table 1 for the ideal diagnostic radiopharmaceutical for imaging because PET radionuclides emit β^+ particles by nature. However, the resulting coincident γ-rays from the β^+ annihilation form the basis for the technique.

Additionally, in consideration of the above principles, a plan must be considered on how to insert the radionuclide into the molecule at a point in the synthetic process with minimal handling yet late enough in the synthesis to minimize loss due to chemical yield and radioactive decay. For these reasons, the preparation of radiopharma-

Received Jul. 19, 2012; revision accepted Nov. 29, 2012.
For correspondence or reprints contact: Azahari Kasbollah, Discipline of Medical Radiations, School of Medical Sciences, RMIT University, P.O. Box 71, Bundoora, Victoria 3083, Australia.
E-mail: azahari@nuclearmalaysia.gov.my
Published online Jan. 17, 2013.

TABLE 1
Properties of Ideal Diagnostic Radiopharmaceutical for Imaging

Properties	Notes
1. Easy availability	Be readily available at low cost
2. Particle emission	Diagnostic purpose: be a pure γ-emitter—that is, have no particle emission such as α and β because these contribute radiation dose to patient without providing diagnostic information
	Therapeutic purpose: have particle emission such as α and β because these are useful for damaging abnormal cells
3. High target–to–nontarget activity ratio	Provide maximum efficacy in diagnosis (therapy), and minimize radiation dose to patient
4. Proper metabolic activity	Possess proper metabolic activity—that is, follow or be trapped in metabolic process of interest

ceuticals requires good planning and techniques that are not encountered by traditional synthetic chemistry.

PET and Immuno-PET

In the beginning of the 1950s, Wrenn et al. proposed the use of coincidence techniques to image positron-emitting radionuclides to study ^{64}Cu in brain tumors using opposing sodium iodine detectors (*5*). Soon, the Anger camera was launched onto the market in 1954 and was quickly applied to positron emitters (*6*). Na(I) detectors with coincidence capabilities were used in clinical investigations during the 1960s (*7*). In the beginning of the 1970s, an important progression in this field occurred with the introduction of the tomography principle (*8*), leading to the development of the PET technique. Thus, PET arose from the outcome of 2 Nobel Prize awards, the tracer principle (de Hevesy in Chemistry in 1943) and the tomographic principle (Godfrey N. Houndsfield and Allan M. Cormack in Medicine in 1979) (*1*).

PET is a nuclear medicine technique that produces a 3-dimensional image or map of functional processes in the body. The system detects pairs of γ-rays emitted indirectly by a positron-emitting radioisotope, which is introduced into the body on a metabolically active molecule. The PET radioisotope sends out a positron that eventually finds an electron, forming a complex atom called positronium that rapidly decays and emits 2 annihilation photons. PET cameras detect the 511-keV photons that are emitted at 180° from each other and enable the production of a 3-dimensional image (*1*). PET images generate physiologic and functional information for the observer, but the anatomic structures are sometimes hard to distinguish. Therefore, most new PET scanners come as dual-imaging devices known as PET/CT scanners, enabling the functional information from PET to be displayed with the structural information from CT.

Immuno-PET, a combination of PET and monoclonal antibodies (mAbs), is an attractive novel tumor imaging option because it has the potential to improve diagnostic tumor characterization by combining the high sensitivity and resolution of PET/CT with the specificity of a mAb localization (*9*). In fact, each mAb that targets a specific tumor cell is a candidate for use in immuno-PET, allowing for the development of a new generation of mAb-based imaging probes.

PET also has the potential for quantification of molecular interactions, which is especially attractive when immuno-PET is used as a prelude to therapy with one of the approved mAbs. In a personalized therapeutic approach, immuno-PET enables the confirmation of tumor targeting and the quantification of mAb accumulation. Immuno-PET might also play a role in the efficient selection, characterization, and optimization of novel high-potential mAbs or mAb-conjugate candidates for diagnosis and therapy (*10*).

^{89}Zr Radioisotope

In more recent years, there has been increased interest in such nonconventional positron emitters as ^{89}Zr. Since the introduction of the long-lived positron emitter ^{89}Zr as a residualizing radionuclide for immuno-PET, procedures have been developed for large-scale production of ^{89}Zr and its stable coupling to mAbs (*11,12*). To have a successful diagnostic in PET for solid tumors, a radionuclide's half-life must be suitable for target accumulation and nonspecific clearance. The most commonly used PET radionuclides such as ^{18}F and ^{11}C, which have short half-lives of 109.7 and 20 min, respectively, are not suitable for detection of solid tumors because they would undergo appreciable radioactive decay before reaching the center of the tumor (*13*). Although ^{18}F-FDG is used to find tumors because the sugar molecule targets quickly, the clearance time of radioimmunoconjugates is relatively long; thus, good target-to-blood ratios are not achieved within 24 h after administration with the relatively short half-life of ^{18}F. ^{124}I, on the other hand, has a half-life of 4.2 d, but there are substantial isotopic enrichment costs involved and the added danger of exposure of thyroid tissue (in particular) to free radioactive iodine. ^{89}Zr has ideal physical characteristics for immuno-PET and has been suggested for use in quantifying slow processes and deposition of mAbs in tissue and tumor. Because intact antibodies need around 2–4 d to penetrate to a solid tumor, the half-life of ^{89}Zr (3.3 d), with 23% positron emission (β^+) decay and 77% electron capture, is compatible with the time needed for these mAbs to achieve optimal tumor–to–nontumor uptake ratios (*14*). In contrast, to achieve good visualization, a large dose—

which is costly and, more important, dangerous to the patient with regard to radiation exposure—would need to be administered (*15*). The relatively low translational energy of the emitted positron for ^{89}Zr results in high-resolution images comparable to those observed using the ^{18}F and ^{64}Cu radionuclides (*16–18*). Table 2 breaks down the characteristics of selected PET radionuclides for radioimmunoimaging (*19*). ^{89}Zr has good γ-energies, allowing imaging using PET scanners. Without this property, visualization of the antibodies would not be possible. Another factor to consider is the daughter nuclides formed by the positron decay of zirconium: ^{89}Y. This radionuclide is stable and will not cause any damage in vivo (*20*). The biggest challenges preventing ^{89}Zr from becoming a widely used radioisotope for immuno-PET are its limited availability and the high-energy γ-emission at 908.97 keV, which may limit the radioactive dose that can be administered to patients. Moreover, a free ^{89}Zr can target to bone marrow instead of solid tumor (*21*). So ^{89}Zr must be well bonded with mAbs or other pharmaceuticals for the radiotracer to securely reach the center of the tumor.

PRODUCTION PROCEDURES OF ^{89}ZR RADIOISOTOPE

Target Materials and Irradiation

A cyclotron target is a container into which the target material to be irradiated is introduced. Target material can be gas, liquid, or solid, depending on the radioisotope of interest. Targets specially designed for the production of the most common positron emitters (^{18}F, ^{11}C, ^{13}N, and ^{15}O) are a standard feature in conventional cyclotrons, and this design has been optimized over many years. The ^{89}Zr radioisotope is an example of a nonconventional positron emitter that has limited commercial availability but can be produced from a starting material of ^{89}Y solid target. The target is usually bombarded in a cyclotron with a certain beam current and time to finally produce the ^{89}Zr radioisotope.

Yttrium Target for Production of ^{89}Zr

Yttrium target is an example of solid target material that is introduced into a cyclotron container for irradiation to produce the ^{89}Zr radioisotope. There are a few types of, and techniques for preparation of, yttrium solid target as a starting material.

Yttrium Foil. Dejesus and Nickles used water-cooled yttrium foils to produce ^{89}Zr via the (p,n) reaction on ^{89}Y with 11-MeV protons (*14*). The target was bombarded with protons (1-cm-diameter beam) typically for 2 h, with a beam current of 10 μA. Then the target was dissolved in concentrated HCl (5 mL) as reported by Link et al. (these authors found that HCl gave less insoluble material) (*22*).

Yttrium Pellet. Zweit et al. described the production of no-carrier-added ^{89}Zr for PET from deuteron irradiation of natural yttrium targets (*23*). The target material of natural yttrium powder (100% ^{89}Y) was pressed into 10-mm-diameter pellets ranging in thickness from 240 to 340 mg/cm^2, which were placed in the target holders. Then the pellets were covered with high-purity aluminum foil 0.005–0.36 mm thick depending on the incident deuteron energy required. The beam currents used were 3 and 5 μA, with irradiation times of 12 and 20 min, respectively. The energy window used for the ^{89}Y(d,2n)^{89}Zr reaction was from 16 to 7 MeV. This window was considered to be optimum to minimize the production of the long-lived ^{88}Zr formed by the ^{89}Y(d,3n) reaction with a threshold energy of 15.5 MeV.

Yttrium Sputtering. A different ^{89}Y target can be prepared using the sputtering technique. Meijs et al. reported that the target can be prepared by sputtering an yttrium layer (25 μm) on a copper support. In this process, the yttrium atoms are ejected as a result of momentum transfer between accelerated argon ions and the yttrium source. The yttrium atoms cross a vacuum chamber (7×10^{-3} torr) and finally deposit on the copper support (*11*).

Yttrium Deposition. Films of yttrium are usually produced by vapor deposition, dry processes, and sputtering, but electroplating would be advantageous in view of the cost and productivity. Kumbhar and Lokhande reported the electrodeposition of yttrium from a nonaqueous (ethanol) bath (*24*). The distance between anode and cathode was 0.2 cm. Deposition was performed under unstirred conditions and in the potentiostatic mode. The study indicated that at

TABLE 2
Characteristic of Selected PET Radionuclides for Radioimmunoimaging (*19*)

Radionuclide	Half-life	Production	positron emission maximum energy (β^+_{max}) MeV	β^+ yields (%)	γ-energies MeV	γ-energies Yields (%)	Intrinsic spatial resolution loss (mm)
^{89}Zr	78.4 h	^{89}Y(p,n)^{89}Zr	0.909	23	—		1.0
		^{89}Y(d,2n)^{89}Zr					
^{124}I	100.2 h	^{124}Te(p,n)^{124}I	2.14	24	0.60	61	2.3
		^{124}Te(d,2n)^{124}I					
		^{125}Te(p,2n)^{124}I					
^{18}F	1.83 h	^{20}Ne(d,α)^{18}F	0.63	97	0.14	41	0.7
		^{18}O(p,n)^{18}F					

room temperature, the thickness of the deposit increases linearly with time up to 1 h. The effect of temperature showed that good-quality uniform white–gray deposits could be obtained at up to 45°C. Sadeghi et al. reported 2 special sedimentation methods to deposit a thick layer of yttrium oxide (Y_2O_3) on copper substrate for the production of ^{89}Zr (*25*). A thick layer of Y_2O_3 was deposited on the copper substrate (surface area, 11.69 cm^2) by ethyl cellulose and methyl cellulose methods. The target was irradiated with up to a 20-μA current with 13-MeV protons, and no degradation was observed.

Production of ^{89}Zr

There are 2 nuclear reactions that have been explored for the production of ^{89}Zr and typically by cyclotron bombardment of ^{89}Y. The first and most commonly used is the ^{89}Y(p,n)^{89}Zr reaction (*14,26*), because a higher yield of ^{89}Zr can be produced from ^{89}Y, which is 100% naturally abundant in the earth's crust. Typically in this reaction, a proton beam with 14- to 14.5-MeV energy is used to bombard an yttrium foil solid target for 2–3 h with a 65- to 80-μA beam current. Because yttrium has only 1 stable isotope and the product can be made relatively pure at low energy, this reaction is ideal for the production of ^{89}Zr. The other reaction that has been used for the production of ^{89}Zr in the cyclotron is the ^{89}Y(d,2n)^{89}Zr reaction (*23*). Usually in this reaction, an yttrium pellet is used and irradiated with a 16-MeV deuteron beam, and ^{89}Zr can be purified and separated from the target by ion-exchange chromatography. Theoretically, all the bifunctional chelating agents, such as diethylenetriamine pentaacetic acid (DTPA) and 1DOTA derivatives, for ^{111}In and ^{90}Y labeling can be used for ^{89}Zr labeling of biomolecules (*27*). The dominant oxidation number of zirconium is +4—which, when combined with a relatively small size, leads to an extensive hydrolyzed aqueous chemistry with a largely covalent nature. Donor ligands containing oxygen, nitrogen, and chloride are especially stable, commonly creating complexes with coordination numbers of 7, 8, or higher. High coordination numbers (7 and 8) are characteristic of zirconium complexes, and the ligands are normally labile, resulting in the great variety of stereochemistries. Different radiometals have significant differences in their coordination chemistry. Because the radiometal chelate can significantly affect biologic properties, the biodistribution of a target-specific radiopharmaceutical can be systematically changed either by modifying the coordination environment around the radiometal with a variety of chelators or by using various coligands if the radiometal chelate contains 2 or more ligands (*28*).

Purification of ^{89}Zr

One of the biggest challenges preventing ^{89}Zr from becoming a widely used radioisotope for immuno-PET is the process to rid it of other impurities. Bombardment of the yttrium solid target results in a large number of radiochemical impurities, along with the radionuclide impurity of trace ^{88}Zr (~0.01%). The target itself contains a copper metal backbone and trace amounts of titanium, iron, and gadolinium. After bombardment, trace products of ^{65}Zn, ^{48}V, ^{56}Co, and ^{156}Tb are formed to the trace metals located on the target (*12*). These unwanted impurities must be separated from ^{89}Zr because they might compete in the labeling step with the antibodies (*11*). Purification of ^{89}Zr usually involved the separation process of ^{89}Zr radionuclide from its impurities and starting materials, followed by elution of the radionuclide from the retention column. The ^{89}Zr can be dissolved in hydrochloric acid and separated from other radioisotopes and the target material on an ion-exchange column (*11,23*). In some cases, a wet chemical extraction preceded the ion-exchange separation (*22*). It was found that the hydroxamic function had high specific affinity for zirconium. Even at high acid concentrations—that is, at concentrations higher than 1 M HCl—zirconium is able to form complexes with hydroxamates, whereas its impurities are not (*23*). The latest method of removing these impurities uses a hydroxamate resin column (*12,20*). The hydroxamate resin column can produce 99.9% carrier-free ^{89}Zr; however, the extraction technique proved to be counterintuitive to the purpose of purification (*14*). Because the ^{89}Zr is ionically bonded to the column, a stronger anion exchanger is needed to remove it. It was found that the most convenient solution for transchelating the ^{89}Zr from the column was oxalic acid in a concentration of at least 0.5 M (*11*). Verel et al. have successfully transchelated 97% of the total activity from the hydroxamate column using 1 M oxalic acid over 5 separate elutions, with an initial 40% yield in the first 2 elutions and a purity of more than 99.9% (*12*).

However, there are some issues that arise with oxalic acid as an extraction chemical for purifying ^{89}Zr. Oxalic acid is highly toxic to the human body, causing blood decalcification—which is detrimental to neural and muscle function—as well as renal tubule obstruction via calcium oxalate precipitation (*20*). Hence, the in vivo use of ^{89}Zr-bound oxalic acid cannot be considered. It was demonstrated that removing the oxalic acid required the use of another strong anion-exchange column and the flushing of a large volume of water through the column, followed by chloride exchange using HCl. The resultant acid solution could then be boiled off at 110°C under a continuous stream of argon and reconstituted in 0.9% NaCl solution (*12*). After this purification process, a carrier-free, purified ^{89}Zr was then able to be bound to a mAb desferrioxamine complex (*29*).

Radiolabeling of Antibodies with ^{89}Zr

Over the past 20 y, attempts have been made to label proteins and antibodies with ^{89}Zr using DTPA derivatives and porphyrins as chelating agents (*22,30*), as well as desferrioxamine conjugates (*31,32*). The process incorporates desferrioxamine groups onto mAbs in a 2-step procedure in which maleimide groups were incorporated into the protein and the thioester of desferrioxamine that was formed was

further converted to a free thiol with hydroxylamine to facilitate reaction with the maleimide groups of the antibody, with subsequent radiolabeling with ^{89}Zr (*31,32*). In 2010, Perk et al. introduced the novel bifunctional chelating agent *p*-isothiocyanatobenzyl-desferrioxamine B (Df-Bz-NCS) for the facile radiolabeling of mAbs with ^{89}Zr for immuno-PET. They also compared its performance in ^{89}Zr for immuno-PET with the reference bifunctional TFP-*N*-sucDf (*12*) and demonstrated that the novel Df-Bz-NCS allowed the efficient and easy preparation of optimally performing ^{89}Zr-labeled mAbs, facilitating further exploration of ^{89}Zr immuno-PET as an imaging tool, with oxalic acid being used to extract the ^{89}Zr from the hydroxamate resin column (*33*). The step-by-step procedure was then described for the facile radiolabeling of mAbs or other proteins with ^{89}Zr using Df-Bz-NCS. First, Df-Bz-NCS was coupled to the lysine-NH_2 groups of a mAb at pH 9.0 (premodification), and then it was purified using gel filtration. Next, the premodified mAb was labeled to ^{89}Zr at room temperature by the addition of ^{89}Zr-Zr-oxalic acid solution, and then it was purified using PD-10 column gel filtration to remove the unlabeled product and oxalic acid from the labeled compound (*34*).

In Vitro and In Vivo Studies of the ^{89}Zr Complex

After the mAb has been successfully labeled with ^{89}Zr, it is usual for the complex to be studied in vitro and in vivo to evaluate its effectiveness in binding with the specific tumors and the potential effectiveness of the complex in PET for detecting and monitoring treatment responses. Chopra (*35*) determined the in vitro binding characteristics of ^{89}Zr-trastuzumab and ^{111}In-trastuzumab using SKVO3 cells (human ovarian cancer cell line overexpressing human epidermal growth factor receptor 2 [HER2]) and GLC4 cells (human small cell cancer cell line, HER2-negative) by a flow cytometric method (*36*). Little change in the immunoreactive fraction of ^{89}Zr-trastuzumab was noted during 7 d of storage either at 4°C (from 0.87 to 0.85 ± 0.06) or at 37°C in human serum (from 0.87 to 0.78 ± 0.01). A similar trend in the immunoreactivity of ^{111}In-trastuzumab was reported at the 2 storage temperatures.

Once in vitro studies are completed, the radiopharmaceutical can be assessed with in vivo studies using animals such as mice (*31,33*), followed by human studies (*37,38*). Basically, before the targeted imaging technique can be used in humans, it is necessary to evaluate the effectiveness of the trastuzumab-*N*-sucDf-^{89}Zr in animals to evaluate biodistribution, tumor concentration, and PET detection capabilities. Sampath et al. used BALB/c nude mice, that had received the human breast cancer tumor cell line SKBR-3 transplanted into the dorsal region of the left flank, to look at the biodistribution and concentration of trastuzumab-*N*-sucDf-^{89}Zr in the tumor site and the ability of the PET scanner to detect tumors using this complex. The tumors were grown to 0.5–0.8 cm in diameter, and the mice were then injected via the tail vein with 200 μg of trastuzumab-*N*-sucDf-^{89}Zr and imaged right after injection and 2–48 h after injection (*39*). Our preliminary results on biodistribution and imaging experiments showed a selective accumulation of ^{89}Zr-Df-trastuzumab in tumor-bearing mice (Fig. 1). The introduction of a mouse model allows the radionuclide to be assessed in the context of a full biologic system (*19*) and as a preliminary step in translating bench research into a means of identifying and perhaps subsequently treating cancer in human subjects.

PET of ^{89}Zr-Labeled mAbs

The most common applications of PET are in the field of oncology, cardiology, and neurology. Since the introduction of the long-lived positron emitter ^{89}Zr as a residualizing radionuclide for immuno-PET, procedures have been developed for the large-scale production of ^{89}Zr and its stable coupling to mAbs (*12,20*).

A feasibility study has been performed to determine the optimal dosage and time of imaging of the mAb ^{89}Zr-trastuzumab to enable PET of HER2-positive lesions. Fourteen patients with HER2-positive metastatic breast cancer received 37 MBq of ^{89}Zr-trastuzumab using 1 of 3 doses (10 or 50 mg for those who were trastuzumab-naive and 10 mg for those who were already on trastuzumab treatment). The patients underwent at least 2 PET scans between days 2 and 5. The results of the study showed that the best time for assessment of ^{89}Zr-trastuzumab uptake by tumors was 4–5 d

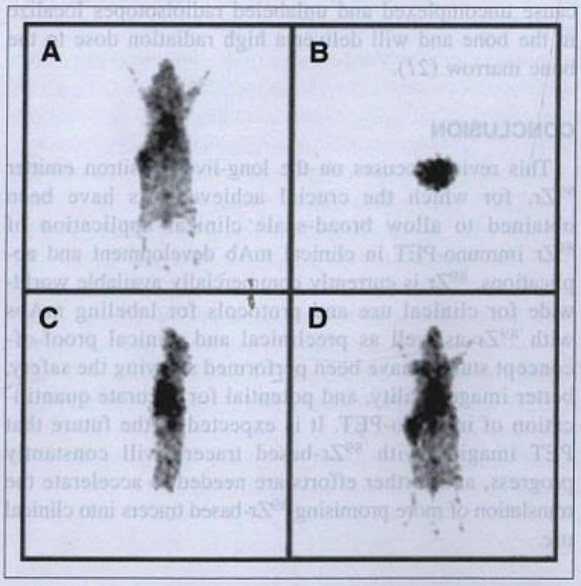

FIGURE 1. PET images of HER2-expressing LS174T tumor–bearing mouse (tumor size, 180 mm^3) at 24 h after injection with 1.85 MBq of ^{89}Zr-Df-trastuzumab using small-animal PET facility at Peter MacCallum Cancer Centre, Melbourne, Victoria, Australia. Four views are shown: posterior (A), slice view (B), side view (C), and posterior (D).

after the injection (*38*). For optimal PET scan results, trastuzumab-naïve patients required a 50-mg dose of ^{89}Zr-trastuzumab, and patients already on trastuzumab treatment required a 10-mg dose. The accumulation of ^{89}Zr-trastuzumab in lesions allowed PET imaging of most of the known lesions and some that had been undetected earlier. The relative uptake values (mean ± SEM) were 12.8 ± 5.8, 4.1 ± 1.6, and 3.5 ± 4.2 in liver, bone, and brain lesions, respectively, and 5.9 ± 2.4, 2.8 ± 0.7, 4.0 ± 0.7, and 0.20 ± 0.1 in normal liver, spleen, kidneys, and brain tissue, respectively. PET scanning after administration of ^{89}Zr-trastuzumab at appropriate doses allowed the visualization and quantification of uptake in HER2-positive lesions in patients with metastatic breast cancer.

Several clinical trials with ^{89}Zr-labeled mAbs have recently been taking place, such as a study of ^{89}Zr-trastuzumab for the detection of HER2-positive tumor lesions in breast cancer patients and for the quantification of HER2 expression levels (*37*). The highest uptake was found in HER2-positive tumors at 144 h after injection (40 percentage injected dose per gram of [%ID/g] tissue for ^{89}Zr-trastuzumab and 47 % ID/g for ^{111}In-ITC-DTPA-trastuzumab), compared with 8 % ID/g tissue in HER2-negative control tumors. Liver uptake was low (8–12 %ID/g of tissue). Preliminary results from the first patients in that study showed excellent tumor tracer uptake and a resolution that was much better than that observed in previous SPECT studies with ^{111}In-trastuzumab (*40*). In PET, the need for stable chelation chemistry remains an important consideration with this element because uncomplexed and unlabeled radioisotopes localize in the bone and will deliver a high radiation dose to the bone marrow (*21*).

CONCLUSION

This review focuses on the long-lived positron emitter ^{89}Zr, for which the crucial achievements have been obtained to allow broad-scale clinical application of ^{89}Zr immuno-PET in clinical mAb development and applications. ^{89}Zr is currently commercially available worldwide for clinical use and protocols for labeling mAbs with ^{89}Zr as well as preclinical and clinical proof-of-concept studies have been performed showing the safety, better image quality, and potential for accurate quantification of immuno-PET. It is expected in the future that PET imaging with ^{89}Zr-based tracers will constantly progress, and further efforts are needed to accelerate the translation of more promising ^{89}Zr-based tracers into clinical use.

DISCLOSURE

Financial support was provided by the Ministry of Science, Technology and Innovation (MOSTI), Malaysia. No other potential conflict of interest relevant to this article was reported.

REFERENCES

1. Hans Lundqvist ML, Tolmachev V. Positron emission tomography. *Eur J Nucl Med.* 1998;19:537–552.
2. Buck AK, Herrmann K, Stargardt T, Dechow T, Krause BJ, Schreyögg J. Economic evaluation of PET and PET/CT in oncology: evidence and methodologic approaches. *J Nucl Med Tech.* 2010;38:6–17.
3. Eckelman WC. The status of radiopharmaceutical research. *Int J Rad Appl Instrum B.* 1991;18:iii–vi.
4. Ruth TJ. The production of radionuclides for radiotracers in nuclear medicine. *Reviews of Accelerator Science and Technology.* 2009;02:17–33.
5. Wrenn FR. GML, Handler P The use of positron-emitting radioisotopes for the localization of brain tumors. *Science.* 1951;113:525–527.
6. Anger HO. Radioisotope camera instrumentation in nuclear medicine. In: Hine, G J ed. *Instrumentation in Nuclear Medicine.* New York, NY: Academic; 1967: 485–552.
7. Aronow S. Positron scanning instrumentation in nuclear medicine. In: Hine, G J ed. *Instrumentation in Nuclear Medicine.* New York, NY: Academic; 1967:461–483.
8. Phelps ME, Hoffman EJ, Mullani NA, Ter-Pogossian MM. Application of annihilation coincidence detection to transaxial reconstruction tomography. *J Nucl Med.* 1975;16:210–224.
9. Lawrentschuk N, Davis ID, Bolton DM, Scott AM. Positron emission tomography (PET), immuno-PET and radioimmunotherapy in renal cell carcinoma: a developing diagnostic and therapeutic relationship. *BJU Int.* 2006;97:916–922.
10. Boswell CA, Brechbiel MW. Development of radioimmunotherapeutic and diagnostic antibodies: an inside-out view. *Nucl Med Biol.* 2007;34:757–778.
11. Meijs WE, Herscheid JDM, Haisma HJ, et al. Production of highly pure no-carrier added ^{89}Zr for the labelling of antibodies with a positron emitter. *Appl Radiat Isot.* 1994;45:1143–1147.
12. Verel I, Visser GWM, Boellaard R, Stigter-van Walsum M, Snow GB, van Dongen GAMS. ^{89}Zr Immuno-PET: comprehensive procedures for the production of ^{89}Zr-labeled monoclonal antibodies. *J Nucl Med.* 2003;44:1271–1281.
13. Phelps ME. Molecular imaging and its biological applications. *Eur J Nucl Med Mol Imaging.* 2004;31:1544.
14. Dejesus OT, Nickles RJ. Production and purification of ^{89}Zr, a potential PET antibody label. *Int J Rad Appl Instrum [A].* 1990;41:789–790.
15. Verel I, Visser GW, Boerman OC, et al. Long-lived positron emitters zirconium-89 and iodine-124 for scouting of therapeutic radioimmunoconjugates with PET. *Cancer Biother Radiopharm.* 2003;18:655–661.
16. Nayak TK, Brechbiel MW. Radioimmunoimaging with longer-lived positron-emitting radionuclides: potentials and challenges. *Bioconjugate Chemistry.* 2009;20:825–841.
17. Lewis Jason S, Singh Rajendra K. Welch Michael J. Long lived and unconventional PET radionuclides. *Molecular Imaging in Oncology;* 2008:283–292.
18. Hohn A, Zimmermann K, Schaub E, Hirzel W, Schubiger PA, Schibli R. Production and separation of "non-standard" PET nuclides at a large cyclotron facility: the experiences at the Paul Scherrer Institute in Switzerland. *Q J Nucl Med Mol Imaging.* 2008;52:145–150.
19. Van Dongen GA, Visser GW, Lub-de Hooge MN, De Vries EG, Perk LR. Immuno-PET: a navigator in monoclonal antibody development and applications. *Oncologist.* 2007;12:1379–1389.
20. Holland JP, Sheh Y, Lewis JS. Standardized methods for the production of high specific-activity zirconium-89. *Nucl Med Biol.* 2009;36:729–739.
21. Bowen H. The biogeochemistry of the elements. In: *Trace Elements in Biochemistry.* London, U.K.: Academic Press. 1966:173–239.
22. Link JM, Krohn KA, Eary JF, et al. ^{89}Zr for antibody labelling and positron tomography. *J Labelled Comp Radiopharm.* 1986;23:1296–1297.
23. Zweit J, Downey S, Sharma HL. Production of no-carrier-added zirconium-89 for positron emission tomography. *Int J Rad Appl Instrum [A].* 1991;42:199–201.
24. Kumbhar PP, Lokhande CD. Electrodeposition of yttrium from a nonaqueous bath. *Met Finish.* 1995;93:28, 30–31.
25. Sadeghi M, Kakavand T, Taghilo M. Targetry of Y_2O_3 on a copper substrate for the non-carrier-added ^{89}Zr production via ^{89}Y(p, n) ^{89}Zr reaction. *Kerntechnik.* 2010;75:298–302.
26. Saha GB, Porile NT, Yaffe L. (p, xn) and (p, pxn) Reactions of Yttrium-89 with 5-85-MeV Protons. *Phys Rev.* 1966;144:962.
27. Liu S. Bifunctional coupling agents for radiolabeling of biomolecules and target-specific delivery of metallic radionuclides. *Adv Drug Deliv Rev.* 2008;60:1347–1370.
28. Greenwood NN, Earnshaw A. *Chemistry of the Elements.* Oxford, UK: Pergamon Press; 1984.

29. Meijs WE, Herscheid JDM, Haisma HJ, Pinedo HM. Evaluation of desferal as a bifunctional chelating agent for labeling antibodies with Zr-89. *Int J Rad Appl Instrum [A].* 1992;43:1443–1447.
30. Ali SA, Shankland EG. Radiochemical synthesis of ^{89}Zr-porphyrin for positron label of monoclonal antibodies. *J Labelled Comp Radiopharm.* 1991;30:326.
31. Meijs WE, Haisma HJ, Klok RP, et al. Zirconium-labeled monoclonal antibodies and their distribution in tumor-bearing nude mice. *J Nucl Med.* 1997;38: 112–118.
32. Meijs WE, Haisma HJ, Van Der Schors R, et al. A facile method for the labeling of proteins with zirconium isotopes. *Nucl Med Biol.* 1996;23:439–448.
33. Perk L, Vosjan M, Visser G, et al. *p*-Isothiocyanatobenzyl-desferrioxamine: a new bifunctional chelate for facile radiolabeling of monoclonal antibodies with zirconium-89 for immuno-PET imaging. *Eur J Nucl Med Mol Imaging.* 2010;37: 250–259.
34. Vosjan MJWD, Perk LR, Visser GWM, et al. Conjugation and radiolabeling of monoclonal antibodies with zirconium-89 for PET imaging using the bifunctional chelate p-isothiocyanatobenzyl-desferrioxamine. *Nat Protoc.* 2010;5:739–743.
35. Chopra A. *^{89}Zr-Labeled Trastuzumab, A Humanized Monoclonal Antibody Against Epidermal Growth Factor Receptor* 2. Molecular Imaging and Contrast Agent Database (MICAD) [database online]. Bethesda, MD: National Library of Medicine, NCBI; 2004–2009; 2010. Available from: http://micad.nih.gov.
36. Dijkers ECF, Kosterink JGW, Rademaker AP, et al. Development and characterization of clinical-grade ^{89}Zr-trastuzumab for HER2/neu ImmunoPET imaging. *J Nucl Med.* 2009;50:974–981.
37. Dijkers E, Lub-de Hooge MN, Kosterink JG, et al. Characterization of ^{89}Zr-trastuzumab for clinical HER2 immunoPET imaging. *J Clin Oncol.* 2007;25 (18S):3508.
38. Dijkers EC, Oude Munnink TH, Kosterink JG, et al. Biodistribution of ^{89}Zr-trastuzumab and PET Imaging of HER2-positive lesions in patients with metastatic breast cancer. *Clin Pharmacol Ther.* 2010;87:586–592.
39. Sampath L, Kwon S, Ke S, et al. Dual-Labeled trastuzumab-based imaging agent for the detection of human epidermal growth factor receptor 2 overexpression in breast cancer. *J Nucl Med.* 2007;48:1501–1510.
40. Perik PJ, Lub-De Hooge MN, Gietema JA, et al. Indium-111–labeled trastuzumab scintigraphy in patients with human epidermal growth factor receptor 2–positive metastatic breast cancer. *J Clin Oncol.* 2006;24:2276–2282.
41. Liu Y, Welch MJ. Nanoparticles labeled with positron emitting nuclides: advantages, methods, and applications. *Bioconjug Chem.* 2012;23:671–682.

Appendix J. Establishing Reliable Production of the PET Isotope ^{89}Zr for Research Use: From Target Fabrication to Preclinical Imaging

Establishing Reliable Production of the PET Isotope ^{89}Zr for Research Use: From Target Fabrication to Preclinical Imaging

R.K. Scharli[a,b], R.I. Price[a,b], S. Chan[a], D. Cryer[a], C.M. Jeffery[a,c,d], A.H. Asad[a,d,e], L. Morandeau[a], P. Eu[f], C. Cullinane[g], A. Kasbollah[f,h] & A. Katsifis[i]

[a]RAPID PET Labs, Sir Charles Gairdner Hospital, Perth, WA 6009 Australia; [b]Physics, University of Western Australia, Perth WA 6009 Aus; [c]Centre for Forensic Science, University of Western Australia, Nedlands, WA, 6009, Aus; [d]ARC Centre of Excellence in Anti-Matter Matter Studies, Australian National University, Canberra, ACT 0200 Aus; [e]Applied Physics, Curtin University, Perth, WA 6009 Aus; [f]Centre of Molecular Imaging and [g]Research Division, Peter MacCallum Cancer Centre, Melbourne, VIC 3000 Aus; [h]School of Medical Sciences, RMIT University, Melbourne, VIC 3083 Aus; [i]PET & Nuclear Medicine, Royal Prince Alfred Hospital, Sydney, NSW 2000 Aus

Abstract. A semi-automated, in-house external beamline, ≤40 μA at 11.7 MeV for 120 min (degraded from 18 MeV to suppress ^{88}Y & ^{88}Zr co-production) produced ^{89}Zr from ^{89}Y(p,n)^{89}Zr. EOB activity (by HPGe γ-spectr.) of ^{89}Zr in target discs, derived from multiple runs, was 1.42 GBq (±0.45 GBq [SD], n=4) which was 67% (±21%, n=4) of the theoretical activity, with a maximum of 1.84 GBq (87% of theory) achieved. Recovery was 88% (±9%, n=4), radionuclidic purity >99% (n=4) and chemical purity 0.2 ppm Zr (±0.3 ppm, n=3, ICP-MS). The Zr:Y ratio improved from 1:10000 in the pre-filtered solution to 1:10 in the product purified by hydroxamate column. Efficiency of radiolabeling to monoclonal antibody (mAb; trastuzumab) was 100% and purified ^{89}Zr did not bind non-specifically to mAb. Chelator:mAb ratio was 1.3:1. No-carrier-added specific activity of purified ^{89}Zr was 408 MBq/μg (±26 MBq/μg, n=2) via the titration-by-chelator method. Minimum ligand concentration for which 100% labeling occurred was 302 nmol/L. Small animal PET imaging (Philips Mosaic; scan acquisition time 10 min; decay & randoms corrected; image reconstructed using a 3-D RAMLA algorithm) demonstrated marked tumor-specific uptake of ^{89}Zr-labeled mAb but nil 'free' ^{89}Zr (as chloride) tumor uptake.

Keywords: Positron emission tomography, radiopharmaceuticals, immuno-PET, solid targetry, ^{89}Zr, zirconium, production, separation, purification, radiolabeling, specific activity, small animal PET imaging.
PACS: 87.57.uk Positron emission tomography (PET); 87.57.un Radiopharmaceuticals.

INTRODUCTION

The PET radionuclide zirconium-89 (^{89}Zr), with its relatively long half-life (78 hr, β^+max=0.897 MeV, β^+mean=0.397 MeV; 23%) is a candidate for immuno-PET imaging, particularly when extended monoclonal-antibody (mAb) circulation time facilitates tumor penetration [1]. Hitherto, challenges in purification of ^{89}Zr and its labeling to mAb had restricted its use. Introduction of an isothiocyanate group to the desferrioxamine (DFO)-based conjugation of mAb [2], plus improvements in ^{89}Zr targetry have expanded applications of ^{89}Zr.

14th International Workshop on Targetry and Target Chemistry
AIP Conf. Proc. 1509, 101-107 (2012); doi: 10.1063/1.4773949

Trastuzumab (Herceptin®, Genentech Inc, South San Francisco, USA) is an anti-human EGFR receptor-2 mAb, indicated in patients with HER2/neu overexpressing breast cancer. In this 'proof-of-concept' study, we produced ^{89}Zr of acceptable radionuclidic, radiochemical and chemical purity, used it to radiolabel trastuzumab, and performed small animal PET imaging on a murine tumor model for HER2+ expressing colorectal cancer.

MATERIALS & METHODS

Production of ^{89}Zr

A semi-automated in-house designed and built external beamline was attached to a port of an IBA 18/9 cyclotron (IBA Group, Louvain-la-Neuve, BEL). An yttrium (Y) foil target (99.9% purity, American Elements, Los Angeles, USA) was proton bombarded at $\leq$40 µA at 11.7 MeV for 120 min to produce ^{89}Zr via the reaction ^{89}Y(p,n)^{89}Zr, which has a production threshold of 3.7 MeV [3]. In order to limit production of competing radionuclides, it was necessary to reduce the primary proton beam energy from the measured value leaving the stripper foil (18.08 MeV ±0.09 MeV [SD], n=5) to approximately 11.7 MeV (11.68 MeV ±0.18 MeV, n=3). This eliminated the reaction ^{89}Y(p,2n)^{88}Zr which has a threshold energy of 13.1 MeV and significantly restricted the reaction ^{89}Y(p,pn)^{88}Y with a threshold energy of 5.61 MeV. Figure 1 shows the solid targetry external beam line plus its schematic.

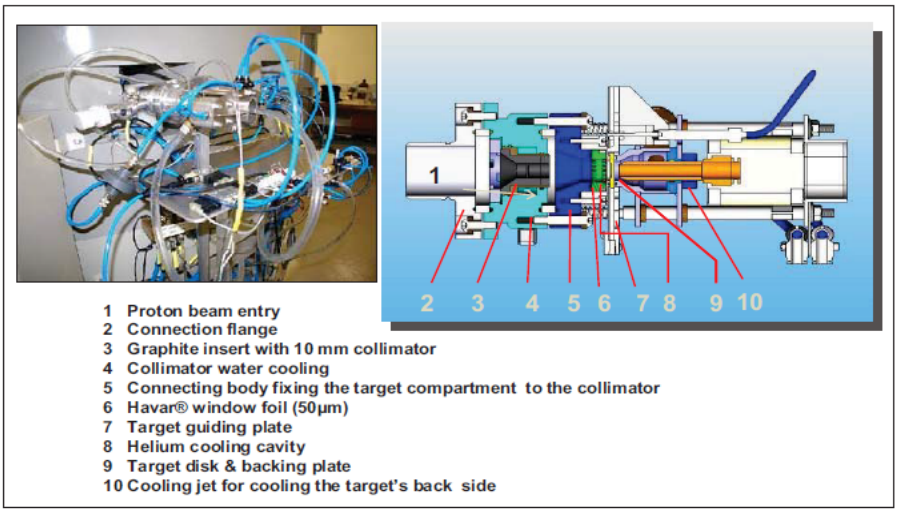

FIGURE 1. In-house designed & constructed solid targetry beamline & its schematic.

The proton beam enters the beam line at (1) then passes through a cooled graphite collimator at (3). For the present study where the primary beam energy of the beam was reduced, a graphite degrader of 1020 µm thickness was inserted at (4) to reduce the beam energy to 11.7 MeV. The volume (5) is for water cooling of the collimator. The energy-degraded beam then passes through the connecting body fixing the target component to the collimator and is further degraded by a 50 µm Havar® (Goodfellow Cambridge Ltd, Huntingdon, UK) window (6,7). This window forms the vacuum seal

between the cyclotron on one side and the target space on the other. Between the window and the front face of the target lies a space (8) through which cooling helium gas flows, conducting heat away from the window foil and the front face of the target in its backing plate (9). The target is held in position by a guiding plate and an in-house designed specially shaped water cooling jet is at (11) to cool the back side of the target.

The target comprised of two stacked pure (99.9%) yttrium foils each (mean) 127 μm thick and 15 mm in diameter. This design minimized the mass of target not exposed to the beam and thus reduced the burden on the chemical process designed to separate Zr from Y. The yttrium foils were cradled in an aluminum (99.999% purity, Goodfellow Cambridge Ltd) backing plate and front disc insert, as shown in Fig. 2. Following insertion of the target, the front face of the target assembly is pressed pneumatically against a Viton® O-ring seal (E. I. du Pont de Nemours and Company, Wilmington, USA) and (as noted above) helium-gas cooled on the beam side. The water cooling jet deployed on the backing plate at the rear of the target was optimized using finite-element heat-flow modeling of candidate designs.

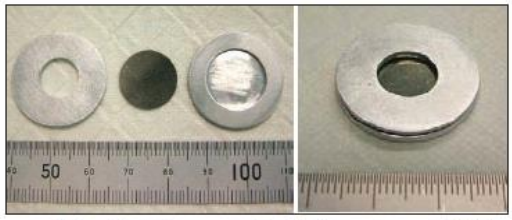

FIGURE 2. 'Sandwich' assembly of yttrium stacked-discs target. Following slotting into external beamline, pneumatic compression of target assembly permits helium-gas cooling on front (between Havar® vacuum 'window' and target surface) plus water cooling on the back.

Separation & Purification of ^{89}Zr

Preparation of hydroxamate column mass

The preparation of an hydroxamate column from a weak cation exchange resin (Accell Plus CM, Waters, Milford, USA) involved first the activation of the carboxylic acid groups into activated ester (tetrafluorophenol ester), followed by reaction with hydroxylamine hydrochloride. This procedure has been published by Verel *et al.,* 2003 [4]. The method below was scaled up fivefold, following Holland *et al.,* 2009 [5].

Separation & Purification of ^{89}Zr

Based on the method of Holland *et al.,* 2009 [5], the bombarded yttrium foils were dissolved in 4 x 0.5 mL 6 M HCl (diluted from 12 M HCl, Sigma-Aldrich, St. Louis, USA), then 25 μL hydrogen peroxide (30% v/v, Sigma-Aldrich) was added to ensure all Zr was in the +4 oxidation state, followed by 5 mL Milli-Q® water (18.2 MΩ.cm @ 25°C, Millipore, Billerica, USA) to give a 2 M HCl solution concentration. This pre-filtered solution was eluted through a hydroxamate ion-exchange column, followed by washes of HCl (2 M), then water. Zr was then eluted with 5 mL 1M oxalic acid (Sigma-Aldrich).

Radiolabeling with ^{89}Zr

Radiolabeling was based on the method of Perk *et al.,* 2010 [2] utilising the bifunctional chelator *p*-isothiocyanatobenzyl-desferrioxamine B (*p*-SCN-Bz-DFO; Macrocyclics, Dallas, USA) to premodify the mAb (trastuzumab) prior to radiolabeling with ^{89}Zr-oxalate. ^{89}Zr was also investigated for non-specific binding to mAb without bifunctional chelator.

The chelator:mAb ratio was determined by labeling the immunoconjugate with a known excess of Zr (Zr-oxalate 'spiked' with ^{89}Zr). Generally following Perk *et al.,* 2010 [2], DFO-mAb was labeled with ^{89}Zr at room temperature for 1 hr and purified by size-exclusion chromatography (GE Life Sciences, Buckinghamshire, UK); then analyzed by instant thin layer chromatography (ITLC) with ITLC-SA paper (pre-heated to >90°C for >24 hr, Varian Inc, Palo Alto, USA) and 0.5 M sodium citrate (pH4-5). The mAb concentration was determined via high performance liquid chromatography (HPLC) analysis using HPLC column (BioSuite 125, 5 µm HR SEC, 7.8 x 300 mm, Waters) and mobile phase described by Perk *et al.,* 2010 [2].

No-carrier added (NCA) specific activity was measured using chelator titration with DFO (Desferal, Novartis, Basel, CH) and analysed by ITLC (Varian ITLC-SA paper and 0.5 M sodium citrate [pH4-5]) to determine chelated vs. 'free' ^{89}Zr. Radiolabeling was carried out using neutralised ^{89}Zr-oxalate and DFO 1:2 serial dilution solutions.

Small Animal PET Preclinical Imaging

Tumor Model & Labeling

Balb/c nude mice were injected subcutaneously on the right flank with the HER2 positive LS174T colorectal tumour cells (CellBank Australia, Westmead, AUS). Two weeks later when the tumours reached a volume of approximately 150 mm^3 the imaging studies to compare 'free' ^{89}Zr (chloride) vs. ^{89}Zr-DFO-trastuzumab uptake at 24 hr were performed. The mAb radiolabel was prepared as described by Perk *et al.,* 2010 [2]. The ^{89}Zr-chloride was prepared based on Holland *et al.,* 2009 [5]. The integrity of the label was verified by HPLC.

Imaging

Mice were injected via the tail vein with 200 µL of 3.7 MBq ^{89}Zr (chloride) in saline, or with 200 µL of 1.85 MBq ^{89}Zr-DFO-trastuzumab in saline. Twenty four hours later the mice were anaesthetized in 3% isofluorane in 50% oxygen in air and placed on the bed of a Philips Mosaic small animal PET scanner (Royal Philips Electronics, Amsterdam, NED). Image data was acquired over 10 minutes; decay and randoms corrected, and images reconstructed using a 3-D RAMLA algorithm [6].

RESULTS & DISCUSSION

Production of ^{89}Zr

The end of bombardment (EOB) activity (by HPGe γ-spectroscopy) of ^{89}Zr in target discs, derived from multiple runs, was 1.42 GBq (±0.45 GBq [SD], n=4) which was

67% (±21%, n=4) of the theoretical activity, with a maximum of 1.84 GBq (87% of theory) achieved. Part of this variation was likely due to a difference in the 'apparent' beam current (determined from electrometer measurement on the target) versus 'true' beam current. The latter is measurable using a Faraday cup or reference-reaction calibration via bombardment of copper and aluminum foils; such measurements were not performed in this experiment. However, related experiments in our laboratory suggest an approximately 5% disparity between these currents.

The beam energy of 11.7 MeV was chosen to be convenient also for the production of ^{64}Cu, which is also performed routinely in our laboratory. ^{89}Zr production can be selectively produced at higher beam energies but exchanging degraders is both inconvenient and a dose burden. In this study the other beam parameters have been set to give >1 GBq EOB activity. The next in-house engineering upgrade of the external beamline will facilitate easy switching of degraders.

Separation & Purification of ^{89}Zr

The product recovery was 88% (±9% [SD], n=4), the radionuclidic purity >99% (n=3, HPGe γ-spectr.) and chemical purity 0.2 ppm Zr (±0.3 ppm, n=3, ICP-MS). This is comparable to published data [5]. The Zr:Y ratio improved from 1:10000 in the pre-filtered solution to 1:10 in the purified product.

Radiolabeling with ^{89}Zr

Radiolabeling efficiency was determined to be 100% and purified ^{89}Zr did not bind non-specifically to trastuzumab (Fig. 3). Therefore *p*-SCN-Bz-DFO is necessary to facilitate ^{89}Zr binding to trastuzumab. For ITLC analysis Holland *et al.*, 2009 [5] and Perk *et al.*, 2010 [2] used ITLC-SG strips (Pall Corp, Port Washington, USA) which were out of production at the time of these experiments. Varian ITLC-SA papers were sourced instead and performed best with 0.5 M sodium citrate (pH4-5) in the separation of bound from 'free' ^{89}Zr.

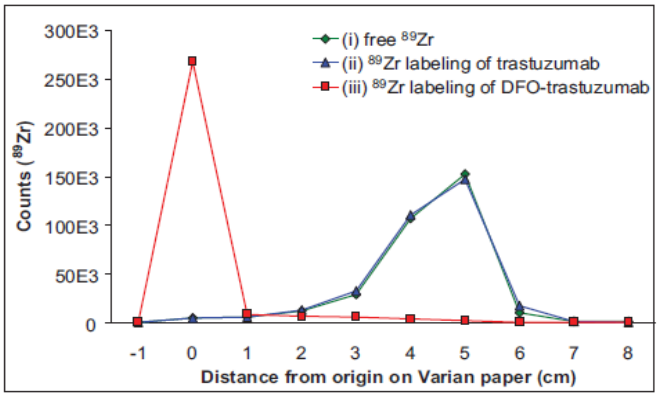

FIGURE 3: ITLC separation analyses of (i) 'free' ^{89}Zr-oxalate; (ii) 'free' ^{89}Zr plus non-conjugated trastuzumab, &; (iii) ^{89}Zr-DFO-trastuzumab.

The chelator:mAb ratio determined in this study was 1.3:1, in satisfactory agreement with Perk *et al.*, 2010 [2], who reported 1.5:1.

NCA Specific Activity

Figure 4 shows a plot of the percentage of zirconium chelated by DFO vs. the DFO concentration. From the line of best fit of the positive linear region of the plot, the minimum ligand concentration for which 100% labeling occurred was determined to be 302 nmol/L (2 x DFO concentration at 50% Zr chelation).

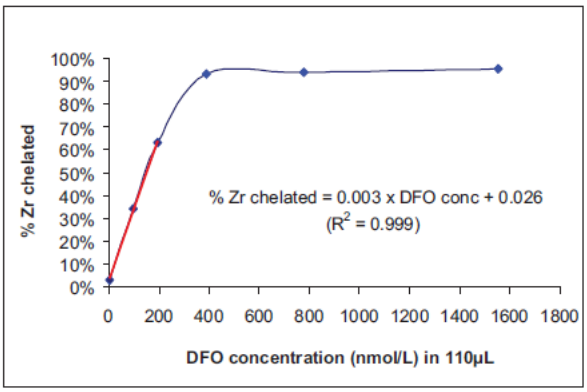

Figure 4: Titration by chelator method for determining specific activity of ^{89}Zr. Minimum ligand concentration for which 100% labeling occurred was 302 nmol/L.

The theoretical 'carrier-free' specific activity is 16600 MBq/µg. The NCA specific activity of purified ^{89}Zr was 408 MBq/µg (±26 MBq/µg, n=2), comparable to published data of Holland *et al.*, 2009 [5] of 196-496 MBq/µg and Hong *et al.*, 2011 [7] of 225 (±24 MBq, n=6), via the titration by chelator method. NCA specific activity via ICP-MS analysis will also be performed in future experiments.

Proof-of-concept Small Animal PET Preclinical Imaging

Small animal PET imaging demonstrated marked tumor-specific uptake of ^{89}Zr-labeled trastuzumab but nil 'free' ^{89}Zr tumor uptake at 24 hr (Fig. 5).

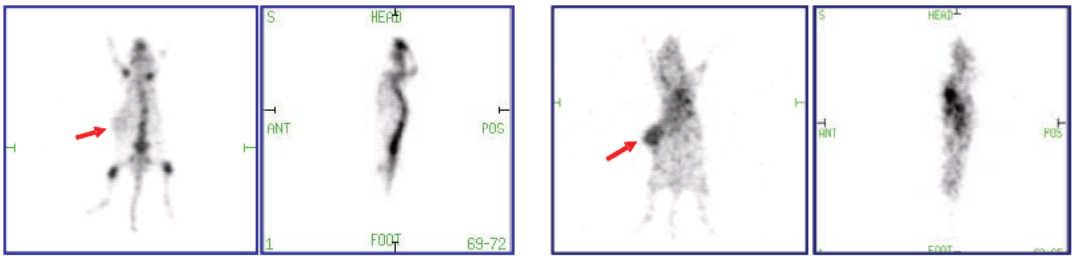

FIGURE 5: Small animal PET maximum intensity projection images taken at 24 hr post-injection of HER2-expressing LS174T tumor bearing mice. (a) Mouse injected with 3.7 MBq ^{89}Zr (chloride i.e. 'free' ^{89}Zr). Skeletal uptake of 'free' ^{89}Zr at that time was noted. There was minimal uptake in the tumor (denoted by the arrow). (b) Mouse injected with 1.85 MBq ^{89}Zr-DFO-trastuzumab. Integrity of label verified by HPLC. Specific tumour uptake is denoted by the arrow. There was also an indication of cardiac uptake in accord with the known pharmacokinetics of trastuzumab [8].

Figure 5(a) shows ^{89}Zr tracer as ^{89}Zr-chloride (i.e. 'free' ^{89}Zr), applied to a nude mouse bearing a HER2 positive LS174T tumor on the right flank. Skeletal uptake of 'free' ^{89}Zr was noted. There was minimal uptake in the tumor. Figure 5(b) shows ^{89}Zr-DFO-trastuzumab, applied to another tumor-bearing mouse. Marked tumor uptake of the radiolabel was noted. There was also an indication of cardiac uptake, in accord with the known pharmacokinetics of trastuzumab [8].

CONCLUSION

This study has demonstrated the stages leading to reliable (research-level) production of ^{89}Zr of acceptable radionuclidic, radiochemical and chemical purities, plus NCA specific activity – from targetry design and construction through to 'proof-of-principle' validation of product use in preclinical imaging of a mouse tumor model.

ACKNOWLEDGMENTS

The authors acknowledge the RAPID, SCGH Lab PET Team for cyclotron, engineering, logistical and radiation safety support. Australian Nuclear Science and Technology Organisation (ANSTO), Sydney for equipment funding. RKS acknowledges an AINSE Scholarship ALNGRA11052, AINSE ID No 6777.

REFERENCES

1. A. Wu, *J. Nucl. Med.* **50**, 2-5 (2009).
2. L. R. Perk, G. W. M. Visser, M. Budde, M. J. W. D. Vosjan, P. Jurek, G. E. Kiefer and G. A. M. S. van Dongen, *Eur. J. Nucl. Med. Mol. Imag.* **37**, 250-259 (2010).
3. M. A. Avila-Rodriguez, J. Rajander, J. O. Lill, K. Gagnond, J. Schlesingera, J. S. Wilsond, S. A. McQuarried, O. Solina, *Nucl. Inst. Meth. Phys. Res. B* **267**, 1867-1872 (2009).
4. I. Verel, G. W. M. Visser, R. Boellaard, O. C. Boerman, M. Stigter-van Walsum, G. B. Snow and G. A. M. S. van Dongen, J. Nucl. Med. **44**, 1271-1281 (2003).
5. J. P. Holland, Y. Sheh and J. S. Lewis, *Nucl. Med. Biol.* **36**, 729-739 (2009).
6. C. Cullinane, D. S. Dorow, S. Jackson, B. Solomon, E. Bogatyreva, *J. Nucl. Med.* **52**, 1261-1267 (2011).
7. H. Hong, G. W. Severin, Y. Yang, J. W. Engle, Y. Zhang, T. E. Barnhart, G. Liu, B. R. Leigh, R. J. Nickles, W. Cai, *Eur. J. Nucl. Med. Mol. Imag.* **39**, 138-148 (2011).
8. D. J. Slamon, B. Leyland-Jones, S. Shak, H. Fuchs, *N. Engl. J. Med.* **344**, 783-92 (2001).